CORE
Metadata, citation and similar papers at core.ac.uk
Provided by Texas A&M Repository

ANALYTICAL TIME DOMAIN ELECTROMAGNETIC FIELD PROPAGATORS AND CLOSED-FORM SOLUTIONS FOR TRANSMISSION LINES

A Dissertation

by

JAEHOON JEONG

Submitted to the Office of Graduate Studies of
Texas A&M University
in partial fulfillment of the requirements for the degree of

DOCTOR OF PHILOSOPHY

December 2006

Major Subject: Electrical Engineering

ANALYTICAL TIME DOMAIN ELECTROMAGNETIC FIELD PROPAGATORS AND CLOSED-FORM SOLUTIONS FOR TRANSMISSION LINES

A Dissertation

by

JAEHOON JEONG

Submitted to the Office of Graduate Studies of
Texas A&M University
in partial fulfillment of the requirements for the degree of

DOCTOR OF PHILOSOPHY

Approved by:

Chair of Committee,	Robert D. Nevels
Committee Members,	Steven Wright
	Philip Hemmer
	Muhammad Zubairy
Head of Department,	Costas N. Georghiades

December 2006

Major Subject: Electrical Engineering

ABSTRACT

Analytical Time Domain Electromagnetic Field Propagators and Closed-Form Solutions for Transmission Lines.

(December 2006)

Jaehoon Jeong, B.S., Hong-Ik University, South Korea

Chair of Advisory Committee: Dr. Robert D. Nevels

An analytical solution for the coupled telegrapher's equations in terms of the voltage and current on a homogeneous lossy transmission line and multiconductor transmission line is presented. The resulting telegrapher's equation solution is obtained in the form of an exact time domain propagator operating on the line voltage and current. It is shown that the analytical equations lead to a stable numerical method that can be used in the analysis of both homogeneous and inhomogeneous transmission lines. A numerical dispersion relation is derived proving that this method has no numerical dispersion down to the two points per wavelength Nyquist limit. Examples are presented showing that exceptionally accurate results are obtained for lossy single and multiconductor transmission lines. The method is extended to represent the general solution to Maxwell's differential equations in vector matrix form. It is shown that, given the electromagnetic field and boundary conditions at a given instant in time, the free space time domain propagator and corresponding dyadic Green's functions in 1-, 2-, and 3-dimensions can be used to calculate the field at all subsequent times.

DEDICATION

To wife, Eun-Kyung,
and
my family.

ACKNOWLEDGMENTS

I would like to express my sincere gratitude to Dr. Robert D. Nevels for his support and guidance with regards to my Ph.D. studies and research at Texas A&M University. I also appreciate Dr. Steven Wright, Dr. Philip Hemmer, and Dr. Muhammad Zubairy for serving as members on my dissertation committee and for their helpful comments. I would like to extend an added thank you to Dr. Ic-Pyo Hong for his technical assistance and invaluable discussions.

I would like to thank all my dear friends for their support. I would also like to thank my parents, parents-in-law, sister's family, younger sister, and sister-in-law for their constant love, encouragement, and support. Finally, I would like to express my deep appreciation to my lovely wife Eun-Kyung for her patience, love, and support during my graduate studies. This work would not have been possible without her support and patience.

TABLE OF CONTENTS

Page

ABSTRACT iii

DEDICATION iv

ACKNOWLEDGMENTS v

TABLE OF CONTENTS vi

LIST OF FIGURES viii

CHAPTER

I INTRODUCTION 1

1.1. Time domain techniques for lossy transmission line 1
1.2. Time domain techniques for multiconductor transmission line 5
1.3. Time domain Green's function for Maxwell's equations 8
1.4. Research 9

II TIME DOMAIN ANALYSIS OF LOSSY TRANSMISSION LINE 13

2.1. Telegrapher's equations for lossy transmission line 13
2.2. The propagator 14
2.3. Explicit solution form 18
2.4. Discrete implementation 21
2.5. Three uniform T.L. 23
2.6. Linear taper T.L. 25
2.7. Exponential taper T.L. 27
2.8. Numerical dispersion 29
2.9. Compatibility between EP and FDTD in magic time step 33
2.10. Tapered microstrip line 38
2.11. Summary 42

III TIME DOMAIN ANALYSIS OF MULTICONDUCTOR TRANSMISSION LINE 44

3.1. Multiconductor line equations for TEM lines 44

CHAPTER Page

3.2. Multiconductor line equations for quasi -TEM lines 49
3.3. Uniform coupled strip lines....53
3.4. Non-uniform coupled strip lines 56
3.5. Three asymmetric coupled strip lines 60
3.6. Uniform coupled microstrip lines 64
3.7. Three coupled microstrip lines having different widths....73
3.8. Non-uniform coupled microstrip lines 78
3.9. Summary 82

IV TIME DOMAIN GREEN'S FUNCTION AND PROPAGATOR FOR MAXWELL'S EQUATIONS 83

4.1. Maxwell's equations 83
4.2. Time domain Green's function and propagator 84
4.3. One-dimensional Green's functions $\bar{\mathbf{G}}^{(1)}$ 90
4.4. Two-dimensional Green's functions $\bar{\mathbf{G}}^{(2)}$ 91
4.5. Three-dimensional Green's functions $\bar{\mathbf{G}}^{(3)}$ 94
4.6. Verification and examples....97
4.7. Summary 100

V SUMMARY AND RECOMMENDATIONS 102

5.1. Summary 102
5.2. Recommendations for future research....106

REFERENCES....107

APPENDIX A 114

APPENDIX B 115

APPENDIX C 118

APPENDIX D 119

VITA 129

LIST OF FIGURES

FIGURE Page

1. (a) Three concatenated transmission lines sections. Each section has the same set of distributed parameters L, G, and C, but R is zero on the two outside sections and non-zero on the center section. S_{11} versus frequency comparison between exact results and numerical calculations based on the EP method with (b) a low-loss and (c) a high-loss center section. 23

2. (a) Lossless transmission line with a linear taper and (b) S_{11} versus frequency comparison between exact results with numerical calculations based on the EP method. 26

3. (a) Exponential tapered lossy transmission line with (b) S_{11} versus frequency comparison between exact results and EP method numerical calculations 28

4. A Gaussian pulse propagated 15m, comparison between FDTD and EP methods. (a) $s=1$ (b) $s=0.5$, and (c) $s=0.25$ 31

5. Current $\left(I|_i^n\right)$ expression in time-spatial numerical grid. 34

6. (a) Imaginary grid points with $i\pm\frac{1}{2}$ and $n-\frac{1}{2}$ (b) Equivalent expression for $I|_i^n$ 35

7. Computation for I_1 and I_2 36

8. Layout Two different expressions (EP and FDTD) for voltage $\left(V|_i^n\right)$ in magic time step 37

9. (a) Geometry of tapered microstrip line, (b) its modeling and (c) its applied circuit for transient simulation. (d) Response at node 1 and (e) Response at node 2 39

10. (a) Geometry of uniform coupled strip lines, (b) its applied circuit for transient simulation. (c) responses at node V_{ne1} and V_{fe1} and (d) responses at node V_{ne2} and V_{fe2}. 54

FIGURE Page

11. (a) Nonuniform coupled strip lines and its applied circuit for transient simulation, (b) numerical modeling, (c) responses at node V_{ne1} and V_{fe1} and (d) responses at node V_{ne2} and V_{fe2}. 58

12. (a) Asymmetric three coupled strip lines, (b) its applied circuit for transient simulation, (c) responses at node V_{ne1} and V_{fe1}, (d) responses at node V_{ne2} and V_{fe2} , and (e) responses at node V_{ne3} and V_{fe3} 61

13. Electric field distributions of coupled microstirp for (a) *a*-mode (b) *b*-mode 65

14. (a) Geometry of coupled microstrip lines, (b) its applied circuit for transient simulation, (c) Sets of voltage sources for the fundamental modes, responses at (d) V_{ne1} and V_{fe1} and (e) V_{ne2} and V_{fe2} 71

15. (a) Geometry of three coupled microstrip lines, (b) its applied circuit for transient simulation, (c) Sets of voltage sources for the fundamental modes, (d) Voltage responses at V_{ne1} and $V_{fe1,}$ (e) V_{ne2} and V_{fe2} and (f) V_{ne3} and V_{fe3}. 74

16. (a) Geometry of nonuniform coupled microstrip lines, (b) Sets of voltage sources for the fundamental modes, (c) Voltage responses at V_{ne1} and $V_{fe1,}$ and (d) V_{ne2} and V_{fe2}. 79

17. Illustration of Simpson’s integration rule. 115

CHAPTER I

INTRODUCTION

1.1. Time domain techniques for lossy transmission line

Nonuniform transmission lines appear in a variety of microwave circuits. Applications of nonuniform lines include impedance matching devices, impedance transformers, filters and directional couples. Resistive loss also plays a key role in the overall transmission line response and can be especially important when analyzing the behavior of broadband time domain signals. However, nonuniform lossy transmission lines are difficult to accurately characterize and simulate in the time domain as compared to other microwave components. There is no general analytical solution for the Telegraphers equations when the transmission line is dissipative and nonuniform except for the special case in which the line is distortionless. However, a number of numerical methods have been developed to solve for the time domain voltage and current on a lossy and/or nonuniform transmission line.

The lumped element model (LEM) [1] is a method in which a lossy transmission line is represented by a cascade of infinitesimally small cells, each characterized by its distributed resistance, conductance, inductance and capacitance (RGLC). In a variation on this method, the lossy line is modeled by a combination of lumped elements and ideal lossless transmission lines [2]. The major advantage of LEM is that equivalent circuits

---

The journal model for this dissertation is *IEEE Transactions on Microwave Theory and Techni*ques.

can be easily and quickly implemented in existing circuit simulators and extended to include coupled transmission lines with an arbitrary termination. This method provides an accurate analysis of the transmission line transient behavior when the line is terminated by a non-linear circuit. A drawback is that the computation speed suffers because the time domain response is obtained by repeated calculations carried out over a range of frequencies, followed by a numerical convolution (inverse Laplace transformation). In addition, a characteristic of lumped models is that they fail to accurately characterize interconnects at high frequencies.

The Method of Characteristics (MoC), a direct time domain calculation that provides an analytical solution to the wave equation for the lossless case, was first used for transmission lines by Branin [3]. With this method the transmission line response is modeled as a sum of modes. For this reason it is referred to as a modal extraction technique. To include losses, Grudis and Chang [4] suggested a cascaded MoC model. The cascaded MoC performs well for a long line, though for short lines it is not as fast or as accurate as other methods [5]. More recently, a variation of MoC using lumped matrix rational approximations was proposed by Grivet-Talocia, *at el.* [6]. They analyze a lossy transmission line in the frequency domain and then apply fast Fourier Transforms (FFT) and convolution to recover the transient time domain response. This method is useful for short as well as long transmission lines, however, for some signals the response is degraded when the frequency points are poorly sampled by the FFT or the convolution spans a large time interval. Xu, *et al* [7] introduced an improved MoC technique which relies on the Laplace transform rather than on FFT's and convolution.

The modified MoC is not subject to instability and requires less computation time and less memory than previous MoC methods. Because the MoC method requires a Taylor series in the frequency domain as well as a Padé approximation for the exponential terms, it is expected that it would be very difficult to apply in the nonuniform line case.

Time/frequency characteristics of lossy transmission lines have been obtained using the finite element method (FEM) [8,9,10] and finite-difference time-domain (FDTD) [11, 12, 13]. Lee and Konard [8] solved the Telegrapher's equation using FEM, which was shown to give accurate results for lossy structures as well as for the nonuniform line. Recently, Lucic, *et al.* [9] and You, *et al.* [10] developed a hybrid LEM-FEM method. The LEM-FEM method takes advantage of the topology of LEM and removes the disadvantage of an instability that can arise in FEM. FDTD based on Yee's method, is the most general method for transmission line analysis. Recently, a modified 'on-line FDTD' scheme was introduced by Zhong, *et al.* [12] based on a semi-implicit approximation. Although Zhong's method improves computational accuracy and stability when compared to the 2^{nd} order Yee scheme when the line is lossy, it does not match the broad band accuracy of the standard FDTD method. Sekine, *et al.* [13] proposed FDTD with a new boundary condition for the nonuniform transmission line. This method has proven to be faster than MoC and more accurate than other current FDTD absorbing boundary conditions for an inhomogeneous line. A drawback of FDTD is that it is subject to numerical dispersion [13] when the signal is propagated a significant number of time steps. In addition, due to the interleaving structure of FDTD, voltage and current are not computed at the same spatial points on the transmission line.

This can lead to small errors in the characterization of capacitance, inductance and characteristic impedance calculated from numerical results.

Another attractive numerical technique, the Transmission Line Method (TLM) [14,15], belongs to the general class of differential equation time-domain numerical modeling methods. With TLM the transmission line is represented by a series of nodes connected by transmission line segments. The relationship between the incident and scattered voltages and currents at the nodes is determined by a scattering matrix. Additional elements, such as transmission-line stubs, can be added to the connecting nodes so that a nonuniform transmission line can be fashioned. It has been reported [15] that compared with standard 2^{nd} order FDTD, the TLM method has much less numerical dispersion.

There are several specialized techniques for analyzing the nonuniform lossy transmission lines [16,17]. In [16] the authors concatenate small linearly tapered transmission line sections that are each represented by the exact frequency domain ABCD matrix. This allows a piecewise-linear approximation of the characteristic impedance of a general shaped nonuniform transmission line, which is a much more accurate representation than the piecewise constant profile used in other similar methods. The result, which is Fourier transformed in order to obtain the time domain response, is in good agreement with analytical solutions [18]. Xu, *et al.* applied the differential quadrature method (DQM) to Telegrapher's equation in [17]. In this case the differential equations are discretized into a set of algebraic equations and solved in the frequency domain. The time domain response is obtained by inverse Laplace transform and

recursive convolution. It is claimed [17] that DQM-based modeling leads to higher computational efficiency than the conventional FEM, FDTD methods and can be easily applied to nonuniform and multiconductor transmission lines.

1.2. Time domain techniques for multiconductor transmission line

As VLSI attains higher operating speeds, greater miniaturization, and denser layouts, the need for more accurate and simpler analysis methods for multiconductor transmission lines has grown. A determination of the time domain response of multiconductor transmission lines is of particular importance in the analysis of crosstalk, delay, and the distortion of signals in fast digital circuit interconnections.

Numerical techniques for time domain analysis of multiconductor lines can be divided into two major categories, frequency domain convolution methods and direct time domain methods. The greatest value of the former lies in its ability to accurately handle frequency dependent losses [19]. However, frequency domain methods require repeated calculations over a wide frequency range along with a subsequent fast Fourier or Laplace transform of the frequency domain data in order to recover the time domain response [20]. Although this general approach is useful for short as well as long transmission lines, the greater computation speed, coding simplicity, and the fact that nonlinear terminations can best be described in the time domain [21] have encouraged the development of improved time domain methods.

The Method of Characteristics (MoC), as mentioned Section 1.1, is also useful technique for analyzing multiconductor transmission lines. Li, *at el* [22] introduced a

transient analysis technique for the multiconductor line using linear transformation MoC [23]. By enforcing two conditions, that each transmission line is coupled only with the closest one and that the lines are identical and equally spaced and side effects are negligible, telegrapher's equations are decoupled to apply MoC in [23]. Gao, *at el* [24] have evaluated the upper bounds on the errors caused by these two assumptions. In a recent paper by A. R. Chavez, *at el.* [19], a new modified MoC using the Norton equivalent models for the analysis of nonuniform multiconductor transmission lines has been presented. It was shown that the MoC can be extended to nonuniform structures and hence is suitable for the simulation of multiple coupled interconnections in integrated circuits and packaging.

Waveform relaxation (WR) techniques [25] were introduced as a substitution for the conventional time stepping algorithms used by circuit simulators for solving ordinary differential equations. Although a slow convergence rate limits its applicability to interconnect circuits, the WR method is useful for analysis of multiconductor lines having many conductors. More recently, Nakhla, *at el.* [26] introduced the technique of transverse partitioning in place of classical longitudinal partitioning thereby improving convergence rates and significantly reducing computational time.

The wavelet transform (WT) method has recently received much attention, especially in solving multiconductor problems [27,28]. Like the Fourier Transform (FT), WT is a frequency domain technique. However, as a consequence of the limited bandwidth of wavelet basis functions [27], the WT overcomes wide bandwidth requirement of the FT. Grivet-Talocia [28] introduced a new WT formulation that

adaptively selects a minimal number of basis functions, thus saving memory occupation and computing time with respect to more standard discretization schemes.

FDTD [29] is also general numerical method for analyzing multiconductor lines as well as single line. Although FDTD suffers from numerical dispersion, this method directly solves Telegrapher's equations in the time domain and is easily applicable to multiconductor lines [30]. In a modified FDTD technique [30], each line is computed by FDTD and overall voltages and currents are calculated by the state variables. FDTD is very useful for analyzing nonuniform transmission lines that are not long in terms of wavelengths.

The similarity transform method is perhaps the most frequently used technique [29] for analyzing multiconductor TEM lines in the time domain. With this method, multiconductor equations are decoupled using a similarity transform and the modal characteristic impedances and propagation velocities are identified. Then, Branin's method and the Bergeron diagram are applied to each modal voltage and current in order to obtain time domain solutions. Cheldavi [31], *et al.* obtained a time domain solution by applying modal decomposition with an equivalent continuous time linear filter model of the coupled lines. This method gives excellent results for the nonuniform coupled line problem. More recently, Amirhosseini, *et al.* [32], directly applied the mode technique to Telegrapher's equation with voltage and current expressed in terms of a product of a diagonal modal characteristic impedance matrix and the modal voltage vector. It was shown that this technique can be applied to symmetric coupled transmission lines.

The decoupled mode technique, a purely time domain method, is commonly used

to analyze symmetric and lossless multiconductor quasi-TEM lines [33]. With this method a normalized voltage and current eigenvector matrix is calculated from the inductance and capacitance matrices. The characteristic impedance and admittance matrices for the voltage and current equations are then obtained using the voltage and current eigenvector matrix. The Weak-coupling Assumption technique [34, 35] is another useful time domain method for the quasi-TEM line voltages and currents. The weak-coupling assumption is to ignore secondary effectx when the multiconductor equations are solved. Under these conditions, this method yields simple and accurate time domain expressions for lossless, symmetric quasi-TEM lines.

1.3. Time domain Green's function for Maxwell's equations

The solution, both analytical and numerical, to boundary value problems in electromagnetics is often facilitated by the introduction of the free space Green's function for Helmholtz equation.

Frequency domain dyadic Green's functions in electromagnetics have appeared regularly in the literature since the original paper on aperture diffraction by Levine and Schwinger [36]. R. E. Collin has contributed many significant articles on the subject as well as a definitive historical review [37]. A comprehensive and consistent presentation of both antenna and scattering problems can be found in Tai [38]. Time domain forms of the dyadic Green's function are much less common. Perhaps the earliest was a dyadic Green's function for Helmholtz's vector wave equation that appeared in Morse and Feshbach [39]. Several years later it was shown in Felson and Marcuvitz [40] that the

dyadic forms for the wave equation could be derived by a simple set of operations on the scalar Green's function. More recently the main body of literature has tended toward specialized applications, for example the time-domain plane-wave representation found in Hansen and Yaghjian [41]. The primary objective of the majority of recent work has been to obtain the radiated fields due to electric or magnetic sources or due to an initial field known on a boundary.

The advantages of the Maxwell equation Green's function over the Helmholtz and wave equation Green's functions are that it is a single compact expression governing radiation from both electric and magnetic sources as well as the propagation of the initial electric and magnetic field known in a volume of space or over its bounding surface. In addition, the derivation of this Green's function by means of the propagator method [42] which, though common in quantum mechanics literature [43, 44], is rarely seen in classical electromagnetics. The propagator method has never before been applied to solve a dyadic equation.

1.4. Research

In this dissertation, it is focused on the Path Integral (PI) method [43]. Path integrals can be described as a direct application of Huygens principle, whereby the voltage and current are updated in a fixed time increment by application of an operator acting on the present time voltage and current. PI methods, which are one category of many types of propagator methods, have not been widely used in transmission line analysis, although their history extends back to a highly regarded paper by Kac [45].

Kac's solution is novel in that the result for a lossy line allows one to clearly delineate the transient response in the absence of dissipation from that with dissipation. An improvement on Kac's method has been developed by Foong [46]. More recently Rubin [47] presented a PI time-domain behavioral modeling approach to analyze lossy multi-conductor transmission line interconnects. Rubbin used transmission and reflection in individual segments of a transmission line combined to form a series of integrals, each of which is related to a sum of trajectories of a propagated pulse. The solution was shown to be accurate, stable, computationally efficient, and applicable to time domain modeling of an interconnect. An example of a propagator method, described as a Symplectic Integrator (SI) [48,49], has been developed to solve the general 3-D Maxwell equations. The propagator in this case is an exponential operator whose series expansion operates on the electromagnetic field using an interleaving method similar to FDTD. Although not yet applied to the transmission line case, the results have been shown to compare favorably with those of other higher order FDTD methods. Recently an unconditionally stable implicit path integral time-domain method for the electromagnetic field was introduced [50]. In a subsequent explicit version, referred to here as EP (explicit propagator), it was shown that a homogeneous transmission line is not subject to numerical dispersion [51].

Chapeter II presents an extension to the analysis in [51, 52] by including transmission line conductor loss. It is started in the following chapter with a derivation of the exact time domain matrix propagator that is the kernel for the fixed time increment path integral for the coupled dissipative Telegrapher's equations. It is shown

that the propagator equations can be converted into a numerical expression with accuracy $\mathcal{O}(h^5)$, where h is the increment between numerical grid points, and subsequently into a general numerical technique for analyzing an inhomogeneous transmission line or quasi-TEM waveguide. Results are presented in which the reflection coefficient (S_{11}) computed by the EP method described here is compared with the exact analytical reflection coefficient available in cases where the loss is uniform and for a linear and an exponentially tapered inhomogeneous transmission line. As a practical example it is analyzed an inhomogeneous lossy microstrip line. The numerical dispersion produced by the EP method is compared with that of the standard, second order accurate, FDTD method.

As an extension of the analytical and numerical methods described above, chapter III present a time domain analytic solution methods for lossless multiconductor lines. In sub-section, mathematical models were developed for TEM and quasi-TEM lines. For TEM lines the EP method is applied in a straightforward manner and modified, based upon the N-mode conditions [53,54], to handle the more common quasi-TEM lines. The accuracy of this technique is demonstrated by several examples. Uniform and nonuniform, coupled dual and triple TEM and quasi-TEM lines were analyzed. Transient response results obtained with the EP method described here are compared with those of a popular commercial simulator.

Chapter IV presents the complete Green's function for Maxwell's equations, including the source region, in a general form, which will allow solutions for given initial sources, application to Huygens sources, or propagation of a field initially known

throughout the volume of space. The general Green's function expression is then solved to obtain the Maxwell equation Green's functions for each of the three spatial dimensions. Examples are presented for a propagating plane wave and a radiating point source. The time convention used in chapter IV is $\exp(j\omega t)$.

Chapter V concludes this dissertation with a summary and discussion of the research accomplishments and recommendations for further studies.

CHAPTER II

TIME DOMAIN ANALYSIS OF LOSSY TRANSMISSION LINE

A solution to the coupled telegrapher's equations for the voltage and current on a lossy transmission line is presented. The resulting expression is obtained in the form of an exact time domain propagator operating on the line voltage and current. An application of Simpson's rule on an integral appearing in the propagator yields a simple numerical representation of the propagator that is accurate on the order of h^5, where h is the numerical increment between grid points. A numerical dispersion relation is derived proving that this method has no numerical dispersion. Examples are presented showing that exceptionally accurate results are obtained for both lossy and general nonuniform lossy transmission lines. The method is also applicable to many types of practical waveguide structures including the inhomogeneous microstrip line for which results are also presented in this chapter.

2.1. Telegrapher's equations for lossy transmission line

The transmission line equations in the time domain with distributed inductance L, distributed capacitance C, voltage V, and current I and including the distributed line impedance R and conductance G are,

$$C\frac{\partial V}{\partial t} = -GV - \frac{\partial I}{\partial z} \tag{1}$$

$$L\frac{\partial I}{\partial t} = -RI - \frac{\partial V}{\partial z} \tag{2}$$

where the transmission line lies along the *z*-axis. A useful form for this set of equations is obtained by isolating the time derivative on the left hand side thereby creating the vector-matrix equation

$$\frac{\partial}{\partial t}\begin{bmatrix} V \\ I \end{bmatrix} = -\begin{bmatrix} \frac{G}{C} & \frac{1}{C}\frac{\partial}{\partial z} \\ \frac{1}{L}\frac{\partial}{\partial z} & \frac{R}{L} \end{bmatrix}\begin{bmatrix} V \\ I \end{bmatrix} \tag{3}$$

Eqn. (3) can be conveniently expressed as a single equation

$$\frac{\partial \mathbf{F}}{\partial t} = \bar{\mathbf{S}}\mathbf{F} \tag{4}$$

where the voltage-current vector $\mathbf{F}$ and operator matrix $\bar{\mathbf{S}}$ are defined by

$$\mathbf{F} = \begin{bmatrix} V & I \end{bmatrix}^T \tag{5}$$

$$\bar{\mathbf{S}} = -\begin{bmatrix} \frac{G}{C} & \frac{1}{C}\frac{\partial}{\partial z} \\ \frac{1}{L}\frac{\partial}{\partial z} & \frac{R}{L} \end{bmatrix} \tag{6}$$

2.2. The propagator

A solution to (4) can be obtained by first finding the propagator matrix $\bar{\mathbf{K}}(z,t)$ that satisfies [42]

$$\frac{\partial \bar{\mathbf{K}}(z,t)}{\partial t} = \bar{\mathbf{S}}\bar{\mathbf{K}}(z,t) \tag{7}$$

with initial condition

$$\lim_{t\to 0}\bar{\mathbf{K}}(z,t)=\bar{\mathbf{I}}\delta(z-z') \tag{8}$$

where δ is the Dirac delta function, z' is the initial position of the voltage and current at time $t=0$, and $\bar{\mathbf{I}}$ is the identity matrix. A solution to (7), subject to (8), is

$$\bar{\mathbf{K}}=e^{\bar{\mathbf{S}}t}\delta(z-z') \tag{9}$$

Eqn. (9) can be expressed as a spectral integral by expanding the exponential in a power series and by replacing the delta function by its Fourier integral representation as follows,

$$\bar{\mathbf{K}}=\left(\mathbf{1}+\bar{\mathbf{S}}t+\bar{\mathbf{S}}^2t^2/2!+\cdots\right)\frac{1}{2\pi}\int_{-\infty}^{\infty}e^{jk_z(z-z')}dk_z \tag{10}$$

After the term by term operations in (10) are carried out, the series is returned to exponential form producing

$$\bar{\mathbf{K}}=\frac{1}{2\pi}\int_{-\infty}^{\infty}e^{\bar{\mathbf{S}}_f t}\exp\left[jk_z(z-z')\right]dk_z \tag{11}$$

$$\bar{\mathbf{S}}_f=-\begin{bmatrix}\frac{G}{C} & \frac{jk_z}{C}\\ \frac{jk_z}{L} & \frac{R}{L}\end{bmatrix} \tag{12}$$

The exponential $e^{\bar{\mathbf{S}}_f t}$ can be converted to a standard 2×2 transition matrix $\bar{\mathbf{A}}$ via the modal matrix method [55]. First the eigenvalues $\lambda_{1,2}$ of $\bar{\mathbf{S}}_f$ are found by extracting the roots of $\det\left[\lambda\bar{\mathbf{I}}-\bar{\mathbf{S}}_f\right]=0$, which in this case is

$$\det\begin{bmatrix} \lambda + \dfrac{G}{C} & \dfrac{jk_z}{C} \\ \dfrac{jk_z}{L} & \lambda + \dfrac{R}{L} \end{bmatrix} = 0 \tag{13}$$

giving

$$\lambda_{1,2} = -\frac{G}{2C}\left(1 \pm \sqrt{1-\chi^2}\right) - \frac{R}{2L}\left(1 \mp \sqrt{1-\chi^2}\right) \tag{14}$$

$$\chi = (v_p k_z)/(G/2C - R/2L)$$

Next an eigenvector is constructed by selecting one column of $adj\left[\lambda_1 \bar{\mathbf{I}} - \bar{\mathbf{S}}_f\right]$ and one column of $adj\left[\lambda_2 \bar{\mathbf{I}} - \bar{\mathbf{S}}_f\right]$. These are

the respective first and second columns of the modal matrix

$$\bar{\mathbf{M}} = \begin{bmatrix} -Z_0 & -Z_0 \\ \dfrac{1-\sqrt{1-\chi^2}}{j\chi} & \dfrac{1+\sqrt{1-\chi^2}}{j\chi} \end{bmatrix} \tag{15}$$

Even though this is a lossy transmission line, in the above equations it has been convenient to define the terms $\sqrt{L/C} \doteq Z_0$ and $v_p = 1/\sqrt{LC}$, which are respectively the characteristic impedance and phase velocity of a lossless transmission line. The modal matrix and its inverse along with a diagonalized exponential eigenvalue matrix are combined to form the matrix product

$$\bar{\mathbf{A}} = e^{\bar{\mathbf{S}}t} = \bar{\mathbf{M}} \begin{bmatrix} e^{\lambda_1 t} & 0 \\ 0 & e^{\lambda_2 t} \end{bmatrix} \bar{\mathbf{M}}^{-1} \tag{16}$$

The matrix multiplications in (16) produce a transition matrix $\bar{\mathbf{A}}$ with the

following elements

$$A_{11} = e^{-at}\left\{ -\frac{b}{v_p}\frac{\sin\left[tv_p\sqrt{k_z^2 - k_l^{\,2}}\right]}{\sqrt{k_z^2 - k_l^{\,2}}} + \cos\left[tv_p\sqrt{k_z^2 - k_l^{\,2}}\right]\right\}$$

$$A_{12} = -jk_z Z_0 e^{-at}\left\{ \frac{\sin\left[tv_p\sqrt{k_z^2 - k_l^{\,2}}\right]}{\sqrt{k_z^2 - k_l^{\,2}}}\right\}$$

$$A_{21} = {A_{12}}\big/{Z_0^2}$$

$$A_{22} = e^{-at}\left\{ \frac{b}{v_p}\frac{\sin\left[tv_p\sqrt{k_z^2 - k_l^2}\right]}{\sqrt{k_z^2 - k_l^2}} + \cos\left[tv_p\sqrt{k_z^2 - k_l^2}\right]\right\} \tag{17}$$

where $k_l = \left({G}\big/{2Cv_p} - {R}\big/{2Lv_p}\right)$ and $a = \frac{1}{2}\left(\frac{G}{C} + \frac{R}{L}\right)$, $b = \frac{1}{2}\left(\frac{G}{C} - \frac{R}{L}\right)$

The propagator equation expressed in terms of the matrix $\bar{\mathbf{A}}$ now becomes

$$\bar{\mathbf{K}} = \frac{1}{2\pi}\int_{-\infty}^{\infty}\begin{bmatrix} A_{11} & A_{12} \\ A_{21} & A_{22}\end{bmatrix}\exp\left[jk_z\bar{z}\right]dk_z \tag{18}$$

with $\bar{z} \doteq z - z'$. Each of the integrals in (18) can be evaluated analytically (see APPENDIX A for details). The resulting propagator is

$$\bar{\mathbf{K}} = \begin{bmatrix} K_{11} & K_{12} \\ K_{21} & K_{22}\end{bmatrix} \tag{19}$$

$$K_{11} = \frac{e^{-at}}{2}\left\{ \delta\left(\bar{z} + tv_p\right) + \delta\left(\bar{z} - tv_p\right)\right.$$

$$-\frac{b}{v_p}J_0\left[\frac{b}{v_p}\sqrt{(\bar{z})^2-(tv_p)^2}\right]+bt\frac{J_1\left[\frac{b}{v_p}\sqrt{(\bar{z})^2-(tv_p)^2}\right]}{\sqrt{(\bar{z})^2-(tv_p)^2}}\Bigg\}$$

$$K_{12}=-Z_0\frac{e^{-at}}{2}\left\{\delta(\bar{z}+tv_p)-\delta(\bar{z}-tv_p)-\bar{z}\frac{b}{v_p}\frac{J_1\left[\frac{b}{v_p}\sqrt{(\bar{z})^2-(tv_p)^2}\right]}{\sqrt{(\bar{z})^2-(tv_p)^2}}\right\}$$

$$K_{21}=K_{12}\Big/Z_0^2$$

$$K_{22}=\frac{e^{-at}}{2}\Bigg\{\ \delta(\bar{z}+tv_p)+\delta(\bar{z}-tv_p)$$

$$+\frac{b}{v_p}J_0\left[\frac{b}{v_p}\sqrt{(\bar{z})^2-(tv_p)^2}\right]+bt\frac{J_1\left[\frac{b}{v_p}\sqrt{(\bar{z})^2-(tv_p)^2}\right]}{\sqrt{(\bar{z})^2-(tv_p)^2}}\Bigg\} \quad (20)$$

In order to ensure causality, the Bessel functions J_0 and J_1 of the first kind and of the zero and first order respectively are restricted by the requirement $|\bar{z}|\le tv_p$.

2.3. Explicit solution form

The purpose of the propagator is to evolve an initial previous time voltage and current distribution (V(z), I(z)) into the present time voltage and current (V(z,t), I(z,t)) , over a fixed time interval t. Mathematically this operation is a spatial convolution of the

propagator with the initial voltage and current [42], as expressed by

$$\begin{bmatrix} V(z,t) \\ I(z,t) \end{bmatrix} = \int_{-\infty}^{\infty} \bar{\mathbf{K}} \cdot \begin{bmatrix} V(z') \\ I(z') \end{bmatrix} dz' \tag{21}$$

Inserting Eqns. (20) into (21) yields the fixed time increment explicit path integral solution,

$$V(z,t) = \frac{e^{-at}}{2} \left\{ \begin{array}{l} V(z+tv_p) + V(z-tv_p) - Z_0 \left[I(z+tv_p) - I(z-tv_p) \right] \\ \quad + bt \int_{z-tv_p}^{z+tv_p} \dfrac{J_1\left[\dfrac{b}{v_p} \sqrt{(\bar{z})^2 - (tv_p)^2} \right]}{\sqrt{(\bar{z})^2 - (tv_p)^2}} V(z')dz' \\ \quad - \dfrac{b}{v_p} \int_{z-tv_p}^{z+tv_p} J_0\left[\dfrac{b}{v_p} \sqrt{(\bar{z})^2 - (tv_p)^2} \right] V(z')dz' \\ \quad + Z_0 \dfrac{b}{v_p} \int_{z-tv_p}^{z+tv_p} \bar{z} \dfrac{J_1\left[\dfrac{b}{v_p} \sqrt{(\bar{z})^2 - (tv_p)^2} \right]}{\sqrt{(\bar{z})^2 - (tv_p)^2}} I(z')dz' \end{array} \right\} \tag{22}$$

$$I(z,t) = \frac{e^{-at}}{2} \left\{ \begin{array}{l} I(z+tv_p) + I(z-tv_p) - \dfrac{1}{Z_0} \left[V(z+tv_p) - V(z-tv_p) \right] \\ \quad + bt \int_{z-tv_p}^{z+tv_p} \dfrac{J_1\left[\dfrac{b}{v_p} \sqrt{(\bar{z})^2 - (tv_p)^2} \right]}{\sqrt{(\bar{z})^2 - (tv_p)^2}} I(z')dz' \\ \quad + \dfrac{b}{v_p} \int_{z-tv_p}^{z+tv_p} J_0\left[\dfrac{b}{v_p} \sqrt{(\bar{z})^2 - (tv_p)^2} \right] I(z')dz' \\ \quad + \dfrac{1}{Z_0} \dfrac{b}{v_p} \int_{z-tv_p}^{z+tv_p} \bar{z} \dfrac{J_1\left[\dfrac{b}{v_p} \sqrt{(\bar{z})^2 - (tv_p)^2} \right]}{\sqrt{(\bar{z})^2 - (tv_p)^2}} V(z')dz' \end{array} \right\} \tag{23}$$

for the transmission line equations.

An expression convenient for numerical calculation is obtained by evaluating the integrals in (22) and (23) by a 3-point integration rule with the interval tv_p between numerical points. An application of the properties of Bessel functions as described in APPENDIX B yields the final set of equations,

$$V(z,t) \simeq \frac{e^{-at}}{2}\left\{\left[1-\frac{(bt)}{3}+\frac{(bt)^2}{6}\right]\left[V(z+tv_p)+V(z-tv_p)\right]\right.$$
$$-Z_0\left[1+\frac{(bt)^2}{6}\right]\left[I(z+tv_p)-I(z-tv_p)\right] \qquad (24)$$
$$\left.+\frac{4(bt)}{3}\left[I_1(bt)-I_0(bt)\right]V(z)\right\}$$

$$I(z,t) \simeq \frac{e^{-at}}{2}\left\{\left[1+\frac{(bt)}{3}+\frac{(bt)^2}{6}\right]\left[I(z+tv_p)+I(z-tv_p)\right]\right.$$
$$-\frac{1}{Z_0}\left[1+\frac{(bt)^2}{6}\right]\left[V(z+tv_p)-V(z-tv_p)\right] \qquad (25)$$
$$\left.+\frac{4(bt)}{3}\left[I_1(bt)+I_0(bt)\right]I(z)\right\}$$

where I_o and I_1 are *0* and 1st order modified Bessel functions of the first kind.

Notice that the present time voltage, or the present time current, is found by taking simple sum and difference combinations of the previous time voltage and current amplitudes. Therefore, given only the total voltage and current distribution on the lossy transmission line at any point in time, (24) and (25) will automatically filter out the

positive and negative traveling waves and, through successive time steps, provide the complete succeeding time response of the transmission line.

If $R, G \to 0$, then $a, b \to 0$ and (24) and (25) reduce to the lossless transmission line equations [51],

$$V(z,t) = \frac{1}{2}\left\{\left[V(z+tv_p) + V(z-tv_p)\right] - Z_0\left[I(z+tv_p) - I(z-tv_p)\right]\right\} \qquad (26)$$

$$I(z,t) = \frac{1}{2}\left\{\left[I(z+tv_p) + I(z-tv_p)\right] - \frac{1}{Z_0}\left[V(z+tv_p) - V(z-tv_p)\right]\right\} \qquad (27)$$

Similarly for a distortionless (LG=RC) transmission line $b = \frac{1}{2}\left(\frac{G}{C} - \frac{R}{L}\right) = 0$ and (24) and (25) reduce to the lossless case Eqns. (26) and (27), but with a multiplying factor e^{-at}.

In the following section, examples are given that demonstrate the accuracy of the above formulas as well as their low level of numerical dispersion. It will also be shown that these equations can be used to analyze the lossy inhomogeneous line.

2.4. Discrete implementation

In deriving the equations in the above section it was assumed that successive calculations of the voltage and current took place at the times 0 and *t*. For the numerical method, where the current and voltage are calculated at many successive instances in time, it is more convenient to set this time interval between successive calculations to a constant $\tau = t - t'$, where t is the time at which the calculation is being made and t' is

the time of the immediately previous calculation of voltage and current on the line. This change is implemented by making the replacement $t \to \tau$ in the above equations. Also, on a homogeneous transmission line the velocity v is constant so the product of the time increment and the velocity defines the numerical spatial increment $\tau v_p \doteq \Delta z$. These substitutions in (24) and (25), give a set of equations that are convenient for numerical calculation,

$$\begin{aligned} V(z,t) = \frac{e^{-a\tau}}{2}\Bigg\{ & \left[1 - \frac{(b\tau)}{3} + \frac{(b\tau)^2}{6}\right]\left[V(z+\Delta z) + V(z-\Delta z)\right] \\ & -Z_0\left[1 + \frac{(b\tau)^2}{6}\right]\left[I(z+\Delta z) - I(z-\Delta z)\right] \\ & + \frac{4(b\tau)}{3}\left[I_1(b\tau) - I_0(b\tau)\right]V(z)\Bigg\} \end{aligned} \tag{28}$$

$$\begin{aligned} I(z,t) = \frac{e^{-a\tau}}{2}\Bigg\{ & \left[1 + \frac{(b\tau)}{3} + \frac{(b\tau)^2}{6}\right]\left[I(z+\Delta z) + I(z-\Delta z)\right] \\ & -\frac{1}{Z_0}\left[1 + \frac{(b\tau)^2}{6}\right]\left[V(z+\Delta z) - V(z-\Delta z)\right] \\ & + \frac{4(b\tau)}{3}\left[I_1(b\tau) + I_0(b\tau)\right]I(z)\Bigg\} \end{aligned} \tag{29}$$

In (28) and (29), the characteristic impedance Z_0 is evaluated at the point z, while the contributions from the previous time voltage and current are taken from the points z and $z \pm \Delta z$.

2.5. Three uniform T.L.

Fig. 1(a) shows three uniform concatenated transmission line sections each of which can have any set of parameters. For the results presented in Fig. 1(b) and 1(c), the distributed inductance and capacitance are L=0.166 μH/m and C=66.67 pF/m in all three sections and only the center section is lossy. The conductance *G* is set to zero in each section, resulting in $a = \frac{R}{2L}$, $b = -\frac{R}{2L}$ with a characteristic impedance $Z_{02} = \sqrt{\frac{R_2 + j\omega L}{j\omega C}}$ in the center section and $Z_{01} = Z_{03} = Z_0 = \sqrt{L/C}$ in the two end sections. Figs. 1(b)-(c) show the S-parameter $S_{11} = \Gamma$ obtained by discrete Fourier transformation (DFT) of the time domain reflected wave on the first transmission line section calculated using a Gaussian pulse excitation in the propagator formulas (28) and (29). A comparison is made with the exact result obtained by evaluating the exact frequency domain expression [56]

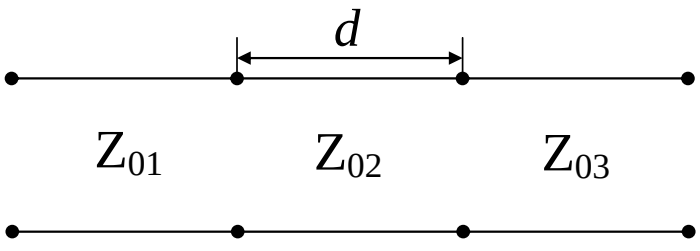

(a)

Fig. 1 (a) Three concatenated transmission lines sections. Each section has the same set of distributed parameters L, G, and C, but R is zero on the two outside sections and non-zero on the center section. S_{11} versus frequency comparison between exact results and numerical calculations based on the EP method with (b) a low-loss and (c) a high-loss center section.

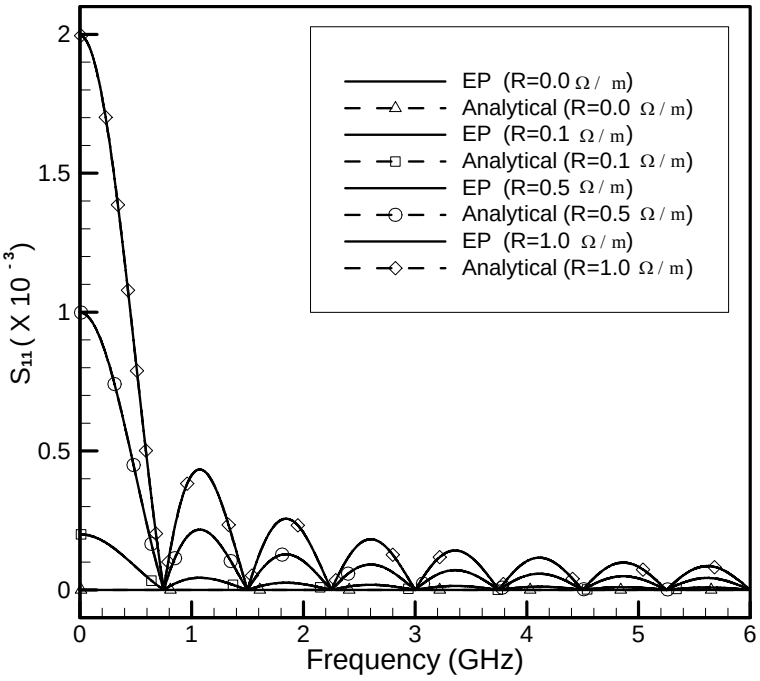

(b)

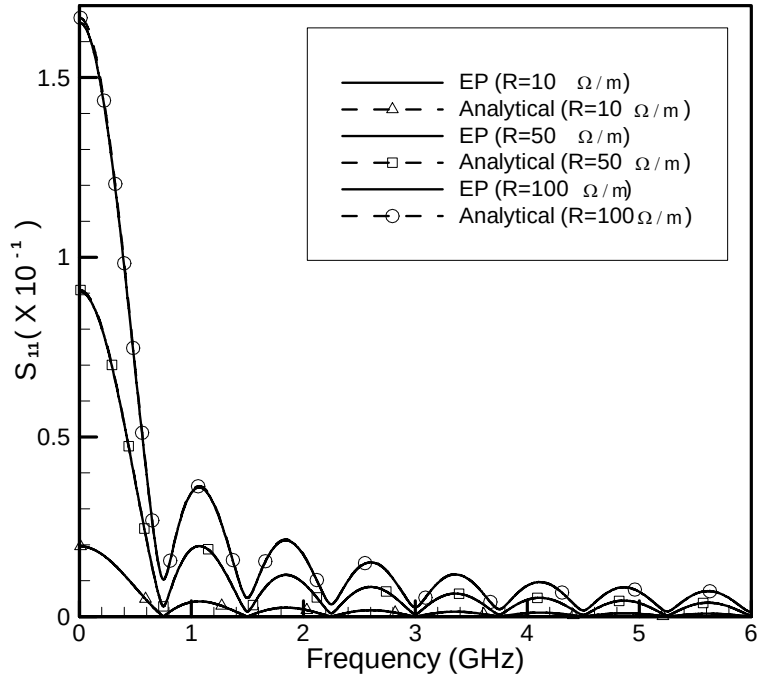

(c)

Fig. 1 Continued.

$$\Gamma = \frac{\Gamma_{12} + \Gamma_{21} e^{2\gamma d}}{1 + \Gamma_{12}\Gamma_{21} e^{2\gamma d}} \tag{30}$$

where $\Gamma_{12} = \dfrac{Z_{02} - Z_{01}}{Z_{02} + Z_{01}}$, $\Gamma_{12} = -\Gamma_{21}$, $\gamma = \sqrt{(R_2 + j\omega L)\, j\omega C}$.

A range of results representative of low loss, R_2 =0.1, 0.5, 1 Ω/m and high loss, R_2 =10, 50, 100 Ω/m, distributed resistances are shown in Figs. 1(b) and 1(c). The lossy line section has a length $d = 0.2m$. In order to apply the EP equations (28) and (29), the center transmission line section is subdivided into 20 cells each of width $\Delta z = 0.01m$. The EP and exact results show excellent agreement over the frequency range $0 - 6GHz$. Greater accuracy or bandwidth can be achieved by using more and smaller segments.

2.6. Linear taper T.L.

In Fig 2(a) the center section is a linearly tapered lossless transmission line. The linear taper is determined by

$$Z_{02}(z) = Z_{01}(1 + qz), \qquad 0 \le z \le d \tag{31}$$

where $Z_{01} = 25\Omega$, $Z_{03} = 275\Omega$, $d = 0.1m$, and $q = 100m^{-1}$.

Consistent with (31) the inductance and capacitance of the center transmission line section are $L_2 = L_1(1 + qz)$ and $C_2 = C_1/(1 + qz)$ where $L_1 = 83.33nH/m$, $C_1 = 0.133nF/m$. The S-parameter S_{11} is compared with the analytical solution [16, 57],

$$S_{11} = \Gamma = \frac{Z_{in} - Z_{01}}{Z_{in} + Z_{01}} \tag{32}$$

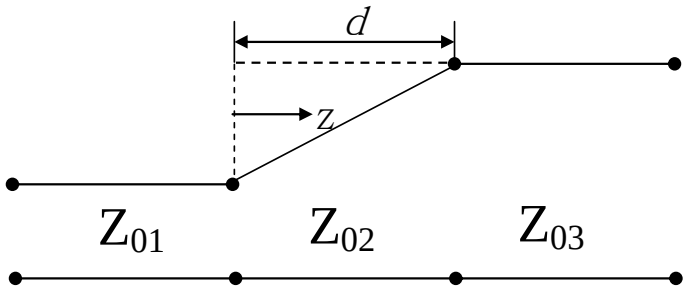

(a)

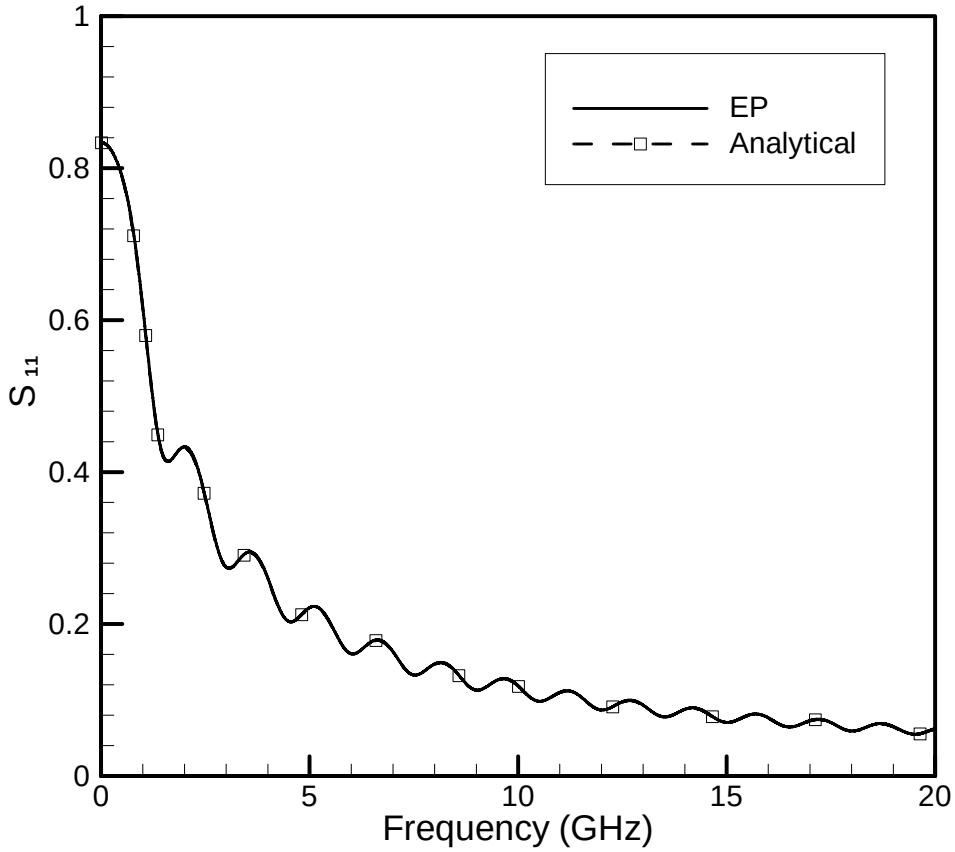

(b)

Fig. 2. (a) Lossless transmission line with a linear taper and (b) S_{11} versus frequency comparison between exact results with numerical calculations based on the EP method.

where $$Z_{in} = \frac{AZ_{02} + B}{CZ_{02} + D} \tag{33}$$

$$A = \frac{\pi\beta_o}{2q}\left[J_1(u_1)Y_0(u_2) - J_0(u_2)Y_1(u_1)\right]$$

$$B = -j\frac{\pi\beta_o}{2q}Z_{01}\left(1+qd\right)\left[J_1(u_2)Y_1(u_1) - J_1(u_1)Y_1(u_2)\right]$$

$$C = j\frac{\pi\beta_o}{2qZ_{01}}\left[J_0(u_1)Y_0(u_2) - J_0(u_2)Y_0(u_1)\right]$$

$$D = -\frac{\pi\beta_o}{2q}\left(1+qd\right)\left[J_0(u_1)Y_1(u_2) - J_1(u_2)Y_0(u_1)\right] \tag{34}$$

with $\beta_o = \omega/v_p$, $u_1 = \beta_o/q$, $u_2 = \left(1+qd\right)u_1$,

$J_n(x)$ is the Bessel function of the first kind of order n , $Y_n(x)$ is the Bessel function of the second kind of order n and ω is the radian frequency. The phase velocity, determined by $v_p = 1/\sqrt{L_2C_2}$, is the same in all three transmission line sections. Fig 2(b) shows the exact result given above compared with that obtained by the EP method. As shown in 2(b), excellent agreement with the exact result is observed when the EP method results were calculated with the linear transmission line section subdivided into 80 cells. As before, more cells on the same length of line will give agreement over a wider frequency range.

2.7. Exponential taper T.L.

A lossy transmission line that is also nonuniform due to an exponential taper in

the distributed parameters in the center section is pictured in Fig 3(a).

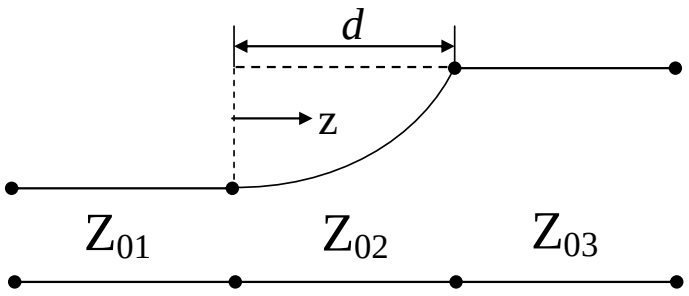

(a)

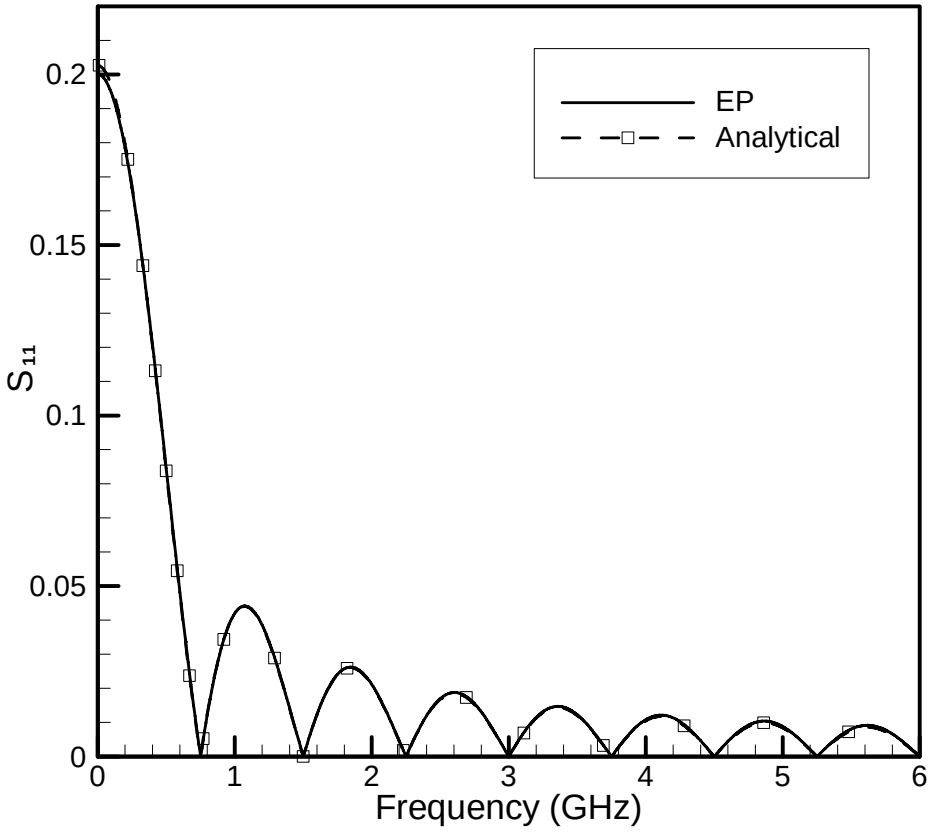

(b)

Fig. 3. (a) Exponential tapered lossy transmission line with (b) S_{11} versus frequency comparison between exact results and EP method numerical calculations.

As before the conductance of all three transmission line sections is zero. In the center section $R_2 = R_1 \exp\left[(z/d)\ln(R_3/R_1)\right]$, $L_2 = L_1 \exp\left[(z/d)\ln(L_3/L_1)\right]$ and $C_2 = C_1 \exp\left[(z/d)\ln(C_3/C_1)\right]$ with $L_1 = 0.166\mu H/m$, $L_3 = 0.25\mu H/m$, $C_1 = 66.66\text{pF}/m$, $C_3 = 44.44\text{pF}/m$, $R_1 = 0.1\Omega/m$ and $R_3 = 0.5\Omega/m$. The length of the tapered section is 0.20 m.

This exponentially tapered line has an analytical solution for the reflection coefficient [18]

$$\Gamma = S_{11} = \frac{1}{4}\frac{1-e^{-2\gamma d}}{\gamma d}\ln\left(\frac{Z_{03}}{Z_{01}}\right) \tag{35}$$

where $\gamma = \sqrt{(R_2 + j\omega L_2)(j\omega C_2)}$. The characteristic impedance of each section is again determined by $Z_{0n} = \sqrt{(R_n + j\omega L_n)/(j\omega C_n)}$ where $n = 1, 2, 3$. For the EP results shown in Fig. 3(b) the center transmission line section is discretized into 50 cells of width 0.004 m. Fig. 3(b) shows a comparison between the EP method, Eqn. (28) and (29), and analytical solution, Eqn. (35). There is excellent agreement up to 6 GHz, but as before agreement over a wider frequency band can be achieved by subdividing the nonuniform center section into more cells.

2.8. Numerical dispersion

A numerical dispersion relation for the EP method can be obtained by first placing Eqns. (26) and (27) in the indexed form,

$$V_i^n = \frac{1}{2}\left[V_{i+1}^{n-1} + V_{i-1}^{n-1}\right] - \frac{Z_0}{2}\left[I_{i+1}^{n-1} - I_{i-1}^{n-1}\right] \tag{36}$$

$$I_i^n = \frac{1}{2}\left[I_{i+1}^{n-1} + I_{i-1}^{n-1}\right] - \frac{1}{2Z_0}\left[V_{i+1}^{n-1} - V_{i-1}^{n-1}\right] \tag{37}$$

Here n represents the time step and i the spatial step. Voltage and current waves propagating through the numerical lattice can be expressed as

$$V_i^n = V_0 e^{j(\omega n\tau - \tilde{k}i\tau v_p)} \tag{38}$$

$$I_i^n = I_0 e^{j(\omega n\tau - \tilde{k}i\tau v_p)} \tag{39}$$

where $\tilde{k}$ is numerical propagation constant. Substituting these expressions into (36) and (37) gives

$$V_0 e^{j\omega\tau} = V_0 \cos(\tilde{k}\tau v_p) + jZ_0 I_0 \sin(\tilde{k}\tau v_p) \tag{40}$$

$$I_0 e^{j\omega\tau} = I_0 \cos(\tilde{k}\tau v_p) + j\frac{Z_0}{V_0}\sin(\tilde{k}\tau v_p) \tag{41}$$

Next, substituting (41) into (40) results in a numerical propagation constant

$$\tilde{k} = \frac{\omega\tau}{v_p\tau} \tag{42}$$

If $v_p\tau$ is equated to Δz then $v_p = c$ the velocity of a wave in a homogeneous medium. However, this definition is not always convenient when the numerical region contains a variety a dielectric materials or expedient when attempting to maintain numerical stability.

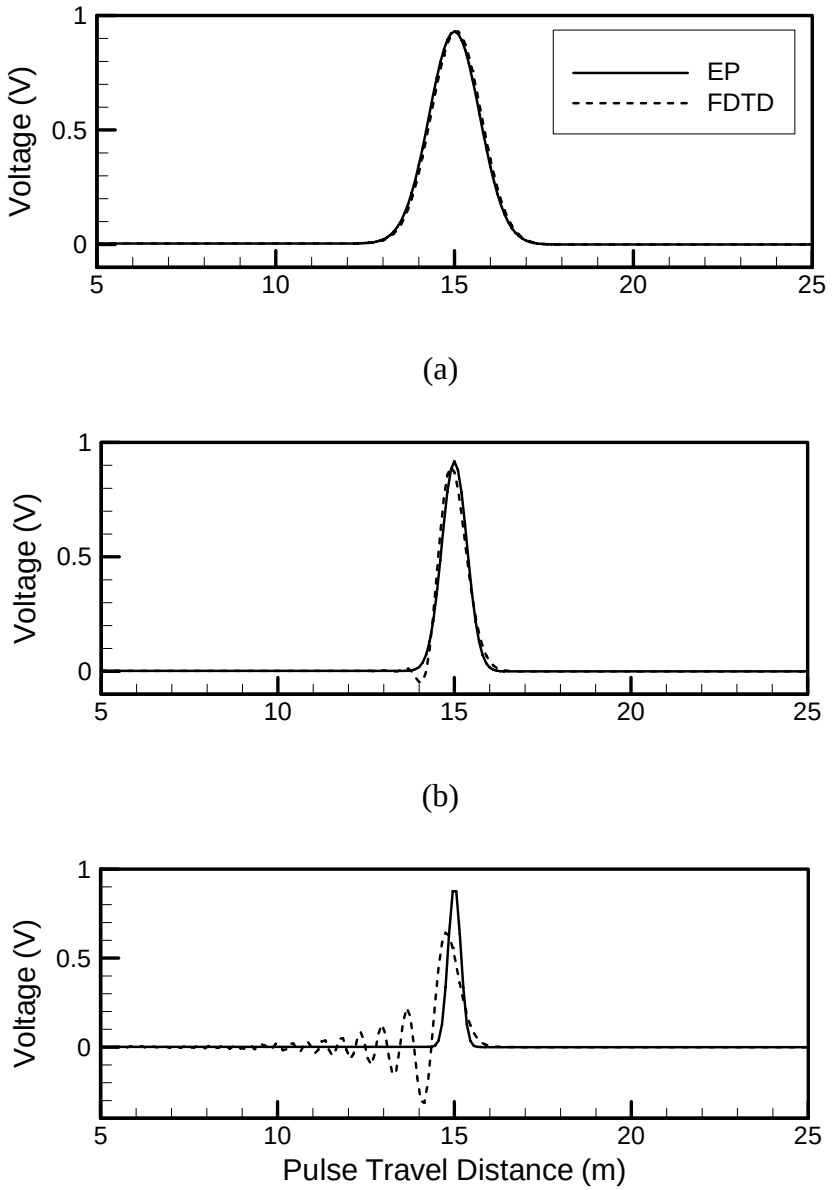

(a)

(b)

(c)

Fig 4. A Gaussian pulse propagated 15m, comparison between FDTD and EP methods. (a) $s=1$ (b) $s=0.5$, and (c) $s=0.25$

For these reasons it can be set,

$$v_p \tau = \frac{\Delta z}{s} \tag{43}$$

where in principle s can be any number. Substituting (43) into (42) gives the numerical dispersion relation

$$\tilde{k} = s\frac{\omega}{c} = sk \tag{44}$$

This result says that the numerical space propagation constant is directly proportional to the physical space propagation constant. Similarly, from (43) the numerical space phase velocity v_p is proportional to the physical space phase velocity according to

$$v_p = \frac{1}{s}c \tag{45}$$

Fig. 4 shows a Gaussian pulse that has propagated approximately 15m in a transmission line modeled with EP and 2nd order FDTD method lattices. Here $L = 0.167\,\mu H/m$, $C = 66.67\,pF/m$, $R = 0.5\Omega/m$, and $G = 0$. The incident Gaussian pulse is formed by

$$\mathrm{V_s}(\mathrm{t}) = \exp\left(-\left(\mathrm{t} - 5\kappa\right)^2 \Big/ \kappa^2\right) \tag{46}$$

where t is the time step and $\kappa = 10$. The numerical space grid size is $L = 0.167\,\mu H/m$ $\Delta z = 0.1m$ and three different time steps ($s = 1, s = 0.5$, and $s = 0.25$) are used. The pulse does not reach the numerical boundary in any of these examples.

The results in Fig. 4(a) show that neither method is subject to numerical dispersion when $s = 1$, the magic time step. However, as seen in Fig 4(b) and 4(c), significant numerical dispersion is observed with the FDTD method, while there is little or no dispersion in the EP method. This is consistent with dispersion relation derived above in

(44) which shows that for the homogeneous lossless case the EP method produces a numerical expression that has no dispersion, faithfully propagating all frequencies up to the Nyquist limit, two numerical points per wavelength.

With both the FDTD and EP methods the voltage and current at each spatial grid point are found by using the previous time field at that point along with the two adjacent grid points. It is clear from Fig. 4 that the FDTD results can be improved by using higher order methods, which typically require more spatial and/or time points. However, the excellent results obtained here and in simulations we have carried out over much greater distances and time periods indicate that a higher order EP method is not needed.

2.9. Compatibility between EP and FDTD in magic time step

Voltage and current for the EP method are introduced in the indexed form,

$$V\Big|_i^n = \frac{1}{2}\left[V\Big|_{i+1}^{n-1} + V\Big|_{i-1}^{n-1} \right] - \frac{Z_0}{2}\left[I\Big|_{i+1}^{n-1} - I\Big|_{i-1}^{n-1} \right] \tag{47}$$

$$I\Big|_i^n = \frac{1}{2}\left[I\Big|_{i+1}^{n-1} + I\Big|_{i-1}^{n-1} \right] - \frac{1}{2Z_0}\left[V\Big|_{i+1}^{n-1} - V\Big|_{i-1}^{n-1} \right] \tag{48}$$

Here n represents the time step and i the spatial step. The voltages and currents along the transmission lines can be written as

$$V\Big|_i^n = V^+\Big|_i^n + V^-\Big|_i^n \text{ and } I\Big|_i^n = I^+\Big|_i^n + I^-\Big|_i^n \tag{49}$$

$$Z_0 = \frac{V^+}{I^+} = -\frac{V^-}{I^-} \tag{50}$$

Applying (49) to (47) , it can be expressed

$$V\Big|_i^n = \frac{1}{2}\left(V^+\Big|_{i+1}^{n-1} + V^-\Big|_{i+1}^{n-1} + V^+\Big|_{i-1}^{n-1} + V^-\Big|_{i-1}^{n-1} \right) - \frac{Z_0}{2}\left(I^+\Big|_{i+1}^{n-1} + I^-\Big|_{i+1}^{n-1} - I^+\Big|_{i-1}^{n-1} - I^-\Big|_{i-1}^{n-1} \right) \tag{51}$$

Using (50), it becomes

$$\begin{aligned} V\Big|_i^n &= \frac{1}{2}\left(V^+\Big|_{i+1}^{n-1} + V^-\Big|_{i+1}^{n-1} + V^+\Big|_{i-1}^{n-1} + V^-\Big|_{i-1}^{n-1} \right) \\ &\quad - \frac{1}{2}\left(V^+\Big|_{i+1}^{n-1} - V^-\Big|_{i+1}^{n-1} - V^+\Big|_{i-1}^{n-1} + V^-\Big|_{i-1}^{n-1} \right) \\ &= V^-\Big|_{i+1}^{n-1} + V^+\Big|_{i-1}^{n-1} \end{aligned} \tag{52}$$

The current can be found from (48), (49), and (50) in the same way.

$$I\Big|_i^n = I^-\Big|_{i+1}^{n-1} + I^+\Big|_{i-1}^{n-1} \tag{53}$$

Eqn. (53) can be shown in time-spatial numerical grid with Fig. 5.

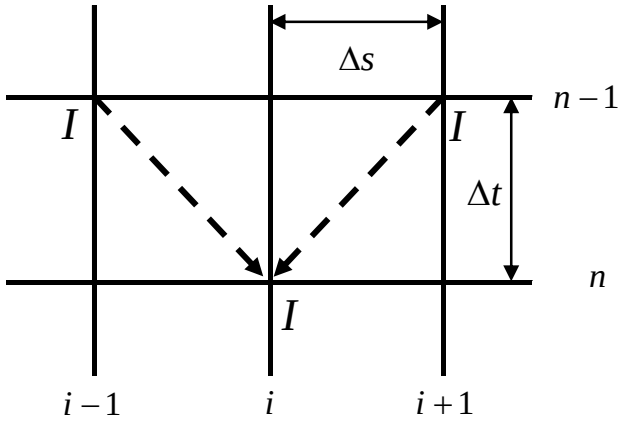

Fig. 5 Current $\left(I\Big|_i^n\right)$ expression in time-spatial numerical grid.

Zero components $V^+\big|_i^{n-1} - V^+\big|_i^{n-1} = 0$ and $V^-\big|_i^{n-1} - V^-\big|_i^{n-1} = 0$ are added in (52).

$$V\big|_i^n = V^-\big|_{i+1}^{n-1} + V^+\big|_{i-1}^{n-1} + \underbrace{V^+\big|_i^{n-1} - V^+\big|_i^{n-1}}_{=0} + \underbrace{V^-\big|_i^{n-1} - V^-\big|_i^{n-1}}_{=0} \quad (54)$$

We can rearrange (54) and apply (50)

$$\begin{aligned} V\big|_i^n &= V^-\big|_i^{n-1} + V^+\big|_i^{n-1} + V^-\big|_{i+1}^{n-1} - V^+\big|_i^{n-1} - V^-\big|_i^{n-1} + V^+\big|_{i-1}^{n-1} \\ &= V^-\big|_i^{n-1} + V^+\big|_i^{n-1} - Z_0\, I^-\big|_{i+1}^{n-1} - Z_0\, I^+\big|_i^{n-1} + Z_0\, I^-\big|_i^{n-1} + Z_0\, I^+\big|_{i-1}^{n-1} \quad (55) \\ &= \underbrace{V^-\big|_i^{n-1} + V^+\big|_i^{n-1}}_{=V_1} - Z_0 \Big[\underbrace{I^-\big|_{i+1}^{n-1} + I^+\big|_i^{n-1}}_{=I_1} - \Big(\underbrace{I^-\big|_i^{n-1} + I^+\big|_{i-1}^{n-1}}_{=I_2} \Big) \Big] \end{aligned}$$

V_1 is represented to single voltage expression using (52).

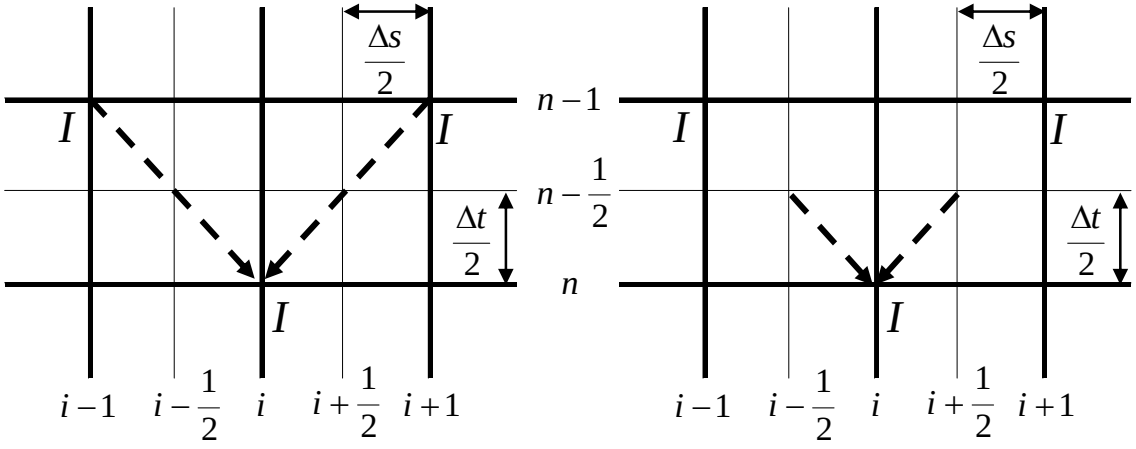

Fig. 6 (a) Imaginary grid points with $i \pm \frac{1}{2}$ and $n - \frac{1}{2}$ (b) Equivalent expression for $I\big|_i^n$

$$V_1 = V^- \Big|_i^{n-1} + V^+ \Big|_i^{n-1} = V \Big|_i^{n-1} \tag{56}$$

Due to (47) and (48), we don't need to calculate $i \pm \frac{1}{2}$ and $n - \frac{1}{2}$ in the EP method. However, we assume if there are imaginary points with $i \pm \frac{1}{2}$ and $n - \frac{1}{2}$, $I\Big|_i^n$ can be expressed by $I^- \Big|_{i+\frac{1}{2}}^{n-\frac{1}{2}}$ and $I^+ \Big|_{i-\frac{1}{2}}^{n-\frac{1}{2}}$ shown in Fig. 6 at the magic time step ($v_o \Delta t = \Delta s$).

$$I\Big|_i^n = I^- \Big|_{i+1}^{n-1} + I^+ \Big|_{i-1}^{n-1} = I^- \Big|_{i+\frac{1}{2}}^{n-\frac{1}{2}} + I^+ \Big|_{i-\frac{1}{2}}^{n-\frac{1}{2}} \tag{57}$$

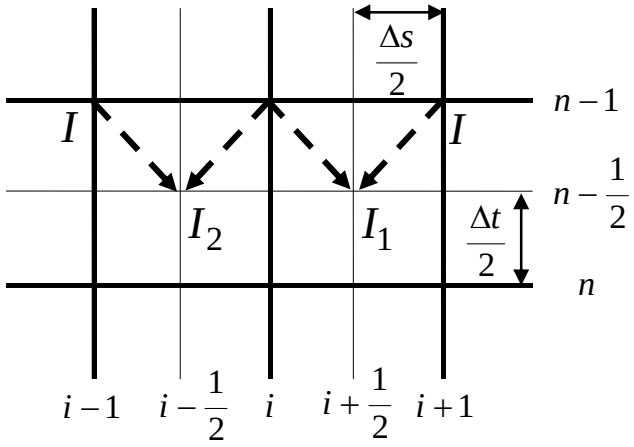

Fig. 7 Computation for I_1 and I_2

According to (57), I_1 and I_2 can be expressed as shown in Fig. 7.

$$I_1 = I^- \Big|_{i+1}^{n-1} + I^+ \Big|_i^{n-1} = I \Big|_{i+\frac{1}{2}}^{n-\frac{1}{2}} \tag{58}$$

$$I_2 = I^- \Big|_i^{n-1} + I^+ \Big|_{i-1}^{n-1} = I \Big|_{i-\frac{1}{2}}^{n-\frac{1}{2}} \tag{59}$$

In magic time step, characteristic impedance $\left(Z_0\right)$ can be calculated

$$Z_0 = \sqrt{\frac{L}{C}} = \frac{\Delta t}{C v_o \Delta t} = \frac{\Delta t}{C \Delta z} \tag{60}$$

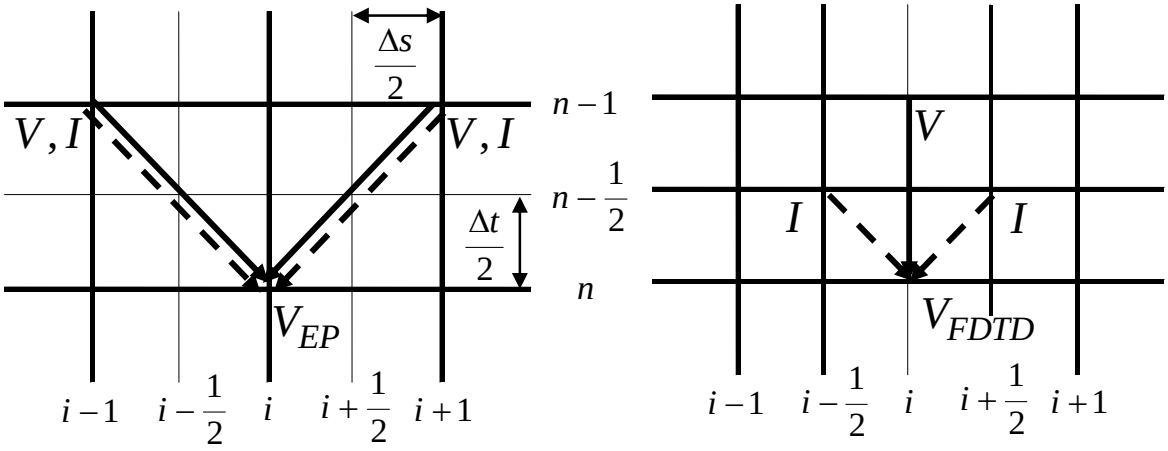

(a)EP (b) FDTD

Fig 8 Two different expressions (EP and FDTD) for voltage $\left(V\big|_i^n\right)$ in magic time step.

Substituting (56), (58), (59) and (60) into (55), it shown to

$$V\big|_i^n = V\big|_i^{n-1} - \frac{\Delta t}{C \Delta z}\left[I \Big|_{i+\frac{1}{2}}^{n-\frac{1}{2}} - I \Big|_{i-\frac{1}{2}}^{n-\frac{1}{2}} \right] \tag{61}$$

Using similar mathematical process, current also can be calculated

$$I\Big|_i^{n-\frac{1}{2}} = I\Big|_i^{n-1} - \frac{\Delta t}{L \Delta z}\left[V \Big|_{i+\frac{1}{2}}^{n-1} - V \Big|_{i-\frac{1}{2}}^{n-1} \right] \tag{62}$$

It is shown that (61) and (62) are same with voltage and current equations of FDTD [11].

Based on (47) and (61), it is drawn in Fig. 8. Solid and dash arrows represent voltage and current, respectively. Fig. 8 shows there are two different expressions ($V_{EP}|_i^n$ and $V_{FDTD}|_i^n$) for voltage $\left(V|_i^n\right)$ in magic time step.

2.10. Tapered microstrip line

The EP method can be used to analyze standard TEM mode transmission lines such as the coaxial cable and stripline, as well to the quasi-TEM microstrip line and co-planar waveguide. As an example, results obtained with the EP approach presented here are compared to those of a popular commercial circuit simulator (ADS) [58] for a non-uniform microstrip line shown in Fig. 9(a) with a width taper given by

$$w(z) = w_0\left(1+ pz\right), \quad 0 \le \mathrm{z} \le d \tag{63}$$

where $p = \left(w_1/w_0 - 1\right)/d$, $w_0 = 0.5mm$, $w_1 = 1.5mm$, d=0.1mm , and $h = 0.5mm$, $s = 0.02mm$. The microstrip has a copper conductor ($\sigma = 5.8\times10^7\ S/m$), an alumina substrate $\varepsilon_r = 9.7$, and a loss tangent 2×10^{-4}. The microstrip line width given in (63) is incorporated into the effective dielectric constant (ε_e) and characteristic impedance (Z_c) at each point on the nonuniform line using the following [18]:

$$\varepsilon_e\left(z\right) = \frac{\varepsilon_r+1}{2} + \frac{\varepsilon_r-1}{2}\left(1+\frac{12h}{w(z)}\right)^{-1/2} - 0.217\left(\varepsilon_r-1\right)\frac{s}{\sqrt{w(z)h}} \tag{64}$$

$$Z_c(z) = \sqrt{\frac{\mu_0 \varepsilon_0}{\varepsilon_e(z)}} \frac{1}{C_a(z)} \tag{65}$$

where μ_o and ε_o are the permeability and permittivity of air respectively, and

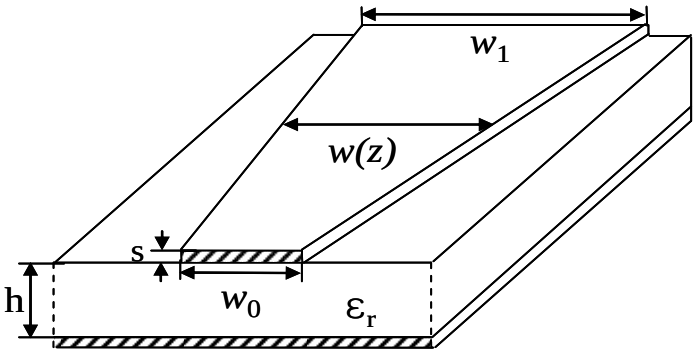

(a)

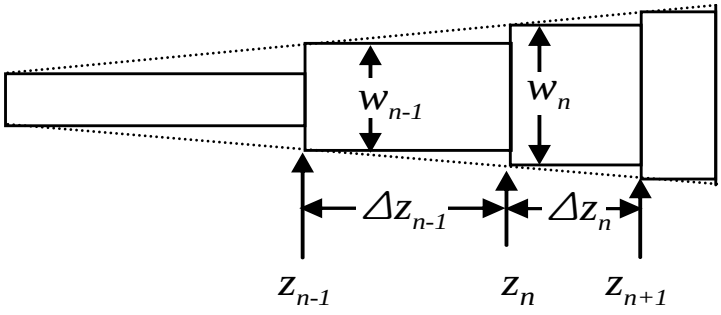

(b)

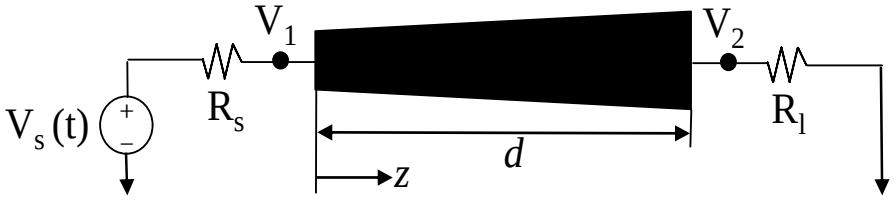

(c)

Fig. 9 (a) Geometry of tapered microstrip line, (b) its modeling and (c) its applied circuit for transient simulation. (d) Response at node 1 and (e) Response at node 2.

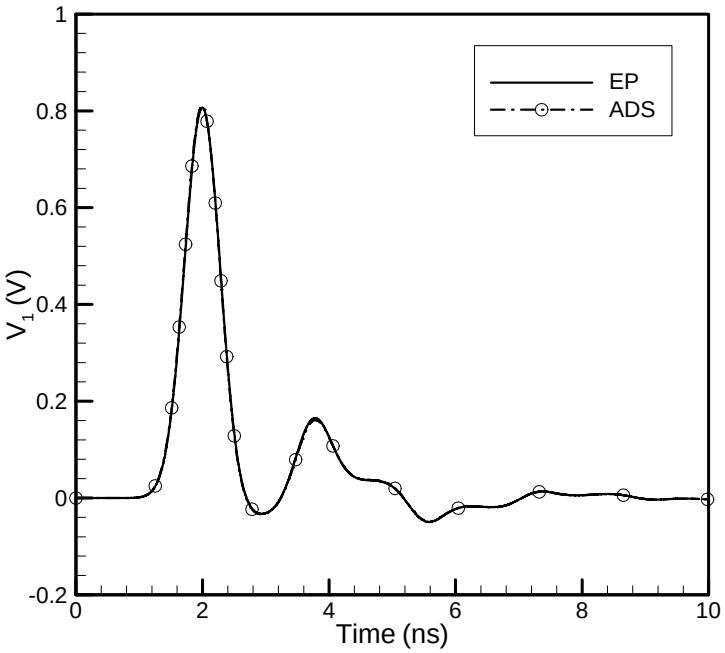

(d)

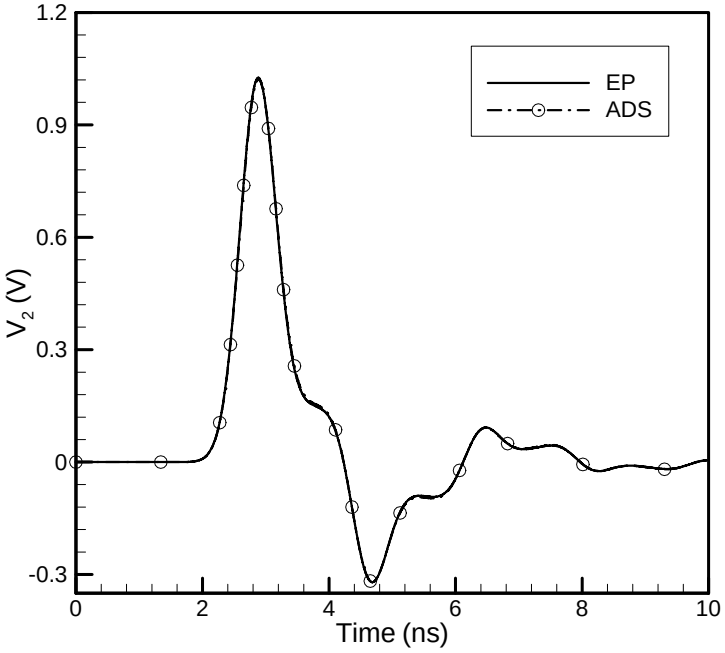

(e)

Fig. 9 Continued.

$$C_a(z) = \varepsilon_0 \left[\frac{w(z)}{h} + 1.393 + 0.667 \ln\left(\frac{w(z)}{h} + 1.444 \right) \right] \tag{66}$$

For the EP numerical method, the lengths Δz_n and widths w_n for each of n microstrip sub-segments are determined by

$$\Delta z_n \doteq \tau v_p(z_n) = \tau c \Big/ \sqrt{\varepsilon_e(z_n)} \tag{67}$$

$$w_n = w(z_n) \tag{68}$$

where $c = speed\ of\ light$.

With a low loss transmission line the phase velocity is approximately a constant because the product of inductance and capacitance is a constant. Constant phase velocity results in a constant sub-segment length given by $\Delta z = \tau v_p$. For the microstrip line the different lengths of the sub-segments given in Eqn. (67) are due to a phase velocity v_p that changes with position, which is in turn attributed to the non-uniform effective dielectric constant ε_e. The microstrip voltage and current equations are adjusted to account for the different sub-section lengths shown in Fig. 9(b) as follows:

$$\begin{aligned} V(z_n,t) = \frac{e^{-a\tau}}{2} \Bigg\{ & \left[1 - \frac{(b\tau)}{3} + \frac{(b\tau)^2}{6} \right] \left[V(z_n + \Delta z_n) + V(z_n - \Delta z_{n-1}) \right] \\ & - Z_0 \left[1 + \frac{(b\tau)^2}{6} \right] \left[I(z_n + \Delta z_n) - I(z_n - \Delta z_{n-1}) \right] \\ & + \frac{4(b\tau)}{3} \left[I_1(b\tau) - I_0(b\tau) \right] V(z_n) \Bigg\} \end{aligned} \tag{69}$$

$$I(z_n,t)=\frac{e^{-a\tau}}{2}\left\{\left[1+\frac{(b\tau)}{3}+\frac{(b\tau)^2}{6}\right]\left[I(z_n+\Delta z_n)+I(z_n-\Delta z_{n-1})\right]\right.$$
$$-\frac{1}{Z_0}\left[1+\frac{(b\tau)^2}{6}\right]\left[V(z_n+\Delta z_n)-V(z_n-\Delta z_{n-1})\right] \qquad (70)$$
$$\left.+\frac{4(b\tau)}{3}\left[I_1(b\tau)+I_0(b\tau)\right]I(z_n)\right\}$$

The inhomogeneous microstrip line section is terminated at each end by impedance matching resistive loads ($R_s=10\Omega$, $R_l=100\Omega$) as shown in Fig. 9(c).

The microstrip is excited by a pulse having a Gaussian time domain voltage distribution, Eqn. (46) , where $\kappa=4\times10^{-10}$. The simulation duration is 10 ns with a time step $\tau=10$ ps . Ten numerical points, which corresponds to ten cascaded uniform transmission-line sections, are used to obtain the EP method results and numerical FORTRAN code showed in APPENDIX D. The voltage response at the input and output points of the non-uniform transmission line section is shown in Fig. 9(d) and 9(e). Good agreement with the results obtained with ADS is observed in both cases. However, because ADS is a time domain simulation based on lumped elements, its assumptions and simplifications are valid primarily at low frequencies. EP provides a much more rapid calculation.

2.11. Summary

A highly accurate and general approach for time domain analysis of lossy inhomogeneous transmission lines has been described in this chapter. The EP method

presented here is an exact solution to the lossy Telegrapher's equations based on the Modal Matrix technique. Simpson's rule is applied to produce a remarkably accurate numerically compatible result. Both lossy and general nonuniform lossy transmission lines examples show that this method is not only simple and efficient, but also an accurate technique for analyzing lossy nonuniform transmission lines with minimal numerical dispersion. In addition, it is shown that this method is compatible with Finite-Difference Time-Domain (FDTD) in magic time step.

CHAPTER III

TIME DOMAIN ANALYSIS OF MULTICONDUCTOR TRANSMISSION LINE

Time domain analytical and simple closed-form solutions to the coupled telegrapher's equations for the voltage and current on a lossless multiconductor transmission line are presented. The resulting expressions are obtained in the form of exact time domain propagators operating on the line voltage and current. Time domain numerical methods are developed and examples are presented showing that exceptionally accurate results are obtained for uniform and nonuniform; coupled and triple; strip and microstrip lines.

3.1. Multiconductor line equations for TEM lines

The transmission line equations in the time domain for N coupled TEM lines are,

$$[C]\frac{\partial}{\partial t}[V] = -\frac{\partial}{\partial z}[I] \tag{71}$$

$$[L]\frac{\partial}{\partial t}[I] = -\frac{\partial}{\partial z}[V] \tag{72}$$

where the transmission lines lie along the *z*-axis. The column vectors $[V]$ and $[I]$ defined the voltages and currents on the conductors. $[L]$ and $[C]$ are the N×N matrices of the per-unit-length inductance and capacitance with,

$$[L][C] = \frac{1}{v_p^{\,2}}\,\bar{\mathbf{I}} \tag{73}$$

where v_p is the phase velocity and $\bar{\mathbf{I}}$ is the identity matrix.

A compacted form for Eqns. (71) and (72) is obtained by gathering the time derivative on the left hand side and capacitance and inductance matrices on right,

$$\frac{\partial}{\partial t}\begin{bmatrix}[V]\\ [I]\end{bmatrix} = -\begin{bmatrix}[0] & [C]^{-1}\dfrac{\partial}{\partial z}\\ [L]^{-1}\dfrac{\partial}{\partial z} & [0]\end{bmatrix}\begin{bmatrix}[V]\\ [I]\end{bmatrix} \tag{74}$$

which can be conveniently expressed as a single equation

$$\frac{\partial \mathbf{F}}{\partial t} = \bar{\mathbf{S}}\,\mathbf{F} \tag{75}$$

where $\mathbf{F}$ is the voltage-current vector and $\bar{\mathbf{S}}$ is the operator matrix in (74)

$$\mathbf{F} = \begin{bmatrix}[V] & [I]\end{bmatrix}^T \tag{76}$$

$$\bar{\mathbf{S}} = -\begin{bmatrix}[0] & [C]^{-1}\dfrac{\partial}{\partial z}\\ [L]^{-1}\dfrac{\partial}{\partial z} & [0]\end{bmatrix} \tag{77}$$

A solution to (75) can be obtained by first finding the propagator matrix $\bar{\mathbf{K}}(z,t)$ that satisfies [42]

$$\frac{\partial \bar{\mathbf{K}}(z,t)}{\partial t} = \bar{\mathbf{S}}\,\bar{\mathbf{K}}(z,t) \tag{78}$$

with initial condition

$$\lim_{t\to 0}\bar{\mathbf{K}}(z,t)=\bar{\mathbf{I}}\delta(z-z') \tag{79}$$

where δ is the Dirac delta function, z' is the initial position of the voltage and current at time $t=0$. A solution to (78), subject to (79), is

$$\bar{\mathbf{K}}=e^{\bar{\mathbf{S}}t}\delta(z-z') \tag{80}$$

Eqn. (80) be expressed as a spectral integral by expanding the exponential in a power series and by replacing the delta function by its Fourier integral representation as follows,

$$\bar{\mathbf{K}}=\left(\mathbf{1}+\bar{\mathbf{S}}t+\bar{\mathbf{S}}^2t^2/2!+\cdots\right)\frac{1}{2\pi}\int_{-\infty}^{\infty}e^{jk_z(z-z')}dk_z \tag{81}$$

After the term by term operations in (81) are carried out, the series is returned to exponential form producing

$$\bar{\mathbf{K}}=\frac{1}{2\pi}\int_{-\infty}^{\infty}e^{\bar{\mathbf{S}}_f t}\exp\left[jk_z(z-z')\right]dk_z \tag{82}$$

$$\bar{\mathbf{S}}_f=-\begin{bmatrix}[0] & jk_z[C]^{-1}\\ jk_z[L]^{-1} & [0]\end{bmatrix} \tag{83}$$

The exponential $e^{\bar{\mathbf{S}}_f t}$ can be converted to a standard 2N×2N transition matrix $\bar{\mathbf{A}}$ via the modal matrix method [55]. First, the eigenvalues $\lambda_{1,\ldots,2N}$ of $\bar{\mathbf{S}}_f$ are found by extracting the roots of $\det\left[\lambda\bar{\mathbf{I}}-\bar{\mathbf{S}}_f\right]=0$, which in this case is

$$\det\begin{bmatrix}\lambda\bar{\mathbf{I}} & jk_z[C]^{-1}\\ jk_z[L]^{-1} & \lambda\bar{\mathbf{I}}\end{bmatrix}=0 \tag{84}$$

By using (73) in (84) we obtain the eigenvalues

$$\lambda_1 = \lambda_2 = ... = \lambda_N = jk_z v_p \doteq \lambda_a \tag{85}$$

$$\lambda_{N+1} = \lambda_{N+2} = ... = \lambda_{2N} = -jk_z v_p \doteq \lambda_b \tag{86}$$

Next, selecting N-columns of eigenvectors each from $adj\left[\lambda_a \bar{\mathbf{I}} - \bar{\mathbf{S}}_f\right]$ and $adj\left[\lambda_b \bar{\mathbf{I}} - \bar{\mathbf{S}}_f\right]$ respectively, forms the modal matrix.

$$\bar{\mathbf{M}} = \begin{bmatrix} -[C]^{-1} & [C]^{-1} \\ v_p \bar{\mathbf{I}} & v_p \bar{\mathbf{I}} \end{bmatrix} \tag{87}$$

The modal matrix and its inverse along with a diagonalized exponential eigenvalue matrix are combined to form the matrix product

$$\bar{\mathbf{A}} = e^{\bar{\mathbf{S}}_f t} = \bar{\mathbf{M}} \begin{bmatrix} e^{\lambda_a t}\bar{\mathbf{I}} & [0] \\ [0] & e^{\lambda_b t}\bar{\mathbf{I}} \end{bmatrix} \bar{\mathbf{M}}^{-1} \tag{88}$$

The matrix multiplications in (88) produce a transition matrix $\bar{\mathbf{A}}$ with the following

$$\bar{\mathbf{A}} = \begin{bmatrix} \cos\left(v_p k_z t\right)\bar{\mathbf{I}} & -jv_p \sin\left(v_p k_z t\right)[L] \\ -jv_p \sin\left(v_p k_z t\right)[C] & \cos\left(v_p k_z t\right)\bar{\mathbf{I}} \end{bmatrix} \tag{89}$$

Each of the integrals in (82) can be evaluated analytically. The resulting propagator is

$$\bar{\mathbf{K}} = \frac{1}{2}\begin{bmatrix} \left\{\delta\left(\bar{z}+v_p t\right)+\delta\left(\bar{z}-v_p t\right)\right\}\bar{\mathbf{I}} & -v_p\left\{\delta\left(\bar{z}+v_p t\right)-\delta\left(\bar{z}-v_p t\right)\right\}[L] \\ -v_p\left\{\delta\left(\bar{z}+v_p t\right)-\delta\left(\bar{z}-v_p t\right)\right\}[C] & \left\{\delta\left(\bar{z}+v_p t\right)+\delta\left(\bar{z}-v_p t\right)\right\}\bar{\mathbf{I}} \end{bmatrix} \tag{90}$$

where $\bar{z} \doteq z - z'$.

The purpose of the propagator is to evolve an initial previous time voltage and current distribution $\left(\left[V(z)\right],\left[I(z)\right]\right)$ into the present time voltage and current $\left(\left[V(z,t)\right],\left[I(z,t)\right]\right)$, over a fixed time interval *t*. Mathematically this operation is a spatial convolution of the propagator with the initial voltage and current [42], as expressed by

$$\begin{bmatrix}\left[V(z,t)\right]\\ \left[I(z,t)\right]\end{bmatrix} = \int_{-\infty}^{\infty} \bar{\mathbf{K}} \cdot \begin{bmatrix}\left[V(z')\right]\\ \left[I(z')\right]\end{bmatrix} dz' \tag{91}$$

Inserting Eqns. (90) into (91) yields the final solution,

$$\left[V(z,t)\right] = \frac{1}{2}\left[V(z+v_p t)+V(z-v_p t)\right] - \frac{1}{2}v_p\left[L\right]\left[I(z+v_p t)-I(z-v_p t)\right] \tag{92}$$

$$\left[I(z,t)\right] = \frac{1}{2}\left[I(z+v_p t)+I(z-v_p t)\right] - \frac{1}{2}v_p\left[C\right]\left[V(z+v_p t)-V(z-v_p t)\right] \tag{93}$$

Notice that final solution sets for multiconductor TEM lines are derived by entirely analytical process. Eqn. (92) and (93) that the present time voltage, or the present time current, is found by taking simple sum and difference combinations of the previous time voltage and current amplitudes. If we consider transmission line having single conductor, then (92) and (93) reduce to the equations [51],

$$V(z,t) = \frac{1}{2}\left\{V(z+tv_p)+V(z-tv_p)\right\} - \frac{1}{2}Z_0\left\{I(z+tv_p)-I(z-tv_p)\right\} \tag{94}$$

$$I(z,t) = \frac{1}{2}\left\{I(z+tv_p)+I(z-tv_p)\right\} - \frac{1}{2}\frac{1}{Z_0}\left\{V(z+tv_p)-V(z-tv_p)\right\} \tag{95}$$

where $Z_0 \doteq \sqrt{L/C}$ and $v_p = 1/\sqrt{LC}$.

3.2. Multiconductor line equations for quasi -TEM lines

It is difficult to find eigenvalues and eigenvectors of $\bar{\mathbf{S}}_f$ because quasi-TEM lines like microstrip line are not satisfied with (73). However, it is known that the inhomogeneous structure lines are related as

$$\left[L \right]\left[C^{o} \right] = \frac{1}{v_0^{\,2}}\,\bar{\mathbf{I}} \tag{96}$$

where v_0 is the phase velocity and $\left[C^o\right]$ is the static capacitance matrix of the structure with an air-filled interface.

N-fundamental modes of propagation for a symmetrical multi-conductor microstrip line can be obtained under the assumption TEM propagation [53]. In order to derive the fundamental modes of propagation, it is necessary to find eigenvalues $\left(\lambda_a, \lambda_b, \lambda_c .....\lambda_n\right)$ and eigenvectors $\left(\mathbf{x_a}, \mathbf{x_b}, \mathbf{x_c} .....\mathbf{x_n}\right)$ of $[C]$. The eigenvalues $\left(\lambda_a^o, \lambda_b^o, \lambda_c^o .....\lambda_n^o\right)$ and eigenvectors $\left(\mathbf{x}_\mathrm{a}^o, \mathbf{x}_\mathrm{b}^o, \mathbf{x}_\mathrm{c}^o .....\mathbf{x}_\mathrm{n}^o\right)$ of $\left[C^o\right]$ will be needed to obtain *N*-fundamental modes. From the eigenvectors N-possible voltage modes can be defined [59]. The modal capacitances and the static capacitances for the same structure with an air-filled substrate are

$$C_a, C_b, C_c .....C_n \text{ and } C_a^o, C_b^o, C_c^o .....C_n^o \tag{97}$$

It is known that following simple relations are always satisfied

$$\begin{cases} \det\left[C \right] = C_a \times C_b \times C_c \times ..... \times C_n \\ \det\left[C^o \right] = C_a^o \times C_b^o \times C_c^o \times ..... \times C_n^o \end{cases} \tag{98}$$

Characteristic impedances and phase velocities for the fundamental mode are defined below

$$\begin{aligned} Z_a &= \frac{1}{v_0 \sqrt{C_a C_a^o}},\ v_a = v_0 \sqrt{\frac{C_a^o}{C_a}} \\ Z_b &= \frac{1}{v_0 \sqrt{C_b C_b^o}},\ v_b = v_0 \sqrt{\frac{C_b^o}{C_b}} \\ &\vdots \qquad\qquad \vdots \\ Z_n &= \frac{1}{v_0 \sqrt{C_n C_n^o}},\ v_n = v_0 \sqrt{\frac{C_n^o}{C_n}} \end{aligned} \tag{99}$$

Using the Eqn. (96), Eqn. (83) for quasi-TEM lines can be converted

$$\bar{\mathbf{S}}_f = -\begin{bmatrix} \left[0 \right] & jk_z \left[C \right]^{-1} \\ jk_z v_0^{\,2} \left[C^a \right] & \left[0 \right] \end{bmatrix} \tag{100}$$

It gives the eigenvalues $\left(\lambda_1, \lambda_2, \lambda_3 ..... \lambda_{2N} \right)$ and eigenvectors $\left(\mathbf{x}_1, \mathbf{x}_2, \mathbf{x}_3 ..... \mathbf{x}_{2N} \right)$ of $\bar{\mathbf{S}}_f$ by same procedures of TEM line.

	Eigenvalue		*Eigenvector*
λ_1	$= jk_z v_a$	$\Rightarrow \mathbf{x}_1$	$= \begin{bmatrix} Z_a \mathbf{x}_a \\ \mathbf{x}_a \end{bmatrix}$
λ_2	$= -jk_z v_a$	$\Rightarrow \mathbf{x}_2$	$= \begin{bmatrix} -Z_a \mathbf{x}_a \\ \mathbf{x}_a \end{bmatrix}$

$$\begin{cases} \lambda_3 = jk_z v_b \Rightarrow \mathbf{x}_3 = \begin{bmatrix} Z_b \mathbf{x}_b \\ \mathbf{x}_b \end{bmatrix} \\ \lambda_4 = -jk_z v_b \Rightarrow \mathbf{x}_4 = \begin{bmatrix} -Z_b \mathbf{x}_b \\ \mathbf{x}_b \end{bmatrix} \end{cases}$$
$$\vdots \qquad\qquad \vdots$$
$$\begin{cases} \lambda_{2N-1} = jk_z v_n \Rightarrow \mathbf{x}_{2N-1} = \begin{bmatrix} Z_n \mathbf{x}_n \\ \mathbf{x}_n \end{bmatrix} \\ \lambda_{2N} = -jk_z v_n \Rightarrow \mathbf{x}_{2N} = \begin{bmatrix} -Z_n \mathbf{x}_n \\ \mathbf{x}_n \end{bmatrix} \end{cases} \tag{101}$$

The modal matrix can be calculated by eigenvectors

$$\begin{aligned} \bar{\mathbf{M}} &= \begin{bmatrix} \mathbf{x}_1 & \mathbf{x}_2 & \cdots & \mathbf{x}_{2N-1} & \mathbf{x}_{2N} \end{bmatrix} \\ &= \begin{bmatrix} \begin{bmatrix} Z_a \mathbf{x}_a \\ \mathbf{x}_a \end{bmatrix} & \begin{bmatrix} -Z_a \mathbf{x}_a \\ \mathbf{x}_a \end{bmatrix} & \cdots & \begin{bmatrix} Z_n \mathbf{x}_n \\ \mathbf{x}_n \end{bmatrix} & \begin{bmatrix} -Z_n \mathbf{x}_n \\ \mathbf{x}_n \end{bmatrix} \end{bmatrix} \end{aligned} \tag{102}$$

Inverse modal matrix is

$$\bar{\mathbf{M}}^{-1} = \frac{1}{2} \begin{bmatrix} \frac{1}{p_a} \begin{bmatrix} \frac{1}{Z_a} \mathbf{x}_a^{\mathrm{T}} & \mathbf{x}_a^{\mathrm{T}} \end{bmatrix} \\ \frac{1}{p_a} \begin{bmatrix} -\frac{1}{Z_a} \mathbf{x}_a^{\mathrm{T}} & \mathbf{x}_a^{\mathrm{T}} \end{bmatrix} \\ \vdots \quad \vdots \\ \frac{1}{p_n} \begin{bmatrix} \frac{1}{Z_n} \mathbf{x}_n^{\mathrm{T}} & \mathbf{x}_n^{\mathrm{T}} \end{bmatrix} \\ \frac{1}{p_n} \begin{bmatrix} -\frac{1}{Z_n} \mathbf{x}_n^{\mathrm{T}} & \mathbf{x}_n^{\mathrm{T}} \end{bmatrix} \end{bmatrix} \tag{103}$$

where $p_n = |\mathbf{x}_n|^2$ and $\mathbf{x}_n^{\mathrm{T}}$ is transverse matrix of $\mathbf{x}_n$.

Using the modal matrix and its inverse, transition matrix $\bar{\mathbf{A}}$ can be solved by

following

$$\bar{\mathbf{A}} = e^{\bar{\mathbf{S}}_f t} = \bar{\mathbf{M}} \begin{bmatrix} e^{\lambda_1 t} & 0 & \cdots & 0 \\ 0 & \ddots & \iddots & \vdots \\ \vdots & \iddots & \ddots & 0 \\ 0 & \cdots & 0 & e^{\lambda_{2N} t} \end{bmatrix} \bar{\mathbf{M}}^{-1} = \begin{bmatrix} [\mathrm{A}_{11}] & [\mathrm{A}_{12}] \\ [\mathrm{A}_{21}] & [\mathrm{A}_{22}] \end{bmatrix} \tag{104}$$

The matrix multiplications in (104) produce a transition matrix $\bar{\mathbf{A}}$ with the following elements

$$\begin{aligned} [\mathrm{A}_{11}] &= \sum_{i=a}^{n} \frac{\cos(v_i k_z t)}{p_i} [\mathrm{A}_i] \\ [\mathrm{A}_{12}] &= \sum_{i=a}^{n} \frac{-jZ_i \sin(v_i k_z t)}{p_i} [\mathrm{A}_i] \\ [\mathrm{A}_{21}] &= \sum_{i=a}^{n} \frac{-j \sin(v_i k_z t)}{Z_i p_i} [\mathrm{A}_i] \\ [\mathrm{A}_{22}] &= [\mathrm{A}_{11}] \end{aligned} \tag{105}$$

where $i = a, b, c, ..., n$ and

$$[\mathrm{A}_i] = \frac{1}{e^{\lambda_i t} + e^{-\lambda_i t}} \begin{bmatrix} \mathbf{x}_i & -\mathbf{x}_i \end{bmatrix} \begin{bmatrix} e^{\lambda_i t} & 0 \\ 0 & e^{-\lambda_i t} \end{bmatrix} \begin{bmatrix} \mathbf{x}_i^{\mathrm{T}} \\ -\mathbf{x}_i^{\mathrm{T}} \end{bmatrix} = \mathbf{x}_i \mathbf{x}_i^{\mathrm{T}} \tag{106}$$

The resulting propagator is

$$\bar{\mathbf{K}} = \begin{bmatrix} [\mathrm{K}_{11}] & [\mathrm{K}_{12}] \\ [\mathrm{K}_{21}] & [\mathrm{K}_{22}] \end{bmatrix} \tag{107}$$

with

$$[\mathrm{K}_{11}] = \frac{1}{2} \sum_{i=a}^{n} \frac{\delta(\bar{z} + v_i t) + \delta(\bar{z} - v_i t)}{p_i} [\mathrm{A}_i]$$

$$[\mathrm{K}_{12}] = -\frac{1}{2}\sum_{i=a}^{n}\frac{\delta(\overline{z}+v_i t)-\delta(\overline{z}-v_i t)}{p_i} Z_i [\mathrm{A}_i]$$

$$[\mathrm{K}_{21}] = -\frac{1}{2}\sum_{i=a}^{n}\frac{\delta(\overline{z}+v_i t)-\delta(\overline{z}-v_i t)}{Z_i p_i} [\mathrm{A}_i]$$

$$[\mathrm{K}_{22}] = [\mathrm{K}_{11}]$$

Inserting (107) into (91), time domain solutions for quasi-TEM line having N-conductors are

$$[V(z,t)] = \frac{1}{2}\sum_{i=a}^{n}\frac{[\mathrm{A}_i]}{p_i}\begin{Bmatrix}[V(z+v_i t)+V(z-v_i t)] \\ -Z_i[I(z+v_i t)-I(z-v_i t)]\end{Bmatrix} \tag{108}$$

$$[I(z,t)] = \frac{1}{2}\sum_{i=a}^{n}\frac{[\mathrm{A}_i]}{p_i}\begin{Bmatrix}[I(z+v_i t)+I(z-v_i t)] \\ -\frac{1}{Z_i}[V(z+v_i t)-V(z-v_i t)]\end{Bmatrix} \tag{109}$$

Notice that these expressions for multiconductor quasi-TEM lines are computed by summing the *N*-fundamental mode voltages and currents. In the following section, examples are given that demonstrate the accuracy of this result.

3.3. Uniform coupled strip lines

For the numerical method, the time increment between initial time (t') and the present time (t) is chosen to be a constant $\tau = t - t'$. This change is implemented by making the replacement $t \to \tau$ in the above equations. The numerical spatial increment is defined by $\tau v_p \doteq \Delta z$ where the velocity v_p is constant. These substitutions in (92) and (93) , give a set of equations that are convenient for numerical calculation,

$$[V(z,\tau)] = \frac{1}{2}[V(z+\Delta z)+V(z-\Delta z)] - \frac{1}{2}v_p[L][I(z+\Delta z)-I(z-\Delta z)] \qquad (110)$$

$$[I(z,\tau)] = \frac{1}{2}[I(z+\Delta z)+I(z-\Delta z)] - \frac{1}{2}v_p[C][V(z+\Delta z)-V(z-\Delta z)] \qquad (111)$$

Fig. 10(a) shows cross section of uniform coupled strip lines. The coupled strip line have dimension $w = 10\mu m$, $s = 20\mu m$, $t = 5\mu m$, $2h = 25\mu m$, and $\varepsilon_r = 3.5$. All metallic parts are assumed to be perfect conductors. The elements of the capacitance matrix $[C]$, obtained by using the formulation in [18,60], are

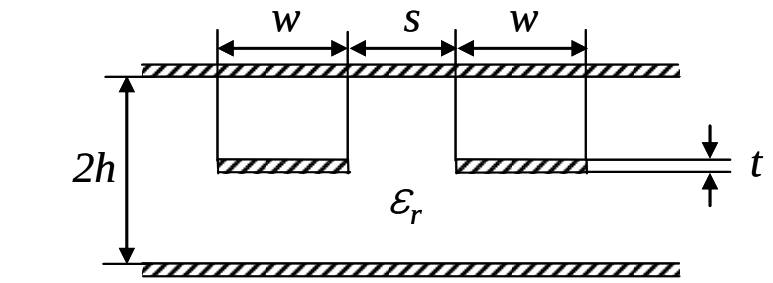

(a)

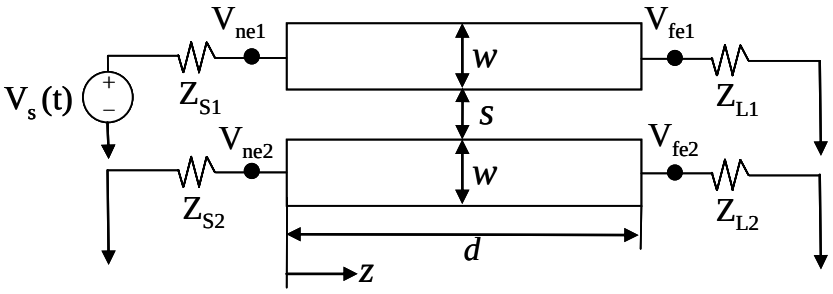

(b)

Fig. 10 (a) Geometry of uniform coupled strip lines, (b) its applied circuit for transient simulation. (c) responses at node V_{ne1} and V_{fe1} and (d) responses at node V_{ne2} and V_{fe2}.

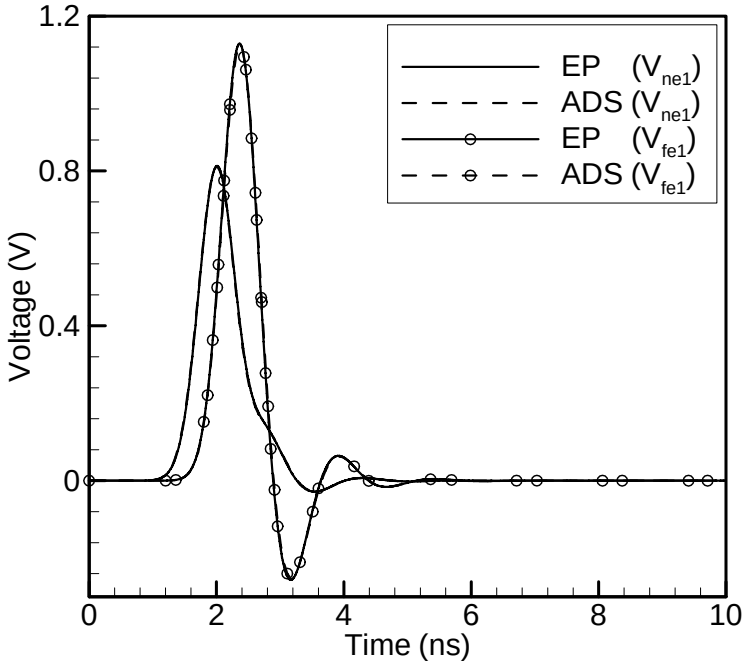

(c)

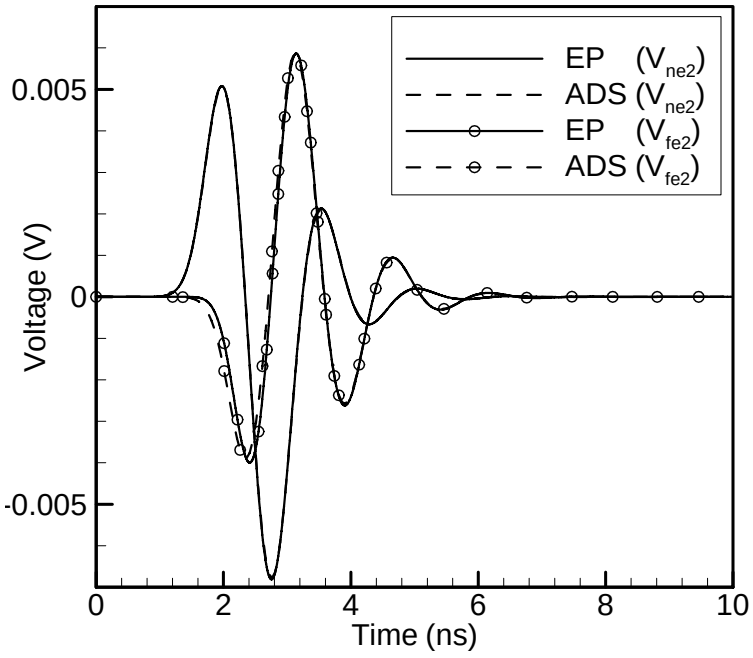

(d)

Fig. 10 Continued.

$$[C]=\begin{bmatrix} 1.476465 & -0.0500974 \\ -0.0500974 & 1.476465 \end{bmatrix} \quad pF/cm \tag{112}$$

and the inductance matrix $[L]$ from (73) is

$$[L]=\begin{bmatrix} 2.640550 & 0.0895955 \\ 0.0895955 & 2.640550 \end{bmatrix} \quad nH/cm \tag{113}$$

The coupled strip lines have equal lengths ($d = 6cm$) and are terminated at each end by impedance matching resistive loads ($Z_{S1} = Z_{S2} = 10\Omega$, $Z_{L1} = Z_{L2} = 100\Omega$) as shown in Fig. 10(b). The strip line is excited by a pulse having a Gaussian time domain voltage distribution

$$\mathrm{V_s}(\mathrm{t}) = \exp\left(-(\mathrm{t}-5\kappa)^2/\kappa^2\right) \tag{114}$$

where $\kappa = 4\times10^{-10}$. The simulation duration is 10 ns with a time step $\tau = 10$ ps.

Results obtained with the direct time domain EP approach presented here are compared to those of a commercial circuit simulator (ADS) [58]. The voltage response at the near ends (V_{ne1}, V_{ne2}) and far ends (V_{fe1}, V_{fe2}) are shown in Fig. 10(c) and (d). Good agreement with the results obtained with ADS is observed in both cases.

3.4 Non-uniform coupled strip lines

In Fig 11(a) the signal lines are nonuniform due to a linear taper. The linear taper is determined by

$$\begin{aligned} w(z) &= w_0(1+pz) \\ s(z) &= s_0(1+qz), \quad 0 \le \mathrm{z} \le d \end{aligned} \tag{115}$$

where $p=\left(w_1/w_0-1\right)/d$, $q=\left(s_1/s_0-1\right)/d$, $w_0=10\,\mu m$, $w_1=20\,\mu m$, $s_0=20\,\mu m$, $s_1=10\,\mu m$, and d=0.1mm. The thickness (t) of conductors, substrate height ($2h$), and permittivity (ε_r) are are the same as in the uniform transmission line example Fig. 10(a). Fig. 11(b) shows the numerical modeling of nonuniform coupled strip lines. The lengths Δz, widths w_m and separation distance s_m for each of m strip sub-segments are determined by

$$\Delta z \doteq \tau v_p = \tau c/\sqrt{\varepsilon_r} \tag{116}$$

$$w_m = w_0\left(1+pz_m\right) \tag{117}$$

$$s_m = s_0\left(1+qz_m\right) \tag{118}$$

where $c=$speed of light. The $\left[C_m\right]$ and $\left[L_m\right]$ matrix elements are determined as follows [61]:

$$\left[C_m\right]=\begin{bmatrix} \mathrm{C}_{11_m} & \mathrm{C}_{12_m} \\ \mathrm{C}_{21_m} & \mathrm{C}_{22_m} \end{bmatrix} \text{ and } \left[L_m\right]=\begin{bmatrix} L_{11_m} & L_{12_m} \\ L_{21_m} & L_{22_m} \end{bmatrix} \tag{119}$$

where

$$\mathrm{C}_{11_m}=\mathrm{C}_{22_m}=\frac{\sqrt{\varepsilon_r}}{2c}\left(\frac{1}{Z_m^e}+\frac{1}{Z_m^o}\right)$$

$$\mathrm{C}_{12_m}=\mathrm{C}_{21_m}=\frac{\sqrt{\varepsilon_r}}{2c}\left(\frac{1}{Z_m^e}-\frac{1}{Z_m^e}\right)$$

$$L_{11_m}=L_{22_m}=\frac{\sqrt{\varepsilon_r}}{2c}\left(Z_m^e+Z_m^e\right)$$

$$L_{12_m}=L_{21_m}=\frac{\sqrt{\varepsilon_r}}{2c}\left(Z_m^e-Z_m^e\right)$$

and [18]

$$Z_m^i = \frac{Z_0\left(2h - t\right)}{4\sqrt{\varepsilon_r}\left(w_m + \left(h/\pi\right)C_f A_m^i\right)} \qquad i = e, o$$

$$A_m^e = 1 + \frac{\ln\left[1 + \tanh\left(\pi s_m / 4h\right)\right]}{\ln 2}$$

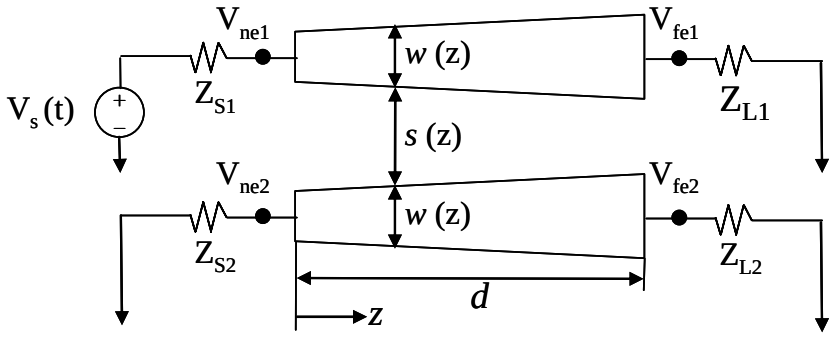

(a)

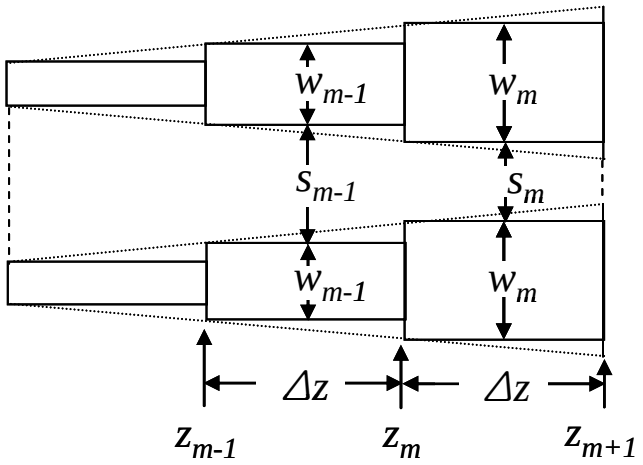

(b)

Fig. 11 (a) Nonuniform coupled strip lines and its applied circuit for transient simulation, (b) numerical modeling, (c) responses at node V_{ne1} and V_{fe1} and (d) responses at node V_{ne2} and V_{fe2}.

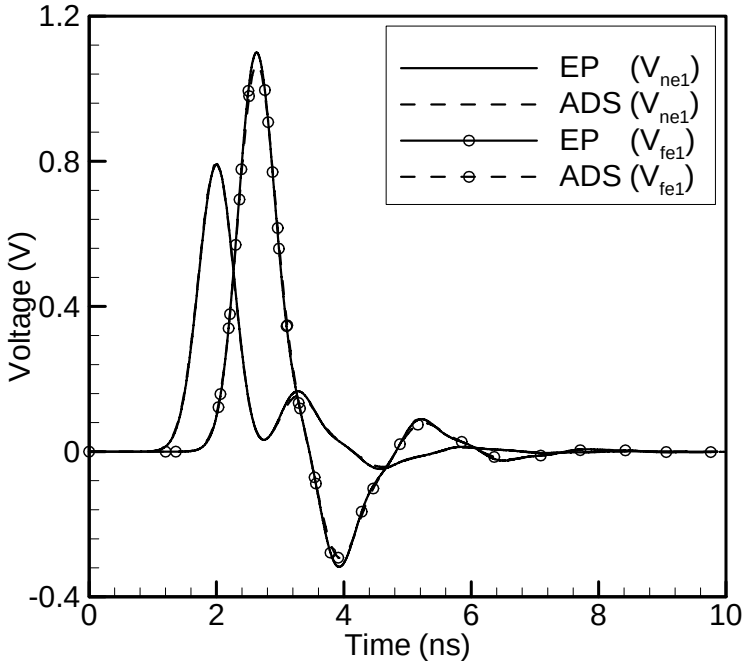

(c)

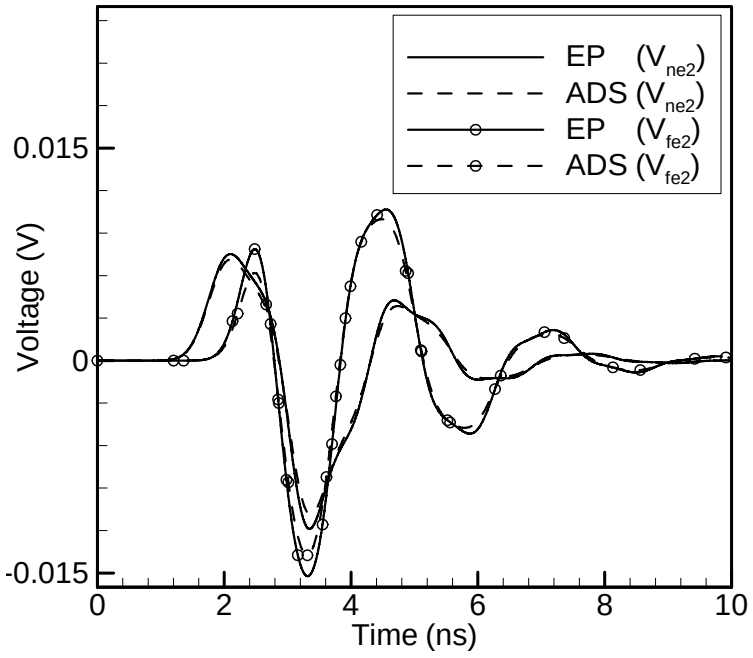

(d)

Fig. 11 Continued.

$$A_m^o = 1 + \frac{\ln\left[1+\coth\left(\pi s_m / 4h\right)\right]}{\ln 2}$$

$$C_f = 2\ln\left(\frac{4h-t}{2h-t}\right) - \frac{t}{2h}\ln\left[\frac{t(4h-t)}{(2h-t)^2}\right]$$

$$Z_0 = 50\Omega$$

Once $[C_m]$ and $[L_m]$ are calculated, EP approach is used to compute transient response of Fig. 11(a). The EP coupled strip voltage and current equations incorporate the different sub-section lengths shown in Fig. 11(b) as follows:

$$\begin{aligned}\left[V(z_m,\tau)\right] = \frac{1}{2}\left[V(z_m+\Delta z)+V(z_m-\Delta z)\right] \\ -\frac{1}{2}v_p\left[L_m\right]\left[I(z_m+\Delta z)-I(z_m-\Delta z)\right]\end{aligned} \tag{120}$$

$$\begin{aligned}\left[I(z_m,\tau)\right] = \frac{1}{2}\left[I(z_m+\Delta z)+I(z_m-\Delta z)\right] \\ -\frac{1}{2}v_p\left[C_m\right]\left[V(z_m+\Delta z)-V(z_m-\Delta z)\right]\end{aligned} \tag{121}$$

For the time domain simulation, nonuniform coupled strip lines are connected by loads ($Z_{S1} = Z_{S2} = 10\Omega$, $Z_{L1} = Z_{L2} = 100\Omega$). The input signal is again the Gaussian voltage distribution given by Eqn. (114). In Fig. 11(c,d), voltages at the near (V_{ne1}, V_{ne2}) and far (V_{fe1}, V_{fe2}) ends of the transmission line show excellent agreement with the ADS generated frequency domain results.

3.5. Three asymmetric coupled strip lines

Fig. 12 shows an example of three asymmetric coupled strip lines. The strip has

substrate height ($h = 1.5mm$), permittivity ($\varepsilon_r = 3.5$), line width ($w_1 = 1.5mm$, $w_2 = 2.0mm$, and $w_3 = 3.5mm$), separation distance ($s_1 = 1.0mm$ and $s_2 = 0.5mm$), conductor thickness ($t = 0.01mm$) and length ($d = 9.0cm$) as shown in Fig. 12(a). Using these dimensions in the [62], we obtain the self and mutual inductances and capacitances

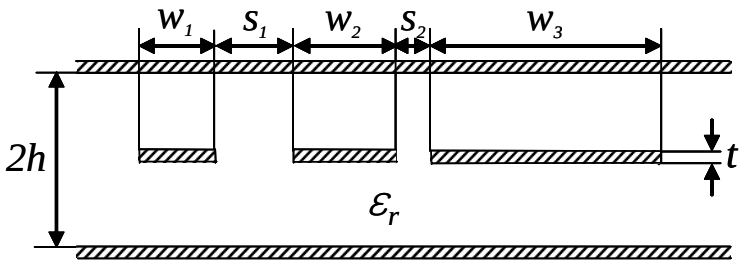

(a)

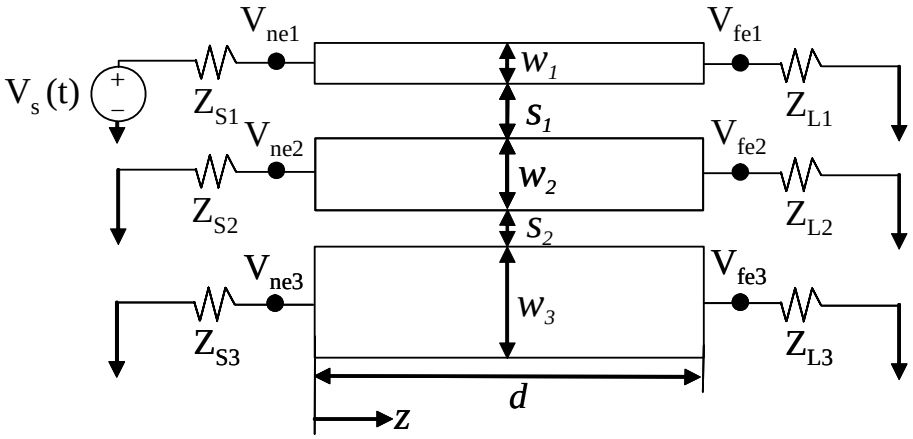

(b)

Fig. 12 (a) Asymmetric three coupled strip lines, (b) its applied circuit for transient simulation, (c) responses at node V_{ne1} and V_{fe1}, (d) responses at node V_{ne2} and V_{fe2} , and (e) responses at node V_{ne3} and V_{fe3}

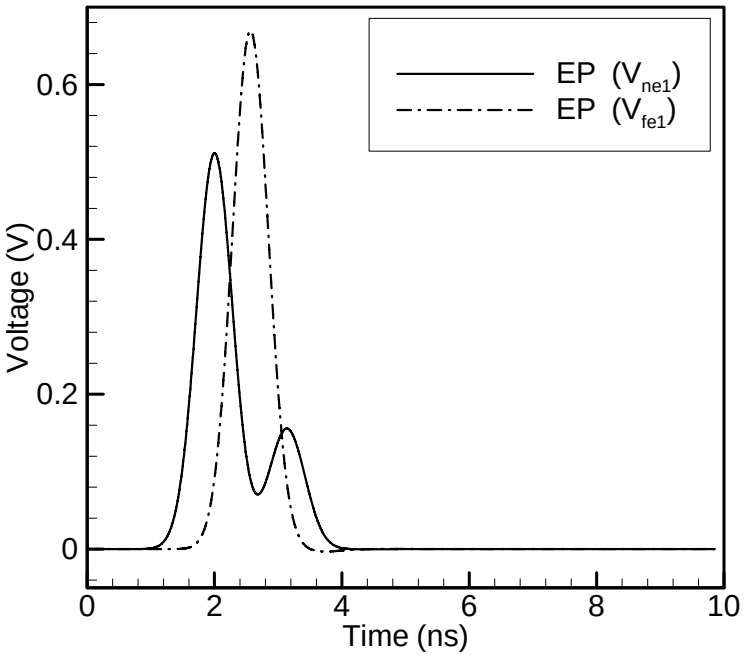

(c)

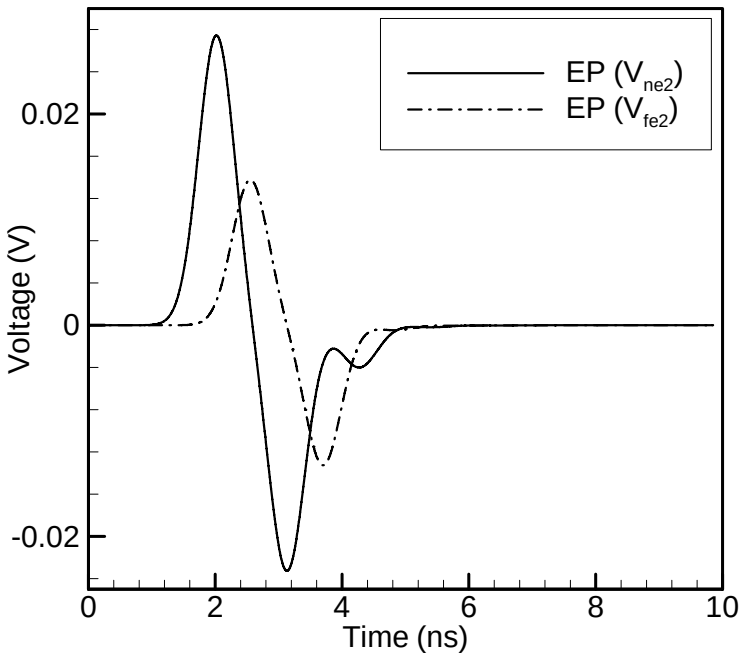

(d)

Fig. 12 Continued.

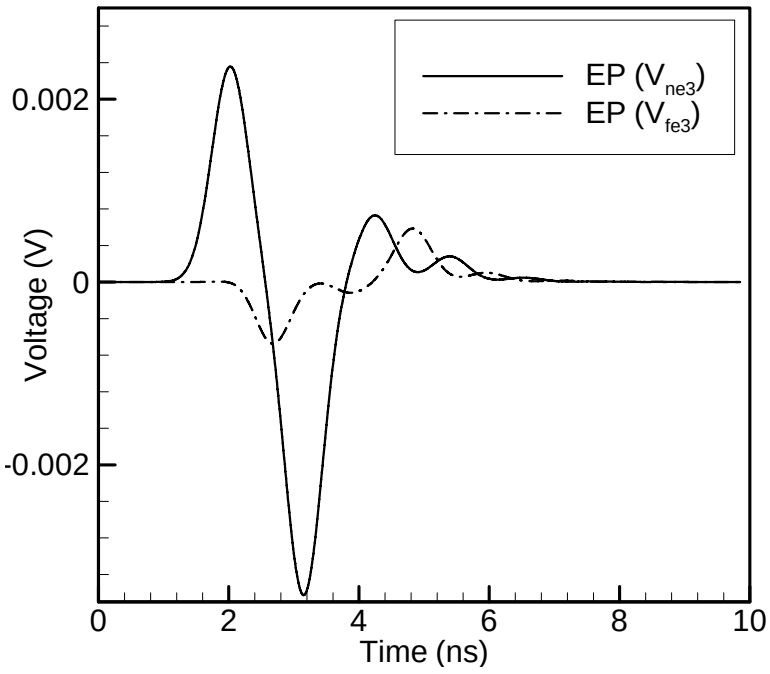

(e)

Fig. 12 Continued.

$$[L] = \begin{bmatrix} 3.282 & 0.3281 & 0.04416 \\ 0.3281 & 2.692 & 0.3547 \\ 0.04416 & 0.3547 & 1.903 \end{bmatrix} \quad nH/cm \tag{122}$$

$$[C] = \begin{bmatrix} 1.201 & -0.1463 & -0.0006074 \\ -0.1463 & 1.501 & -0.2762 \\ -0.0006074 & -0.2762 & 2.097 \end{bmatrix} \quad pF/cm \tag{123}$$

For time domain simulation the strip lines are excited by a Gaussian pulse and terminated by resistive loads ($Z_{S1} = Z_{S2} = Z_{S3} = 50\Omega$, $Z_{L1} = Z_{L2} = Z_{L3} = 100\Omega$) as shown in Fig. 12(b). The EP method transient response on the near ($V_{ne1}, V_{ne2}, V_{ne3}$) and

far ($V_{ne1}, V_{ne2}, V_{ne3}$) ends of the transmission line are shown in Fig 12(c, d, e). Many time domain methods such as ADS and the fundamental modes technique do not provide general solutions for asymmetric lines.

3.6. Uniform coupled microstrip lines

A time domain numerical method is obtained by replacing the time step $0 \to t$ by a time increment τ and the numerical spatial increment $\tau v_i \doteq \Delta z_i$, Eqn. (108) and (109) become

$$\left[V(z,\tau)\right] = \frac{1}{2}\sum_{i=a}^{n} \frac{\left[\mathrm{A}_i\right]}{p_i} \begin{Bmatrix} \left[V(z+\Delta z_i) + V(z-\Delta z_i)\right] \\ -Z_i\left[I(z+\Delta z_i) - I(z-\Delta z_i)\right] \end{Bmatrix} \tag{124}$$

$$\left[I(z,\tau)\right] = \frac{1}{2}\sum_{i=a}^{n} \frac{\left[\mathrm{A}_i\right]}{p_i} \begin{Bmatrix} \left[I(z+\Delta z_i) + I(z-\Delta z_i)\right] \\ -\frac{1}{Z_i}\left[V(z+\Delta z_i) - V(z-\Delta z_i)\right] \end{Bmatrix} \tag{125}$$

As an example, if there are two symmetric microstrip conductors, there will be two fundamental propagating modes ($i = a, b$). The capacitance matrix and the static capacitance matrix for the same structure with an air-filled interface are

$$\left[C\right] = \begin{bmatrix} \mathrm{C}_{11} & \mathrm{C}_{12} \\ \mathrm{C}_{12} & \mathrm{C}_{11} \end{bmatrix} \text{ and } \left[C^o\right] = \begin{bmatrix} \mathrm{C}^o_{11} & \mathrm{C}^o_{12} \\ \mathrm{C}^o_{12} & \mathrm{C}^o_{11} \end{bmatrix} \tag{126}$$

The eigenvalues and corresponding eigenvectors of the capacitance matrix are found by solving $\left(\lambda\bar{\mathbf{I}} - \left[C\right]\right)\mathbf{x} = 0$, which gives

$$\begin{array}{lll} \textit{Eigenvalue} & & \textit{Eigenvector} \\ \lambda_a = C_{11} - C_{12} & \Rightarrow & \mathbf{x}_a = \begin{bmatrix} -1 \\ 1 \end{bmatrix} \\ \lambda_b = C_{11} + C_{12} & \Rightarrow & \mathbf{x}_b = \begin{bmatrix} 1 \\ 1 \end{bmatrix} \end{array} \tag{127}$$

From the eigenvectors $\mathbf{x}_a$ and $\mathbf{x}_b$ we obtain the following conditions for each of the two possible voltage modes:

$$\begin{aligned} a-\text{mode}: \quad & V_{1a} = -V_{2a} \\ b-\text{mode}: \quad & V_{1b} = V_{2b} \end{aligned} \tag{128}$$

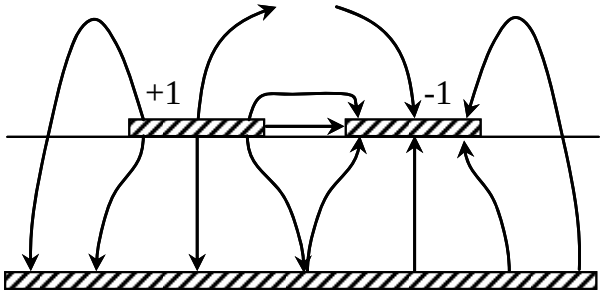

(a)

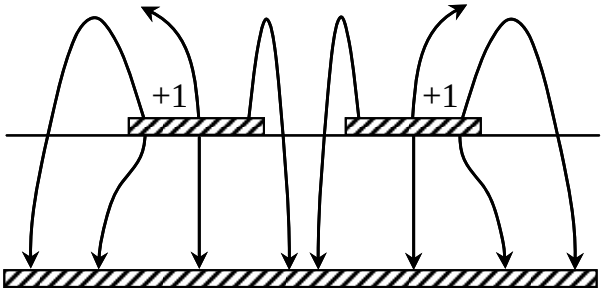

(b)

Fig. 13 Electric field distributions of coupled microstirp for (a) *a*-mode (b) *b*-mode.

where V_{1a} and V_{2a} are the $a-$mode excitation voltages in the 1st and 2nd conductors respectively and V_{1b} and V_{2b} are the $b-$mode applied voltages in 1st and 2nd line. Fig. 13 shows a sketch of the electric field lines for the two fundamental modes given by (128). When there are two symmetric lines, the $a-$mode and $b-$mode are referred to as the *odd*-mode and *even*-mode, respectively [60]. Now suppose that the charges of the conductors are related to the line potentials and capacitances by

$$[Q_i] = [\mathrm{C}] \cdot [V_i] \tag{129}$$

For the $a-$mode, we obtain the modal capacitances

$$\frac{Q_{1a}}{V_{1a}} = \mathrm{C}_{11} - \mathrm{C}_{12} \tag{130}$$

$$\frac{Q_{2a}}{V_{2a}} = \mathrm{C}_{11} - \mathrm{C}_{12} \tag{131}$$

and similarly for the $b-$mode,

$$\frac{Q_{1b}}{V_{1b}} = \mathrm{C}_{11} + \mathrm{C}_{12} \tag{132}$$

$$\frac{Q_{2b}}{V_{2b}} = \mathrm{C}_{11} + \mathrm{C}_{12} \tag{133}$$

These are the redefined fundamental mode capacitances from the *N*-voltage modes. From these equations one gets

$$C_a = \mathrm{C}_{11} - \mathrm{C}_{12} \tag{134}$$

$$C_b = \mathrm{C}_{11} + \mathrm{C}_{12} \tag{135}$$

Also, in the same way we can calculate the $a-\text{mode}$ and $b-\text{mode}$ capacitances of $\left[C^o\right]$,

$$C_a^o = \mathrm{C}_{11}^o - \mathrm{C}_{12}^o \tag{136}$$

$$C_b^o = \mathrm{C}_{11}^o + \mathrm{C}_{12}^o \tag{137}$$

The characteristic impedances (Z_a, Z_b) and phase velocities (v_a, v_b) for each mode can be obtained from Eqns. (99).

The eigenvalues $\left(\lambda_1, \lambda_2\right)$ and eigenvectors $\left(\mathbf{x}_1, \mathbf{x}_2\right)$ of $\bar{\mathbf{S}}_f$ are defined in Eqn. (101). Transient matrix $\bar{\mathbf{A}}$, Eqn. (104) can be calculated using modal matrix Eqn.(102) and its inverse matrix Eqn. (103)

$$\bar{\mathbf{A}} = \begin{bmatrix} [\mathrm{A}_{11}] & [\mathrm{A}_{12}] \\ [\mathrm{A}_{21}] & [\mathrm{A}_{22}] \end{bmatrix} \tag{138}$$

$$[\mathrm{A}_{11}] = \frac{\cos\left(v_a k_z t\right)}{p_a}[\mathrm{A}_a] + \frac{\cos\left(v_b k_z t\right)}{p_b}[\mathrm{A}_b]$$

$$[\mathrm{A}_{12}] = \frac{-jZ_a \sin\left(v_a k_z t\right)}{p_a}[\mathrm{A}_a] + \frac{-jZ_b \sin\left(v_b k_z t\right)}{p_b}[\mathrm{A}_b]$$

$$[\mathrm{A}_{21}] = \frac{-j \sin\left(v_a k_z t\right)}{Z_a p_a}[\mathrm{A}_a] + \frac{-j \sin\left(v_b k_z t\right)}{Z_b p_b}[\mathrm{A}_b]$$

$$[\mathrm{A}_{22}] = [\mathrm{A}_{11}]$$

where $p_a = p_b = 2$,

$$[\mathrm{A}_a] = \begin{bmatrix} 1 & -1 \\ -1 & 1 \end{bmatrix} \text{ and } [\mathrm{A}_b] = \begin{bmatrix} 1 & 1 \\ 1 & 1 \end{bmatrix} \tag{139}$$

The resulting propagator is

$$\bar{\mathbf{K}} = \begin{bmatrix} [\mathrm{K}_{11}] & [\mathrm{K}_{12}] \\ [\mathrm{K}_{21}] & [\mathrm{K}_{22}] \end{bmatrix} \tag{140}$$

with the matrix elements

$$[\mathrm{K}_{11}] = \frac{1}{2}\left\{ \begin{array}{l} \dfrac{\delta(\bar{z}+v_a t)+\delta(\bar{z}-v_a t)}{2}[\mathrm{A}_a] \\ +\dfrac{\delta(\bar{z}+v_b t)+\delta(\bar{z}-v_b t)}{2}[\mathrm{A}_b] \end{array} \right\}$$

$$[\mathrm{K}_{12}] = -\frac{1}{2}\left\{ \begin{array}{l} Z_a \dfrac{\delta(\bar{z}+v_a t)-\delta(\bar{z}-v_a t)}{2}[\mathrm{A}_a] \\ +Z_b \dfrac{\delta(\bar{z}+v_b t)-\delta(\bar{z}-v_b t)}{2}[\mathrm{A}_b] \end{array} \right\}$$

$$[\mathrm{K}_{21}] = -\frac{1}{2}\left\{ \begin{array}{l} \dfrac{\delta(\bar{z}+v_a t)-\delta(\bar{z}-v_a t)}{2Z_a}[\mathrm{A}_a] \\ +\dfrac{\delta(\bar{z}+v_b t)-\delta(\bar{z}-v_b t)}{2Z_b}[\mathrm{A}_b] \end{array} \right\}$$

$$[\mathrm{K}_{22}] = [\mathrm{K}_{11}]$$

Finally, the time domain solutions for coupled quasi-TEM line are

$$[V(z,t)] = \frac{1}{2}\left\{ \begin{array}{l} \dfrac{[\mathrm{A}_a]}{2}\left[V(z+v_a t)+V(z-v_a t)\right] \\ +\dfrac{[\mathrm{A}_b]}{2}\left[V(z+v_b t)+V(z-v_b t)\right] \\ -\dfrac{Z_a[\mathrm{A}_a]}{2}\left[I(z+v_a t)-I(z-v_a t)\right] \\ -\dfrac{Z_b[\mathrm{A}_b]}{2}\left[I(z+v_b t)-I(z-v_b t)\right] \end{array} \right\} \tag{141}$$

$$[I(z,t)]=\frac{1}{2}\left\{\begin{array}{l}\frac{[\mathrm{A}_a]}{2}\left[I(z+v_a t)+I(z-v_a t)\right]\\ \quad+\frac{[\mathrm{A}_b]}{2}\left[I(z+v_b t)+I(z-v_b t)\right]\\ \quad-\frac{[\mathrm{A}_a]}{2Z_a}\left[V(z+v_a t)-V(z-v_a t)\right]\\ \quad-\frac{[\mathrm{A}_b]}{2Z_b}\left[V(z+v_b t)-V(z-v_b t)\right]\end{array}\right\} \tag{142}$$

The two-conductor quasi-TEM transmission line equations reduce to those of the TEM transmission line case, where

$$v_a = v_b = \frac{v_0}{\sqrt{\varepsilon_r}} = v_p \tag{143}$$

$$Z_a = \frac{1}{v_p}\frac{1}{C_a} \quad \text{and} \quad Z_b = \frac{1}{v_p}\frac{1}{C_b} \tag{144}$$

due to $\frac{C_a}{C_a^a}=\frac{C_b}{C_b^a}=\varepsilon_r$.

Substituting (143) into (141) and (142), solutions Eqns. (141) and (142)will convert

$$[V(z,t)]=\frac{1}{2}\left\{\begin{array}{l}\frac{1}{2}\left([\mathrm{A}_a]+[\mathrm{A}_b]\right)\left[V(z+v_p t)+V(z-v_p t)\right]\\ -\frac{1}{2}\left(Z_a[\mathrm{A}_a]+Z_b[\mathrm{A}_b]\right)\left[I(z+v_p t)-I(z-v_p t)\right]\end{array}\right\} \tag{145}$$

$$[I(z,t)]=\frac{1}{2}\left\{\begin{array}{l}\frac{1}{2}\left([\mathrm{A}_a]+[\mathrm{A}_b]\right)\left[I(z+v_p t)+I(z-v_p t)\right]\\ \quad-\frac{1}{2}\left(\frac{[\mathrm{A}_a]}{Z_a}+\frac{[\mathrm{A}_b]}{Z_b}\right)\left[V(z+v_p t)-V(z-v_p t)\right]\end{array}\right\} \tag{146}$$

Sum between $\frac{[\mathrm{A}_a]}{2}$ and $\frac{[\mathrm{A}_b]}{2}$ can be calculated by (139).

$$\frac{1}{2}\left([\mathrm{A}_a]+[\mathrm{A}_b]\right)=\bar{\mathbf{I}}_2 \tag{147}$$

where $\bar{\mathbf{I}}_2$ is $2X2$ identity matrix.Using (144), we can calculate second coefficient matrix of (145) and (146)

$$\frac{1}{2}\left(Z_a[\mathrm{A}_a]+Z_b[\mathrm{A}_b]\right)=\frac{1}{2}\frac{1}{v_p}\left(\frac{[\mathrm{A}_a]}{C_a}+\frac{[\mathrm{A}_b]}{C_b}\right)=\frac{1}{v_p}[C]^{-1}=v_p[L] \tag{148}$$

$$\frac{1}{2}\left(\frac{[\mathrm{A}_a]}{Z_a}+\frac{[\mathrm{A}_b]}{Z_b}\right)=\frac{v_p}{2}\left(C_a[\mathrm{A}_a]+C_b[\mathrm{A}_b]\right)=v_p[C] \tag{149}$$

These (147), (148), and (149) lead that quasi-TEM line solutions (141) and (142) reduce to the TEM line solutions (92) and (93), respectively.

Fig. 14(a) shows an example of two coupled microstrip lines. The microstrip has a substrate height ($h=10\,\mu m$), permittivity ($\varepsilon_r=9.8$), line width ($w=10\mu m$), separation distance ($s=10\mu m$), conductor thickness ($t=5\mu m$) and length ($d=0.1m$).The characteristic impedances ($Z_a=32.0308\,\Omega$, $Z_b=48.7293\,\Omega$) and phase velocities ($v_a=1.4007\times10^8\,m/s$, $v_b=1.1269\times10^8\,m/s$) for each mode are obtained using Line Calculator [58]. The circuit topology for transient simulation of coupled microstrip lines is represented in Fig. 14(b). The coupled microstrip lines are terminated by the resistive loads $Z_{S1}=Z_{S2}=50\Omega$ and $Z_{L1}=Z_{L2}=100\Omega$. A Gaussian pulse, Eqn. (114), is applied as an input signal. According to Eqn. (128), the individual transmission line voltage

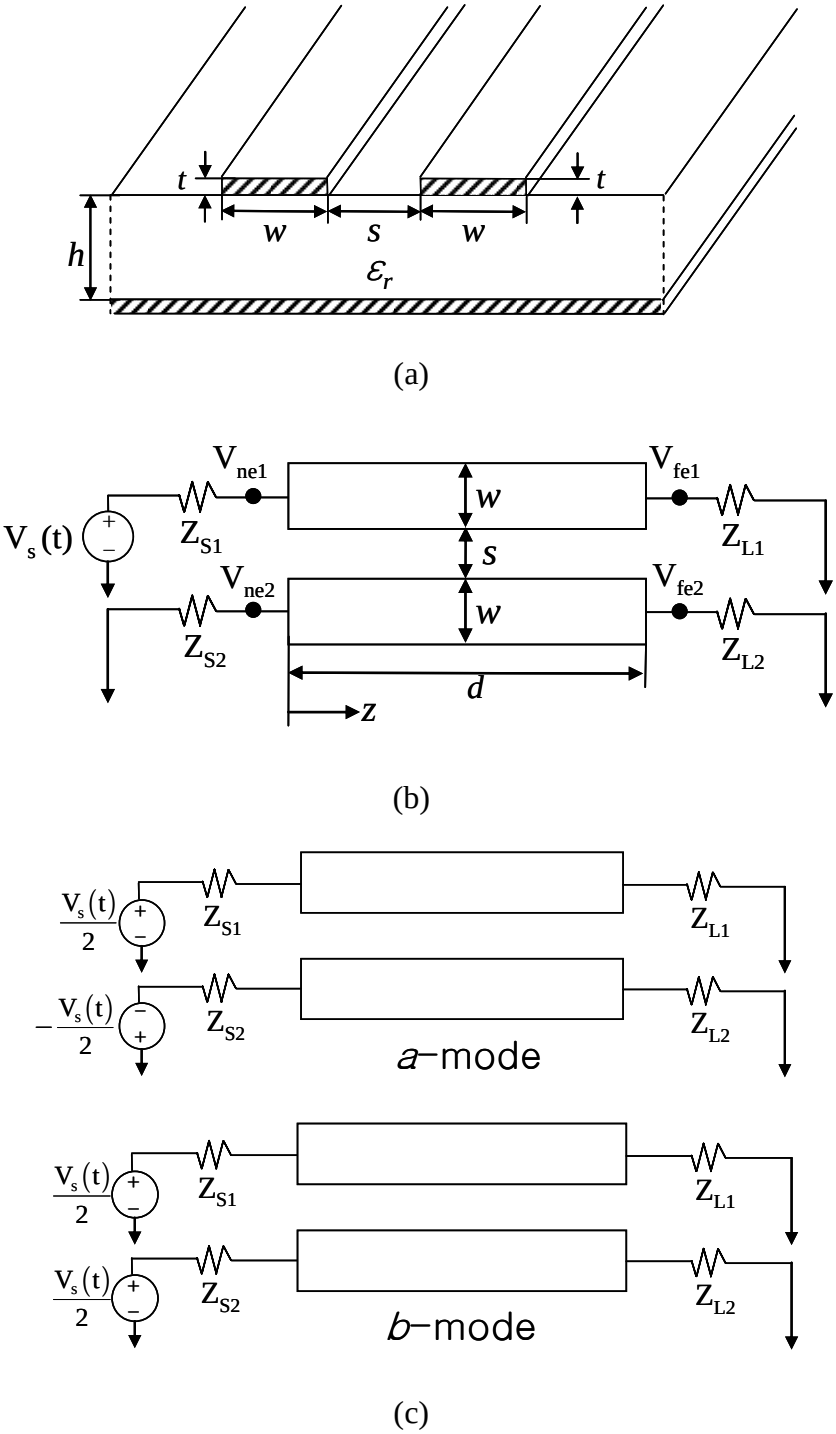

Fig. 14 (a) Geometry of coupled microstrip lines, (b) its applied circuit for transient simulation, (c) Sets of voltage sources for the fundamental modes, responses at (d) V_{ne1} and V_{fe1} and (e) V_{ne2} and V_{fe2}.

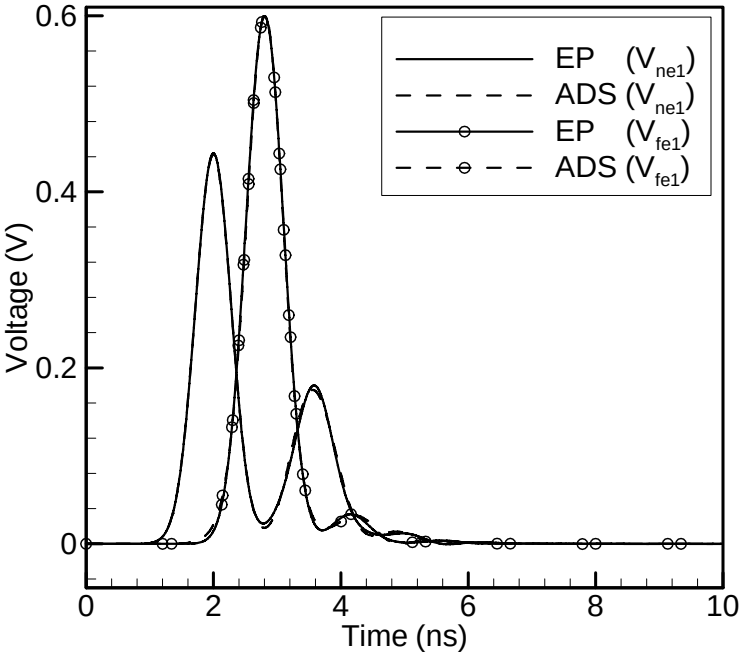

(d)

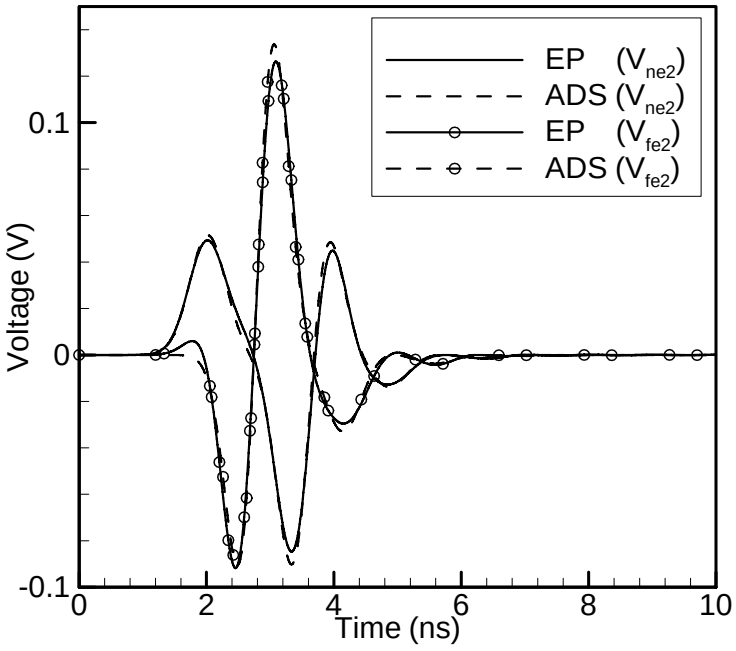

(e)

Fig. 14 Continued.

sources are related to the fundamental modal voltages by

$$\begin{aligned} 1^{st}\ \text{line}: &\quad V_{1a}+V_{1b}=V_s \\ 2^{nd}\ \text{line}: &\quad V_{2a}+V_{2b}=-V_{1a}+V_{1b}=0 \end{aligned} \tag{150}$$

Eqn. (150) then gives the modal voltages

$$V_{1a}=V_{1b}=V_{2b}=\frac{V_s}{2},\quad V_{2a}=-\frac{V_s}{2} \tag{151}$$

shown in Fig.14(c). So by superposition, the excitation of line 1 in Fig. 14(b) can be treated as the sum of the *a*- and *b*- mode excitations shown in Fig. 14(c).

In Fig 14(d, e), the EP method transient voltage responses at the near (V_{ne1}, V_{ne2}) and far (V_{fe1}, V_{fe2}) ends of each transmission line is shown and compared with results obtained using ADS commercial software. Excellent agreement is observed in both cases confirming the accuracy of the EP method.

3.7. Three coupled microstrip lines having different widths

Now consider three coupled microstrip transmission lines having different conductor widths as shown in Fig. 15(a). The microstrip has a substrate height ($h=1.524mm$), permittivity ($\varepsilon_r=4.65$), line width ($w=1.524mm$, $w_1=0.762mm$), separation distance ($s=0.254mm$), conductor thickness ($t=0.0356mm$) and length ($d=30.48cm$).

Using the LINPAR [62], we obtain the capacitance matrix

$$\left[C\right]=\begin{bmatrix} 1.056 & -0.3305 & -0.03524 \\ -0.3305 & 0.9547 & -0.3305 \\ -0.03524 & -0.3305 & 1.056 \end{bmatrix} \quad pF/cm \tag{152}$$

$$\left[C^a\right]=\begin{bmatrix} 0.3532 & -0.1364 & -0.02369 \\ -0.1364 & 0.3504 & -0.1364 \\ -0.02369 & -0.1364 & 0.3532 \end{bmatrix} \quad pF/cm \tag{153}$$

Applying the same procedure as in (126)-(137), we obtain the eigenvalues

$$\mathbf{x}_a = \begin{bmatrix} 1 \\ u \\ 1 \end{bmatrix},\ \mathbf{x}_b = \begin{bmatrix} 1 \\ 0 \\ -1 \end{bmatrix},\ \mathbf{x}_c = \begin{bmatrix} 1 \\ -\dfrac{2}{u} \\ 1 \end{bmatrix} \tag{154}$$

where $u = 1.5177$ and modal capacitances

$$\begin{aligned} &C_a = 0.5192,\ C_b = 1.0912,\ C_c = 1.4563 \quad pF/cm \\ &C_a^a = 0.1468,\ C_b^a = 0.3769,\ C_c^a = 0.5331 \quad pF/cm \end{aligned} \tag{155}$$

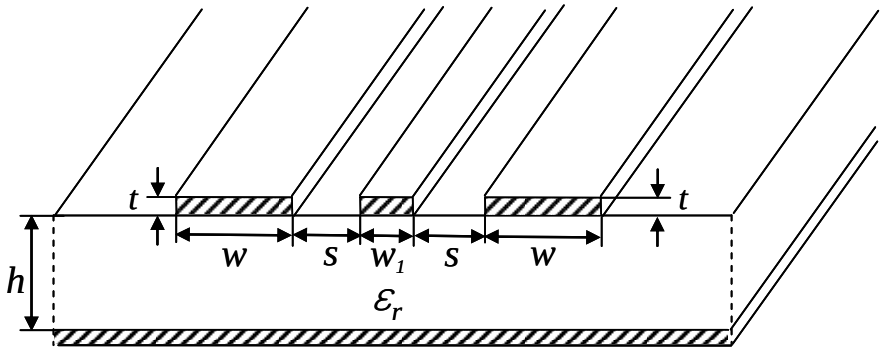

(a)

Fig. 15 (a) Geometry of three coupled microstrip lines, (b) its applied circuit for transient simulation, (c) Sets of voltage sources for the fundamental modes, (d) Voltage responses at V_{ne1} and $V_{fe1,}$ (e) V_{ne2} and V_{fe2} and (f) V_{ne3} and V_{fe3}

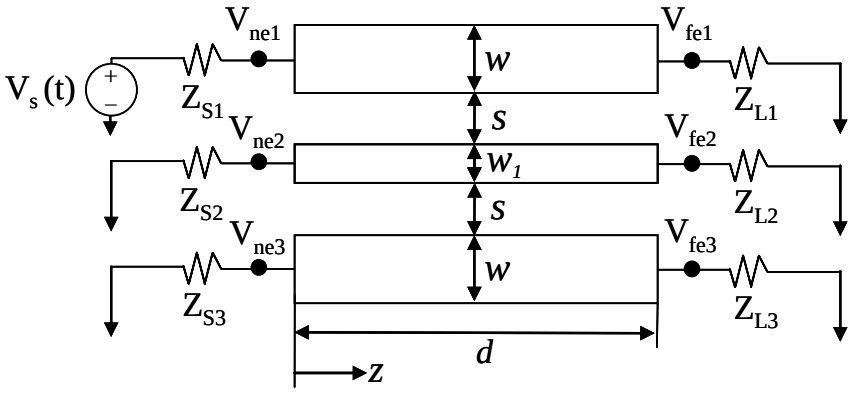

(b)

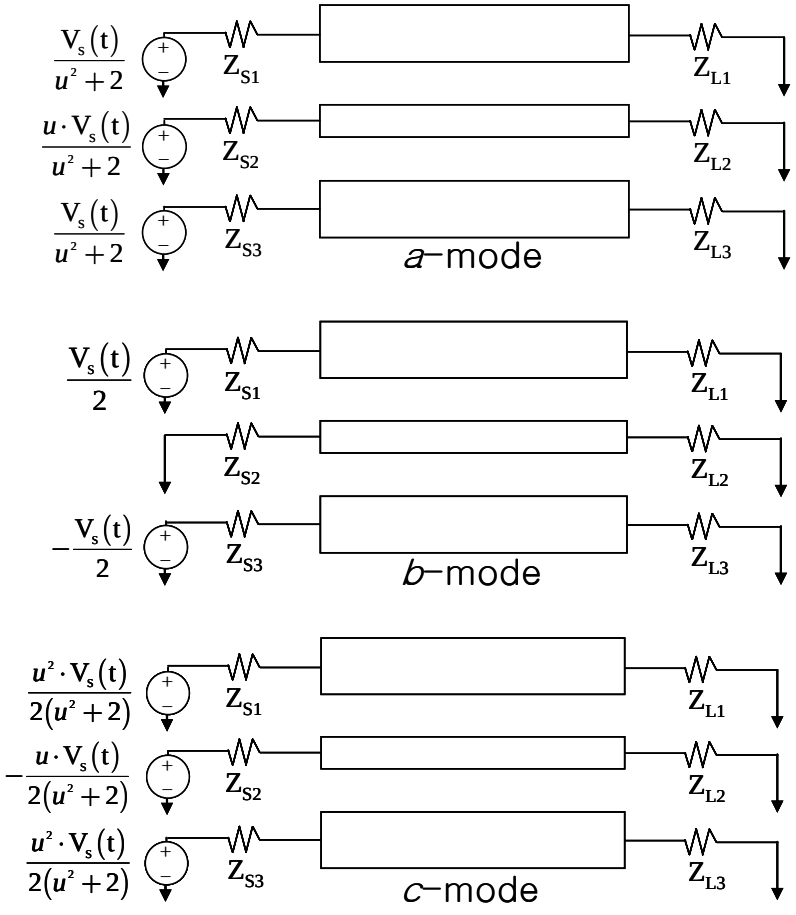

(c)

Fig. 15 Continued.

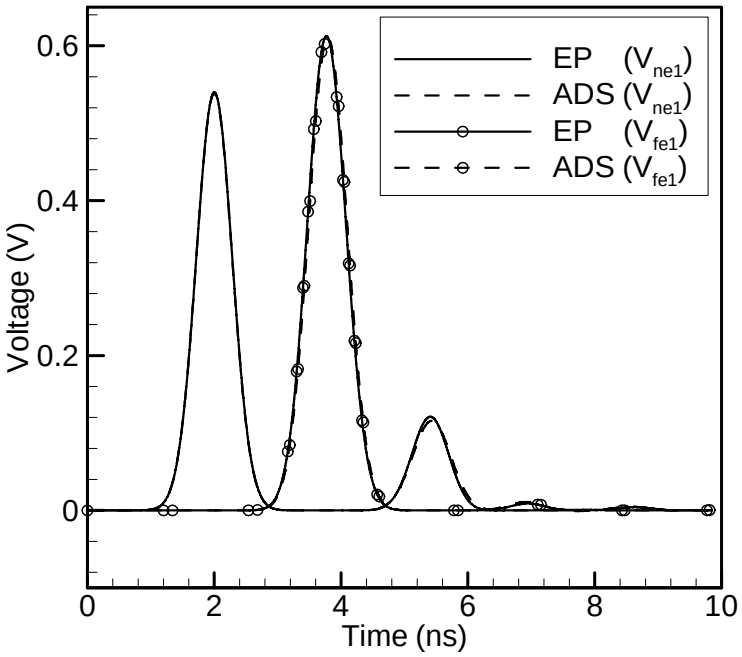

(d)

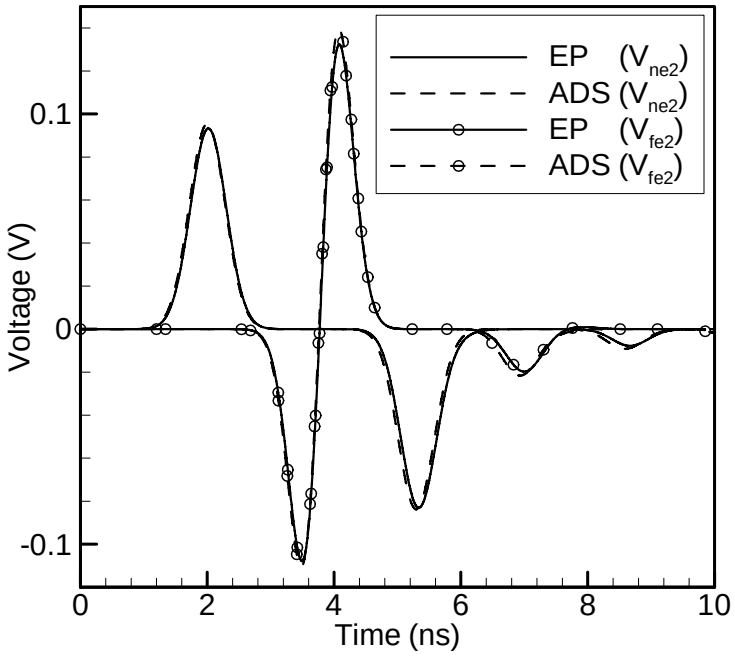

(e)

Fig. 15 Continued.

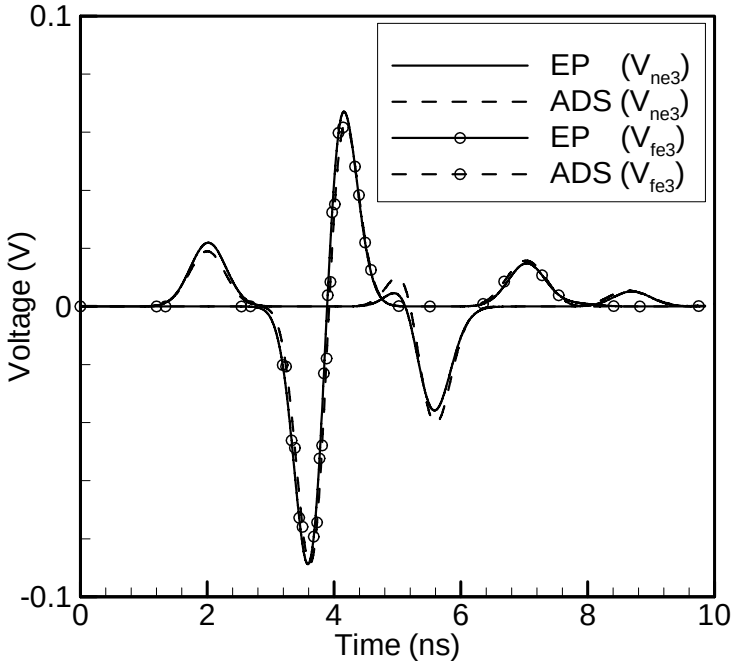

(f)

Fig. 15 Continued.

According to (99) and (101), the modal characteristic impedances and phase velocities are

$$\begin{aligned} Z_a &= 120.7539\Omega,\ v_a = 1.5951\times 10^8\ m/s \\ Z_b &= \ 51.9770\Omega,\ v_b = 1.7631\times 10^8\ m/s \\ Z_c &= \ 37.8299\Omega,\ v_c = 1.8152\times 10^8\ m/s \end{aligned} \tag{156}$$

$$\begin{aligned} \left[\mathrm{A}_a\right] &= \mathbf{x}_a\mathbf{x}_a^{\mathrm{T}},\quad p_a = 4.3034 \\ \left[\mathrm{A}_b\right] &= \mathbf{x}_b\mathbf{x}_b^{\mathrm{T}},\quad p_b = 2.0000 \\ \left[\mathrm{A}_c\right] &= \mathbf{x}_c\mathbf{x}_c^{\mathrm{T}},\quad p_c = 3.7366 \end{aligned} \tag{157}$$

From the eigenvectors $\mathbf{x}_a$, $\mathbf{x}_b$, and $\mathbf{x}_c$, we can derive the following three possible voltage modes [53]:

$$\begin{aligned} a-\text{mode}: &\quad V_{1a} = \frac{V_{2a}}{u} = V_{3a} \\ b-\text{mode}: &\quad V_{1b} = -V_{3b},\ V_{2b} = 0 \\ c-\text{mode}: &\quad V_{1c} = -\frac{u \cdot V_{2c}}{2} = V_{3c} \end{aligned} \tag{158}$$

For the time domain numerical simulation, the microstrip lines are terminated by resistive loads $Z_{S1} = Z_{S2} = Z_{S3} = 50\Omega$ and $Z_{L1} = Z_{L2} = Z_{L3} = 100\Omega$ as shown in Fig. 15(b). The applied input signal is defined in Eqn. (114). Following (158), each fundamental mode is represented a set of three voltage sources, as shown in Fig. 15(c) [53]. In Fig. 15(d,e,f), the transient responses at near ends ($V_{ne1}, V_{ne2}, V_{ne3}$) and far ends ($V_{fe1}, V_{fe2}, V_{fe3}$)found by the EP method are compared with those obtained using ADS circuit simulator. In each case there is high degree of accuracy.

3.8. Non-uniform coupled microstrip lines

Fig. 16(a) shows two nonuniform coupled microstrip transmission lines. The widths $w(z)$ and separation distances $s(z)$ are respectively defined by (115). The microstrip has substrate height ($h = 10\,\mu m$), and permittivity ($\varepsilon_r = 9.8$).

The numerical model for the set of nonuniform microstrip lines is shown in Fig. 16(b). The lengths $\Delta z_{m,i}$, widths $w_{m,i}$ and separation distances $s_{m,i}$ for each of m strip sub-segments are determined by

$$\Delta z_{m,i} \doteq \tau v_i \left(z_{m,i} \right) \tag{159}$$

$$w_{m,i} = w\left(z_{m,i}\right) \tag{160}$$

$$s_{m,i} = s\left(z_{m,i}\right) \tag{161}$$

where $i = a$ $(a-\text{mode})$ and b $(b-\text{mode})$.

The voltage and current on each of the *m* sub-segments, obtained from Eqns. (124) and (125), is

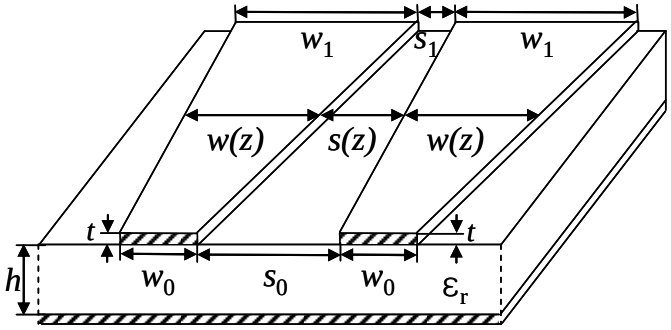

(a)

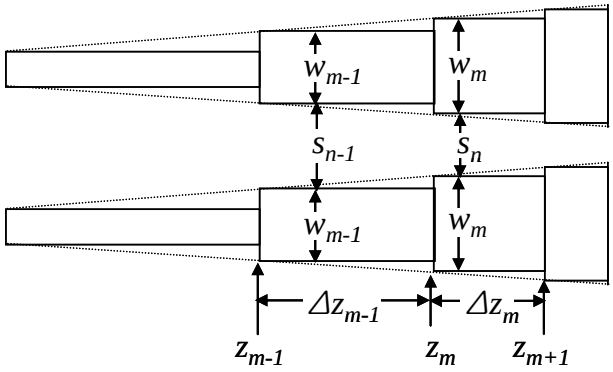

(b)

Fig. 16 (a) Geometry of nonuniform coupled microstrip lines, (b) its numerical modeling, (c) Sets of voltage sources for the fundamental modes, (d) Voltage responses at V_{ne1} and $V_{fe1,}$ and (e) V_{ne2} and V_{fe2}

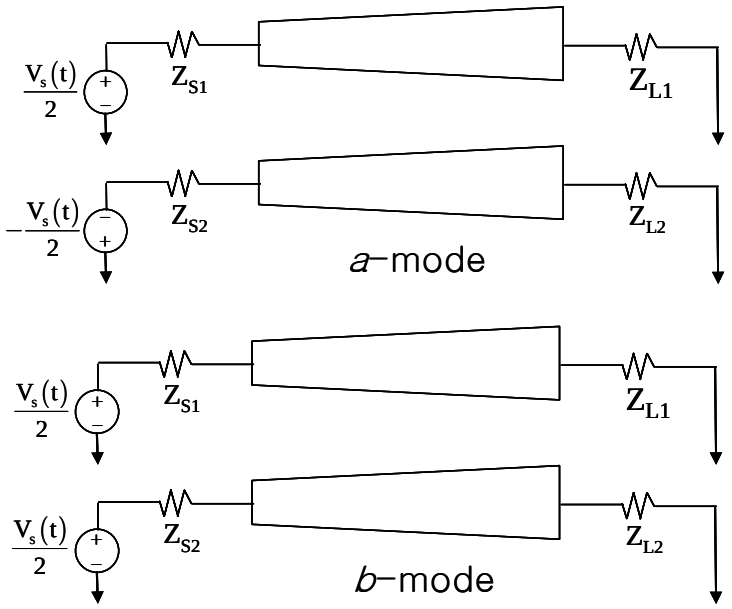

(c)

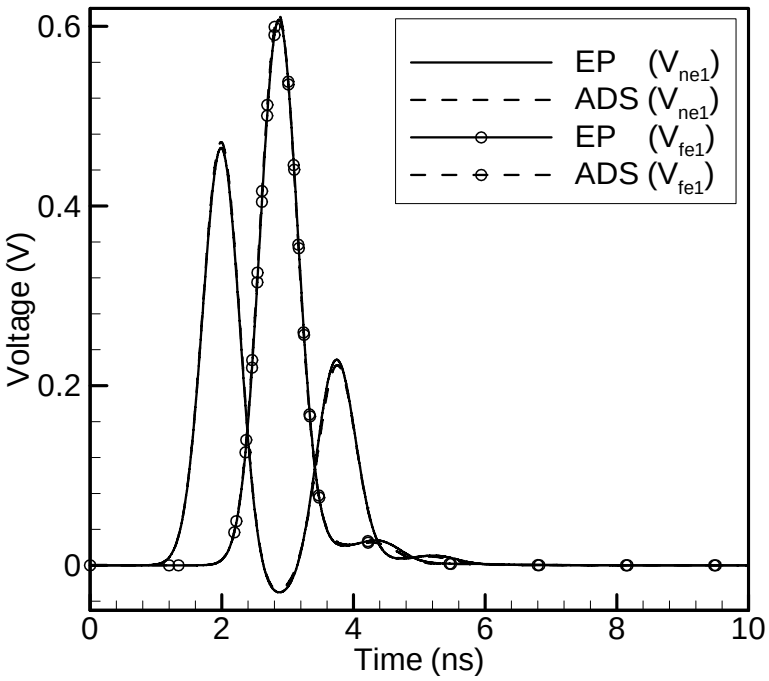

(d)

Fig. 16 Continued.

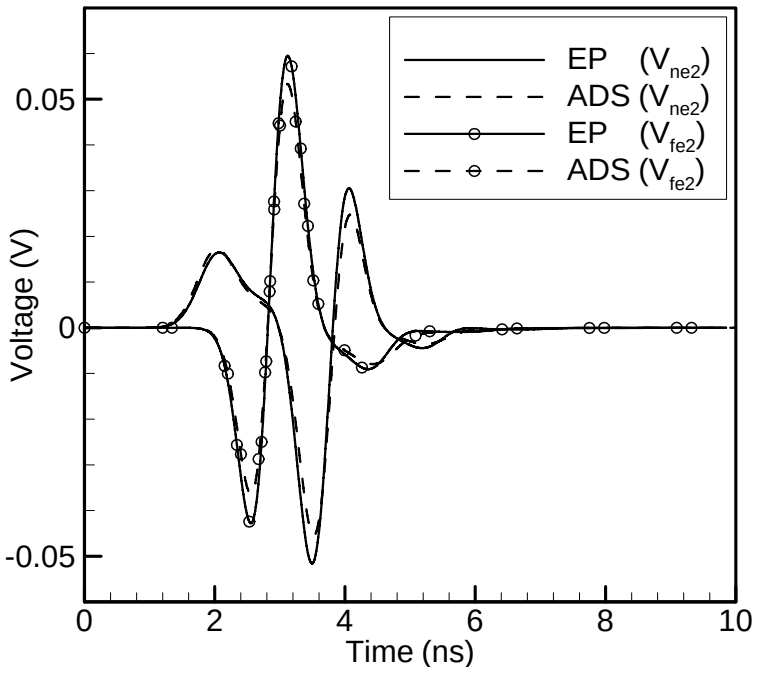

(e)

Fig. 16 Continued.

$$\left[V(z_m,\tau)\right]=\frac{1}{2}\sum_{i=a}^{b}\frac{\left[\mathrm{A}_i\right]}{p_i}\begin{Bmatrix}\left[V(z_{m,i}+\Delta z_{m,i})+V(z_{m,i}-\Delta z_{m,i})\right]\\-Z_{m,i}\left[I(z_{m,i}+\Delta z_{m,i})-I(z_{m,i}-\Delta z_{m,i})\right]\end{Bmatrix} \quad (162)$$

$$\left[I(z_m,\tau)\right]=\frac{1}{2}\sum_{i=a}^{b}\frac{\left[\mathrm{A}_i\right]}{p_i}\begin{Bmatrix}\left[I(z_{m,i}+\Delta z_{m,i})+I(z_{m,i}-\Delta z_{m,i})\right]\\-\frac{1}{Z_{m,i}}\left[V(z_{m,i}+\Delta z_{m,i})-V(z_{m,i}-\Delta z_{m,i})\right]\end{Bmatrix} \quad (163)$$

The phase velocity ($v_{m,a}$, $v_{m,b}$) and characteristic impedance ($Z_{m,a}$, $Z_{m,b}$) for each mode are found in [63] and [64]. The inhomogeneous coupled microstrip lines are terminated by resistive loads ($Z_{S1}=Z_{S2}=50\Omega$, $Z_{L1}=Z_{L2}=100\Omega$) as shown in Fig 11(a). A Gaussian pulse, given in (114), serves as the source for the numerical

simulation. Each mode source is the same as that given in (128), and shown in Fig 16(c). Ten numerical points, which corresponds to ten cascaded uniform transmission-line sections, are used to obtain the propagator and ADS method results. The voltage response at the near and far ends of the non-uniform transmission line section is shown in Fig. 16(d,e). Good agreement with the results obtained with ADS is observed in both cases.

3.9. Summary

As an extension of the analytical and numerical methods described chapter II, this chapter presents analytical and simple closed-form solutions to the lossless multiconductor transmission line. Mathematical models were developed for TEM and quasi-TEM lines. Both techniques shows that the present time voltage (current) is found by taking simple sum and difference combination of the previous time voltage and current amplitdude. The set of solution for quasi-TEM lines can be reduced to solution of TEM lines when the phase velocity and impedauce of each mode are identical. These explicit sets of equations are simple to implement numerically and has been shown to give good results with TEM lines and with quasi-TEM lines.

CHAPTER IV

TIME DOMAIN GREEN'S FUNCTION AND PROPAGATOR FOR MAXWELL'S EQUATIONS [*]

The free space time domain propagator and corresponding dyadic Green's function for Maxwell's differential equations are derived in 1-, 2-, and 3-dimensions using the propagator method. The propagator method reveals terms that contribute in the source region, which to our knowledge have not been previously reported in the literature (Section 1.3). It is shown that these terms are necessary to satisfy the initial condition, that the convolution of the Green's function with the field must identically approach the initial field as the time interval approaches zero. It is also shown that without these terms, Huygen's principle cannot be satisfied. To illustrate the value of this Green's function two analytical examples are presented, that of a propagating plane wave and of a radiating point source. An accurate propagator is the key element in the time domain path integral formulation for the electromagnetic field.

4.1. Maxwell's equations

In a homogeneous region the time domain Maxwell curl equations in terms of the electric and magnetic field intensities, $\mathbf{E}$ and $\mathbf{H}$, and the electric and magnetic current

[*] © 2004 IEEE. Parts of this chapter are reprinted, with permission, from R. Nevels and J. Jeong, "The Time Domain Green's Function and Propagator for Maxwell's Equations," *IEEE Trans. Antennas Propagat.*, vol. 52, No.11, pp. 3012-3018, Nov. 2004.

densities $\mathbf{J}_e$ and $\mathbf{J}_m$ are given by

$$\varepsilon \frac{\partial \mathbf{E}}{\partial t} = \nabla \times \mathbf{H} - \mathbf{J}_e \tag{164}$$

$$\mu \frac{\partial \mathbf{H}}{\partial t} = -\nabla \times \mathbf{E} - \mathbf{J}_m \tag{165}$$

where μ, ε are respectively the permeability and permittivity in a homogeneous region. Eqns. (164) and (165) can be expressed as the general matrix equation

$$\frac{\partial \mathbf{F}}{\partial t} - \bar{\mathbf{S}} \cdot \mathbf{F} = -\mathbf{J} \tag{166}$$

which has a vector field $\mathbf{F}$ and vector current $\mathbf{J}$, defined by

$$\mathbf{F} = \begin{bmatrix} E_x & E_y & E_z & H_x & H_y & H_z \end{bmatrix}^T, \qquad \mathbf{J} = \begin{bmatrix} \mathbf{J}_e / \varepsilon & \mathbf{J}_m / \mu \end{bmatrix}^T \tag{167}$$

and $\bar{\mathbf{S}}$ is a 6×6 matrix of differential operators, symbolically represented by

$$\bar{\mathbf{S}} = \begin{bmatrix} 0 & \frac{1}{\varepsilon} \nabla \times \\ -\frac{1}{\mu} \nabla \times & 0 \end{bmatrix} \tag{168}$$

4.2. Time domain Green's function and propagator

The goal is to solve Eqn. (166) to find the field $\mathbf{F}(\mathbf{r}, t)$. To this end a free space dyadic Green's function $\bar{\mathbf{G}}(\mathbf{r}, t \,|\, \mathbf{r}', t')$, a 6×6 matrix of elements, must be found. Once $\bar{\mathbf{G}}$ is known, the present time field $\mathbf{F}(\mathbf{r}, t)$ is determined by [42]

$$\mathbf{F}(\mathbf{r},t)=\int_{v}\int_{t_o}^{t+}\bar{\mathbf{G}}(\mathbf{r},t\,|\,\mathbf{r}',t')\cdot\mathbf{J}(\mathbf{r}',t')dt'd\mathbf{r}'+\int_{v'}\bar{\mathbf{G}}(\mathbf{r},t\,|\,\mathbf{r}',t_o)\cdot\mathbf{F}_o(\mathbf{r}')d\mathbf{r}'$$
$$+\int_{s}\int_{t_o}^{t+}\hat{\mathbf{n}}\times\left[\bar{\mathbf{G}}(\mathbf{r},t\,|\,\mathbf{r}',t')\cdot\mathbf{F}_s(\mathbf{r}',t')\right]dt'd\mathbf{s}' \tag{169}$$

The first integral above is the contribution to the present time field due to the current $\mathbf{J}(\mathbf{r},t)$. Generally the time t_o is taken to be the turn on time of the current $\mathbf{J}$, but $\mathbf{F}(\mathbf{r},t)$ t_o can be $-\infty$.The second integral is the present time field contribution due to the initial field $\mathbf{F}(\mathbf{r},t_o)\doteq\mathbf{F}_o(\mathbf{r})$ prescribed for a volume of space at t_o. The third integral in (169) accounts for the contribution from the field on the surface *s* bounding the volume of space in which the present time field is to be found. Extending the volume to infinity causes this term to go to zero due to the radiation condition. For convenience the field vector in this expression is modified by the addition of the medium parameters according to,

$$\mathbf{F}_s=\left[\varepsilon E_x\quad \varepsilon E_y\quad \varepsilon E_z\quad -\mu H_x\quad -\mu H_y\quad -\mu H_z\right]^T \tag{170}$$

If all that needs to be known is the time evolution of the field, then given the initial field throughout space, it is sufficient to find a dyadic propagator $\bar{\mathbf{K}}(\mathbf{r},t\,|\,\mathbf{r}',t')$ that determines the present time field through

$$\mathbf{F}(\mathbf{r},t)=\int_{v'}\bar{\mathbf{K}}(\mathbf{r},t\,|\,\mathbf{r}',t_o)\cdot\mathbf{F}_o(\mathbf{r}')d\mathbf{r}' \tag{171}$$

The propagator can be obtained by solving the homogeneous equation

$$\frac{\partial \bar{\mathbf{K}}}{\partial t} - \bar{\mathbf{S}} \cdot \bar{\mathbf{K}} = 0, \qquad t > t' \tag{172}$$

subject to

$$\bar{\mathbf{K}}(\mathbf{r}, t' \,|\, \mathbf{r}', t') = \bar{\mathbf{I}}\delta(\mathbf{r} - \mathbf{r}'), \quad \text{(at time } t = t'\text{)}, \tag{173}$$

$$\bar{\mathbf{K}} \to 0, \quad \text{as } |\mathbf{r}| \to \infty \tag{174}$$

Eqn. (172) along with the conditions (173) and (174) form what is known as the propagator method [42]. The propagator is a solution to the homogeneous equation (172), therefore it is not the Green's function, which is a solution to the inhomogeneous equation

$$\frac{\partial \bar{\mathbf{G}}}{\partial t} - \bar{\mathbf{S}} \cdot \bar{\mathbf{G}} = \bar{\mathbf{I}}\delta(\mathbf{r} - \mathbf{r}')\delta(t - t') \tag{175}$$

The relationship between the propagator and the Green's function is (see APPENDIX C)

$$\bar{\mathbf{G}}(\mathbf{r}, t \,|\, \mathbf{r}', t') = U(t - t')\bar{\mathbf{K}}(\mathbf{r}, t \,|\, \mathbf{r}', t') \tag{176}$$

where the unit step function,

$$U(t - t') = \begin{cases} 0, & t < t' \\ 1, & t > t' \end{cases} \tag{177}$$

enforces causality. Although the dyadic Green's function can be found using an eigenfunction expansion method [38], eigenfunction expansion can be tedious, not to mention the necessity of acquiring specialized knowledge of several indigenous rules and procedures. For these reasons a much more straightforward plan is to solve (172) subject to (173) and (174) with the additional requirement that causality is enforced

through (176).

To solve (172), $\bar{\mathbf{K}}$ is expressed as a Fourier integral in terms of its spectral (or phase-space) dependence $\mathbf{k}$,

$$\bar{\mathbf{K}}(\mathbf{r},t\,|\,\mathbf{r}',t') = \int_{-\infty}^{\infty} \bar{\mathbf{K}}_p(\mathbf{k},t,\mathbf{r},t')e^{j\mathbf{k}\cdot\mathbf{r}}d\mathbf{k} \tag{178}$$

where in Cartesian coordinates $\mathbf{k} = k_x\hat{\mathbf{x}} + k_y\hat{\mathbf{y}} + k_z\hat{\mathbf{z}}$ and the differential $d\mathbf{k} = dk_x dk_y dk_z$ are in terms of the spatial frequency components k_x, k_y, k_z and, in the exponent, $\mathbf{r} = x\hat{\mathbf{x}} + y\hat{\mathbf{y}} + z\hat{\mathbf{z}}$. Substituting (178) into (172) yields

$$\int_{-\infty}^{\infty}\left[\frac{\partial\bar{\mathbf{K}}_p}{\partial t} - \bar{\mathbf{S}}_p\bar{\mathbf{K}}_p\right]e^{j\mathbf{k}\cdot\mathbf{r}}d\mathbf{k} = 0 \tag{179}$$

where the 6×6 matrix operator $\bar{\mathbf{S}}_p$, the spectral domain dual of (168), can again be expressed symbolically, in this case in terms of algebraic quantities, by

$$\bar{\mathbf{S}}_p(\mathbf{k}) = \begin{bmatrix} 0 & \frac{1}{\varepsilon}\mathbf{k}\times \\ -\frac{1}{\mu}\mathbf{k}\times & 0 \end{bmatrix} \tag{180}$$

Eqn. (179) yields the time dependence of $\bar{\mathbf{K}}_p$:

$$\frac{\partial\bar{\mathbf{K}}_p}{\partial t} - \bar{\mathbf{S}}_p\bar{\mathbf{K}}_p = 0 \tag{181}$$

By substitution it can be shown that a solution to (181) is

$$\bar{\mathbf{K}}_p = e^{\bar{\mathbf{S}}_p t}\bar{\mathbf{K}}_o \tag{182}$$

Substituting (182) into (178), enforcing (173) and using the standard Fourier transform representation of the delta function then gives

$$\int_{-\infty}^{\infty} e^{\bar{\mathbf{S}}_p t'} \bar{\mathbf{K}}_o e^{j\mathbf{k}\cdot\mathbf{r}} d\mathbf{k} = \delta(\mathbf{r}-\mathbf{r}') = \frac{1}{(2\pi)^3} \int_{-\infty}^{\infty} e^{j\mathbf{k}\cdot(\mathbf{r}-\mathbf{r}')} d\mathbf{k} \tag{183}$$

Equating coefficients of $\exp(j\mathbf{k}\cdot\mathbf{r})$ in (183), and substituting the result into (182), yields

$$\bar{\mathbf{K}}_p = \frac{1}{(2\pi)^3} e^{-\bar{\mathbf{S}}_p \tau} e^{-j\mathbf{k}\cdot\mathbf{r}'} \tag{184}$$

Here, for brevity, we write $\tau = t - t'$, which is the time increment between the initial and present time. Finally, substituting (184) into (178) yields the propagator

$$\bar{\mathbf{K}} = \frac{1}{(2\pi)^3} \int_{-\infty}^{\infty} e^{\bar{\mathbf{S}}_p \tau} e^{j\mathbf{k}\cdot(\mathbf{r}-\mathbf{r}')} d\mathbf{k} \tag{185}$$

The exponential matrix term $e^{\bar{\mathbf{S}}_p \tau}$ can be expanded in the power series

$$e^{\bar{\mathbf{S}}_p \tau} = \bar{\mathbf{I}} + \bar{\mathbf{S}}_p \tau + \bar{\mathbf{S}}_p^2 \tau^2 / 2! + \bar{\mathbf{S}}_p^3 \tau^3 / 3! + \cdots \tag{186}$$

When the matrices on the right hand side of (186) are summed, a new 6×6 "evolution operator" matrix $e^{\bar{\mathbf{S}}_p \tau} = \bar{\mathbf{A}}(t, \mathbf{k})$ is created. The power series formed by summing the components of the $\bar{\mathbf{A}}$ matrix yield surprisingly simple closed form expressions:

$$A_{11} = A_{44} = \left[k_x^2 + \left(k_y^2 + k_z^2 \right) \cos(kc\tau) \right] / k^2$$

$$A_{22} = A_{55} = \left[k_y^2 + \left(k_x^2 + k_z^2 \right) \cos(kc\tau) \right] \Big/ k^2$$

$$A_{33} = A_{66} = \left[k_z^2 + \left(k_x^2 + k_y^2 \right) \cos(kc\tau) \right] \Big/ k^2$$

$$A_{12} = A_{21} = A_{45} = A_{54} = k_x k_y \left[1 - \cos(kc\tau) \right] \Big/ k^2$$

$$A_{13} = A_{31} = A_{46} = A_{64} = k_x k_z \left[1 - \cos(kc\tau) \right] \Big/ k^2$$

$$A_{23} = A_{32} = A_{56} = A_{65} = k_y k_z \left[1 - \cos(kc\tau) \right] \Big/ k^2$$

$$A_{15} = -A_{24} = -\eta^2 A_{42} = \eta^2 A_{51} = -\, jk_z \eta \sin(kc\tau)/k$$

$$A_{16} = -A_{34} = -\eta^2 A_{43} = \eta^2 A_{61} = \, jk_y \eta \sin(kc\tau) \big/ k$$

$$A_{26} = -A_{35} = -\eta^2 A_{53} = \eta^2 A_{62} = -\, jk_x \eta \sin(kc\tau)/k$$

$$A_{14} = A_{25} = A_{36} = A_{41} = A_{52} = A_{63} = 0 \qquad (187)$$

where $k^2 = k_x^2 + k_y^2 + k_z^2$ and $c = 1 \big/ \sqrt{\mu\varepsilon}$ and $\eta = \sqrt{\mu/\varepsilon}$ are respectively the phase velocity and intrinsic impedance of the homogeneous medium.

The evolution operator matrices, $\bar{\mathbf{A}}$, for the 1- and 2-dimensional cases can be found by respectively setting two and one of the spectral variables k_x, k_y, k_z in (187) to zero. Unfortunately, the 3-dimensional propagator, which now has the form

$$\bar{\mathbf{K}}(\mathbf{r}, t \,|\, \mathbf{r}', t') = \int_{-\infty}^{\infty} \bar{\mathbf{A}}(t, \mathbf{k}) e^{j\mathbf{k}\cdot(\mathbf{r}-\mathbf{r}')} d\mathbf{k} \qquad (188)$$

once evaluated, can not be readily reduced to the 1- or 2-D propagators. For this reason the 1-, 2- and 3-D cases are presented separately below.

4.3. One-dimensional Green's functions $\bar{\mathbf{G}}^{(1)}$

Consider the case in which $k_x = k_y = 0$. Because this is a one-dimensional field, $k \to k_z$, $1/(2\pi)^3 \to 1/(2\pi)$ and

$$\mathbf{F} = \begin{bmatrix} E_x & H_y \end{bmatrix}^T \tag{189}$$

Eqn. (188) becomes

$$\bar{\mathbf{K}}^{(1)} = \frac{1}{2\pi} \int_{-\infty}^{\infty} \begin{bmatrix} \cos(k_z c\tau) & -j\eta \sin(k_z c\tau) \\ \frac{-j}{\eta} \sin(k_z c\tau) & \cos(k_z c\tau) \end{bmatrix} e^{jk_z(z-z')} dk_z \tag{190}$$

The four matrix elements in brackets are the 1-D forms of the A_{11}, A_{15}, A_{51}, and A_{55} components of (187) above. The integrals in eqn. (190) can be easily evaluated, giving

$$\begin{aligned} \bar{\mathbf{G}}^{(1)} &= U(\tau)\bar{\mathbf{K}}^{(1)} \\ &= \frac{U(\tau)}{2} \begin{bmatrix} [\delta(\mathbf{z}+c\tau)+\delta(\mathbf{z}-c\tau)] & -\eta[\delta(\mathbf{z}+c\tau)-\delta(\mathbf{z}-c\tau)] \\ -[\delta(\mathbf{z}+c\tau)-\delta(\mathbf{z}-c\tau)]/\eta & [\delta(\mathbf{z}+c\tau)+\delta(\mathbf{z}-c\tau)] \end{bmatrix} \end{aligned} \tag{191}$$

where δ represents the Dirac delta function, and for brevity we have defined $\mathbf{z} = z - z'$.

Because the spatial dependence of the 1-D Green's function is entirely contained in delta functions, Eqn. (169) can be easily evaluated giving

$$\begin{bmatrix} E_x(z,t) \\ H_y(z,t) \end{bmatrix} = \frac{U(\tau)}{2} \begin{bmatrix} [E_{xo}(z+c\tau)+E_{xo}(z-c\tau)] & -\eta[H_{yo}(z+c\tau)-H_{yo}(z-c\tau)] \\ -[E_{xo}(z+c\tau)-E_{xo}(z-c\tau)]/\eta & [H_{yo}(z+c\tau)+H_{yo}(z-c\tau)] \end{bmatrix} \tag{192}$$

where a zero in the subscript designates the initial fields. This result, which is the D'Alembert solution for a set of coupled functions, can be interpreted as follows: The field at time *t* at a point *z* in 1-D is determined by simple algebraic combinations of the fields that existed at the previous time t' at the points $z \pm c\tau \doteq z \pm \Delta z$. Even though (192) appears to be a numerical expression, it is in fact an exact solution to (169) and can be applied at the Courant limit without numerical dispersion [51].

4.4. Two-dimensional Green's functions $\bar{\mathbf{G}}^{(2)}$

As an example, take the 2-D TM to *z* case where all fields are zero except $E_z, H_x,$ and H_y. Expressed succinctly as the field vector

$$\mathbf{F} = \begin{bmatrix} E_z & H_x & H_y \end{bmatrix}^T \tag{193}$$

Setting H_y k_z to zero and replacing $1/(2\pi)^3 \rightarrow 1/(2\pi)^2$, $A_{33} \rightarrow A_{11}^{(2)}$, $A_{34} \rightarrow A_{12}^{(2)}$, $A_{35} \rightarrow A_{13}^{(2)}$, $A_{43} \rightarrow A_{21}^{(2)}$, $A_{44} \rightarrow A_{22}^{(2)}$, $A_{45} \rightarrow A_{23}^{(2)}$, $A_{53} \rightarrow A_{31}^{(2)}$, $A_{54} \rightarrow A_{32}^{(2)}$, $A_{55} \rightarrow A_{33}^{(2)}$ in equations (187) results in the creation of a 3×3 2-D evolution operator matrix $\bar{\mathbf{A}}^{(2)}$. Each element of the evolution operator matrix determines a corresponding 2-D propagator matrix element $K_{mn}^{(2)}$, obtained by evaluating (188). For example

$$K_{11}^{(2)} = \frac{1}{(2\pi)^2} \int_{k_x=-\infty}^{\infty} \int_{k_y=-\infty}^{\infty} \cos(kc\tau) e^{jk_x(x-x')} e^{jk_y(y-y')} dk_x dk_y \tag{194}$$

where $k = \sqrt{k_x^2 + k_y^2}$, when evaluated results in the Green's function

$$G_{11}^{(2)} = U(\tau)K_{11}^{(2)} = \frac{U(\tau)}{2\pi}\left\{\frac{\delta(c\tau-\rho)}{\sqrt{(c\tau)^2-\rho^2}} - \frac{(c\tau)U(c\tau-\rho)}{\left[(c\tau)^2-\rho^2\right]^{3/2}}\right\} \tag{195}$$

The remaining terms of the Green's function matrix, which are evaluated with the help of identities found in [65,66], are:

$$G_{12}^{(2)} = \frac{\eta U(\tau)}{2\pi}\left\{\frac{\delta(c\tau-\rho)}{\sqrt{(c\tau)^2-(\rho)^2}} - \frac{\rho U(c\tau-\rho)}{\left[(c\tau)^2-(\rho)^2\right]^{3/2}}\right\}\sin\phi \tag{196}$$

$$G_{13}^{(2)} = \frac{\eta U(\tau)}{2\pi}\left\{-\frac{\delta(c\tau-\rho)}{\sqrt{(c\tau)^2-(\rho)^2}} + \frac{\rho U(c\tau-\rho)}{\left[(c\tau)^2-(\rho)^2\right]^{3/2}}\right\}\cos\phi \tag{197}$$

$$G_{21}^{(2)} = G_{13}^{(2)}/\eta^2 \tag{198}$$

$$\begin{aligned} G_{22}^{(2)} = {} & \frac{\delta(\rho)U(\tau)\cos^2\phi}{2\pi\rho} + \frac{U(\tau)\sin^2\phi}{2\pi}\left\{\frac{\delta(c\tau-\rho)}{\sqrt{(c\tau)^2-\rho^2}} - \frac{(c\tau)U(c\tau-\rho)}{\left[(c\tau)^2-\rho^2\right]^{3/2}}\right\} \\ & - \frac{\cos(2\phi)}{2\pi}\left\{\frac{1}{\rho^2} + \frac{U(c\tau-\rho)}{\sqrt{(c\tau)^2-\rho^2}\left[c\tau+\sqrt{(c\tau)^2-\rho^2}\right]}\right\} \end{aligned} \tag{199}$$

$$G_{23}^{(2)} = \frac{U(\tau)\sin(2\phi)}{2\pi}\left\{ \frac{\delta(\rho)}{2\rho} + \frac{\delta(c\tau-\rho)}{2\sqrt{(c\tau)^2-\rho^2}} - \frac{(c\tau)U(c\tau-\rho)}{2\left[(c\tau)^2-\rho^2\right]^{3/2}} \right.$$
$$\left. - \frac{1}{\rho^2} - \frac{U(c\tau-\rho)}{\sqrt{(c\tau)^2-\rho^2}\left[c\tau+\sqrt{(c\tau)^2-\rho^2}\right]} \right\} \tag{200}$$

$$G_{31}^{(2)} = G_{13}^{(2)} / \eta^2 \tag{201}$$

$$G_{32}^{(2)} = G_{23}^{(2)} \tag{202}$$

$$G_{33}^{(2)} = \frac{\delta(\rho)U(\tau)\sin^2\phi}{2\pi\rho} + \frac{U(\tau)\cos^2\phi}{2\pi}\left\{ \frac{\delta(c\tau-\rho)}{\sqrt{(c\tau)^2-\rho^2}} - \frac{(c\tau)U(c\tau-\rho)}{\left[(c\tau)^2-\rho^2\right]^{3/2}} \right\}$$
$$+ \frac{U(\tau)\cos(2\phi)}{2\pi}\left\{ \frac{1}{\rho^2} + \frac{U(c\tau-\rho)}{\sqrt{(c\tau)^2-\rho^2}\left[c\tau+\sqrt{(c\tau)^2-\rho^2}\right]} \right\} \tag{203}$$

Although these equations are in a relatively compact analytical form, unfortunately they have the awkward property of being non-integrable across the singularities at $\rho = 0$ and $\rho = c\tau$. Away from the singularities these expressions are well defined, but this is of little consequence in evaluating (188). It must therefore be concluded that for all practical purposes the 2-D time domain Maxwell equation Green's functions cannot be used to analytically obtain 2-D electromagnetic field solutions. However, it is noted that it is possible to solve Eqn. (188) numerically provided the 2-D Green's functions are left in integral form [50].

4.5. Three-dimensional Green's functions $\bar{\mathbf{G}}^{(3)}$

The 3-D Green's function is found by evaluating all components of the 6×6 propagator matrix Eqn. (188). For example

$$
\begin{aligned}
K_{11}^{(3)} &= \frac{1}{(2\pi)^3}\int_0^{\infty}\left[\frac{k_x^2+\left(k_y^2+k_z^2\right)\cos\left(kc\tau\right)}{k^2}\right]e^{j\mathbf{k}\bullet(\mathbf{r}-\mathbf{r}')}d\mathbf{k} \\
&= \left[\frac{\delta(c\tau+R)-2\delta(R)+\delta(c\tau-R)}{4\pi R^2}+\frac{\mathrm{sgn}(R)U(c\tau-|R|)}{4\pi R^3}\right]\left[1-\frac{3(x-x')^2}{R^2}\right] \\
&+\left[\frac{\delta'(c\tau+R)-2\delta'(R)-\delta'(c\tau-R)}{4\pi R}\right]\frac{(x-x')^2}{R^2}-\left[\frac{\delta'(c\tau+R)}{4\pi R}-\frac{\delta'(c\tau-R)}{4\pi R}\right]
\end{aligned}
\tag{204}
$$

where

$$(\mathbf{r}-\mathbf{r}') = (x-x')\hat{\mathbf{x}}+(y-y')\hat{\mathbf{y}}+(z-z')\hat{\mathbf{z}},$$

$$R = \left[\left(x-x'\right)^2+\left(y-y'\right)^2+\left(z-z'\right)^2\right]^{1/2}$$

$$\mathrm{sgn}(R) = \begin{cases} +1, R>0 \\ -1, R<0 \end{cases} \tag{205}$$

By rejecting nonphysical solutions, where 6×6 $R<0$, we get

$$
\begin{aligned}
K_{11}^{(3)} &= \left[\frac{\delta(c\tau-R)-\delta(R)}{4\pi R^2}+\frac{U(c\tau-R)-U(-R)}{4\pi R^3}\right]\left[1-\frac{3(x-x')^2}{R^2}\right] \\
&-\left[\frac{\delta'(c\tau-R)-\delta'(R)}{4\pi R}\right]\frac{(x-x')^2}{R^2}+\frac{\delta'(c\tau-R)}{4\pi R}
\end{aligned}
\tag{206}
$$

Arguments concerning which terms from (204) should be retained in (206) have both a mathematical and physical basis. Because of the initial condition $\tau>0$ and the

physical requirement $R > 0$, unit step and delta functions with the argument $(c\tau + R)$ in (204) do not contribute to the volume integrals in (169) and are therefore dropped. Removal of factors of 2 in front of the unit step and delta functions acting at the origin is suggested by the spatial symmetry of the expression in (204) and can be justified by applying the mathematical identities

$$\delta'(R) = -\delta(R)/R, \qquad U(R)\delta(R) = \delta(R)/2 \tag{207}$$

The components of the 3-D Green's function matrix in compact form are

$$G_{11}^{(3)} = G_{44}^{(3)} = L\left[1 - \frac{3(x-x')^2}{R^2}\right] + S\left(\frac{x-x'}{R}\right)^2 + T$$

$$G_{22}^{(3)} = G_{55}^{(3)} = L\left[1 - \frac{3(y-y')^2}{R^2}\right] + S\left(\frac{y-y'}{R}\right)^2 + T$$

$$G_{33}^{(3)} = G_{66}^{(3)} = L\left[1 - \frac{3(z-z')^2}{R^2}\right] + S\left(\frac{z-z'}{R}\right)^2 + T$$

$$G_{12}^{(3)} = G_{21}^{(3)} = G_{45}^{(3)} = G_{54}^{(3)} = -L\left[\frac{3(x-x')(y-y')}{R^2}\right] + S\left[\frac{(x-x')(y-y')}{R^2}\right]$$

$$G_{13}^{(3)} = G_{31}^{(3)} = G_{46}^{(3)} = G_{64}^{(3)} = -L\left[\frac{3(x-x')(z-z')}{R^2}\right] + S\left[\frac{(x-x')(z-z')}{R^2}\right]$$

$$G_{23}^{(3)} = G_{32}^{(3)} = G_{56}^{(3)} = G_{65}^{(3)} = -L\left[\frac{3(y-y')(z-z')}{R^2}\right] + S\left[\frac{(y-y')(z-z')}{R^2}\right]$$

$$G_{15}^{(3)} = -G_{24}^{(3)} = -\eta^2 G_{42}^{(3)} = \eta^2 G_{51}^{(3)} = \eta P \frac{z-z'}{R}$$

$$G_{16}^{(3)} = -G_{34}^{(3)} = -\eta^2 G_{43}^{(3)} = \eta^2 G_{61}^{(3)} = -\eta P \frac{y-y'}{R}$$

$$G_{26}^{(3)} = -G_{35}^{(3)} = -\eta^2 G_{53}^{(3)} = \eta^2 G_{62}^{(3)} = \eta P \frac{x - x'}{R}$$

$$G_{14}^{(3)} = G_{25}^{(3)} = G_{36}^{(3)} = G_{41}^{(3)} = G_{52}^{(3)} = G_{63}^{(3)} = 0 \tag{208}$$

where

$$L = U(\tau)\left[\frac{\delta(c\tau - R) - \delta(R)}{4\pi R^2} + \frac{U(c\tau - R) - U(-R)}{4\pi R^3}\right] \tag{209}$$

$$S = U(\tau)\left[\frac{-\delta'(c\tau - R) - \delta'(R)}{4\pi R}\right] \tag{210}$$

$$T = \frac{U(\tau)\delta'(c\tau - R)}{4\pi R} \tag{211}$$

$$P = U(\tau)\left[\frac{\delta(c\tau - R)}{4\pi R^2} + \frac{\delta'(c\tau - R)}{4\pi R}\right] \tag{212}$$

Eqns. (208) for the free space Maxwell equation Green's function can also be expressed in the compact dyadic form as

$$\bar{\mathbf{G}} = \begin{bmatrix} \bar{\mathbf{G}}_{11} & \bar{\mathbf{G}}_{12} \\ \bar{\mathbf{G}}_{21} & \bar{\mathbf{G}}_{22} \end{bmatrix} \tag{213}$$

with

$$\bar{\mathbf{G}}_{11} = \bar{\mathbf{G}}_{22} = -\frac{\delta'(c\tau - R)}{4\pi R}\bar{\mathbf{I}} - \nabla\nabla\frac{[U(c\tau - R) - U(-R)]}{4\pi R} \tag{214}$$

$$\bar{\mathbf{G}}_{12} = -\eta^2 \bar{\mathbf{G}}_{21} = \nabla \times \frac{\eta\delta(c\tau - R)}{4\pi R}\bar{\mathbf{I}} \tag{215}$$

where $\bar{\mathbf{I}}$ is the identity matrix and $U(\tau)$ has been suppressed. The term $U(-R)$ in (214) does not appear in the Maxwell equation Green's function reported elsewhere

(e.g. [40]). It will be shown below that $U(-R)$ is not needed if the field is due entirely to a current element, the case considered in [40]. However, it must be retained when the field is determined from an initial field distribution, as is the case for the second and third integrals in (169).

This completes the derivation of the 1-, 2- and 3-D free space dyadic Green's functions for Maxwell's equations. In the following section it is shown that the above equations satisfy the limiting conditions given in (173) and (174). Examples are presented in which the propagated field is found given an initial field and the radiated field is determined given an initial current.

4.6. Verification and examples

The Green's functions above can be verified by showing that the initial condition, Eqn. (173), and the radiation condition, Eqn. (174) are satisfied. The radiation condition presents only a few difficulties. In 1-D the delta function components acting at infinity yield no contribution. In 2- and 3-D pervasive $1/\rho$ and $1/R$ multipliers cause each term to go to zero as the causal radius approaches infinity.

Showing that the initial condition is satisfied is more problematic. In 1-D the condition $c\tau \to 0$ readily leads to the expected delta functions in the diagonal components and to off diagonal components that are zero in the Green's function matrix in (191). In 2-D, the problem of a singularity intersecting and delta function prevents any realistic conclusions. In 3-D as $c\tau \to 0$ all off diagonal terms in (208) go to zero due to cancellation of like delta functions and the fact that all unit step functions vanish in the

limit. All diagonal terms become delta functions as expected. For example

$$G_{11}^{(3)} \xrightarrow[c\tau\to 0]{\lim} -\frac{\delta'(R)}{4\pi R} = \frac{\delta(R)}{4\pi R^2} \tag{216}$$

which is unity when integrated over a spherical volume of radius *R*.

As an example of an application of (169), assume that there is no initial current and that the initial field is a plane wave with unity amplitude

$$E_{xo} = \cos\left(\omega t - kz\right) = \cos\left(\omega t - kr\cos\theta\right) \tag{217}$$

with $H_{yo} = E_{xo}/\eta$. The first integral in (169) is eliminated due to lack of an initial current and the last integral goes to zero as the surface enclosing the volume of space under consideration approaches infinity. The second integral becomes

$$E_x(\mathbf{r},t) = \int_{v'}\left(G_{11}^{(3)}(\mathbf{r},t\,|\,\mathbf{r}',t') + G_{15}^{(3)}(\mathbf{r},t\,|\,\mathbf{r}',t')/\eta\right)E_{xo}(\mathbf{r}',t')d\mathbf{r}' \tag{218}$$

Inserting the Green's function components into (218) and expressing the resulting equation in spherical coordinates with $c\tau \doteq r_o$, $\tau = t - t_o$, and $a \doteq \omega t$ gives

$$\begin{aligned} E_x(\mathbf{r},t) = \int_{v'}\Bigg\{&\left[\frac{\delta(r_o-r')-\delta(r')}{4\pi r'^2} + \frac{U(r_o-r')-U(-r')}{4\pi r'^3}\right]\left(1-3\sin^2\theta'\cos^2\phi'\right) \\ &-\left[\frac{\delta'(r_o-r')+\delta'(r')}{4\pi r'}\right]\sin^2\theta'\cos^2\phi' + \frac{\delta'(r_o-r')}{4\pi r'} \\ &+\left[\frac{\delta(r_o-r')}{4\pi r'^2} + \frac{\delta'(r_o-r')}{4\pi r'}\right]\cos\theta'\Bigg\}\cos\left(a - kr'\cos\theta'\right)dv' \end{aligned} \tag{219}$$

The result, after tedious calculation, is

$$
\begin{aligned}
E_x(\mathbf{r},t) = &-\cos a\left[\frac{3\sin(kr_o)}{(kr_o)^3}-\frac{3\cos(kr_o)}{(kr_o)^2}-\frac{\sin(kr_o)}{kr_o}\right] \\
&-\frac{\cos a}{3}+\cos a\left[\frac{\sin(kr_o)}{(kr_o)^3}-\frac{\cos(kr_o)}{(kr_o)^2}\right] \\
&+\cos a\left[\frac{2\sin(kr_o)}{(kr_o)^3}-\frac{2\cos(kr_o)}{(kr_o)^2}-\frac{\sin(kr_o)}{kr_o}\right]+\frac{\cos a}{3} \\
&+\cos a\cos(kr_o) \\
&+\sin a\left[\frac{\sin(kr_o)}{(kr_o)^2}-\frac{\cos(kr_o)}{kr_o}\right] \\
&-\sin a\left[\frac{\sin(kr_o)}{(kr_o)^2}-\frac{\cos(kr_o)}{kr_o}\right]+\sin a\sin(kr_o) \\
=&\cos\left(\omega t-kr_o\cos 0^o\right)=\cos\left(\omega t-kz_o\right)
\end{aligned}
\tag{220}
$$

This example demonstrates that the free space dyadic Green's function propagates a plane wave a distance determined by the product of the time increment and the free space medium velocity, i.e. $z_o = c\tau$. The first term in brackets in (220) results from evaluating the first delta function in brackets in (219). The delta function and unit step at the origin in (219) yields no contribution to the integral. The terms in the second line on the right hand side (RHS) of (220) arise from the unit step in the first bracketed term of (219). The delta function derivatives in the second bracket and the following term in (219) contribute the third and fourth lines respectively on the RHS of (220). The two delta functions in the third bracketed term in (219) respectively produce the fifth and sixth lines of (220). The manner in which the terms in (220) cancel is significant and will be discussed in the following section.

As a second application of the Maxwell equation Green's function, consider an impulsive electric current density $\mathbf{J}_e = \mathbf{p}\delta(\mathbf{r})\delta(t)$ and no initial field in the infinite volume of space. This current gives rise to the space- and time-dependent electric field

$$\mathbf{E}(\mathbf{r},t) = \bar{\mathbf{G}}_{11}(\mathbf{r},t\,|\,0,0)\cdot\mathbf{p} \tag{221}$$

where the Green's functions are as given in (208) with the replacements $z_o = c\tau$ and $R \to r$. In compact dyadic form $\bar{\mathbf{G}}_{11}(\mathbf{r},t\,|\,0,0)$ can be expressed as

$$\begin{aligned}\bar{\mathbf{G}}_{11}(\mathbf{r},t\,|\,0,0) = \left(\bar{\mathbf{I}} - 3\mathbf{rr}\right)\left[\frac{\delta(ct-r)-\delta(r)}{4\pi r^2} + \frac{U(ct-r)-U(-r)}{4\pi r^3}\right] \\ -\mathbf{rr}\left[\frac{\delta'(ct-r)+\delta'(r)}{4\pi r}\right] + \bar{\mathbf{I}}\,\frac{\delta'(ct-r)}{4\pi r}\end{aligned} \tag{222}$$

In the following section we address the physical implication of some of the terms appearing in the examples above.

4.7. Summary

In a sense, there are no surprises in the 1-D and 2-D Green's functions. The 1-D Green's function yields a present time field that depends only upon the previous time field that existed on the causal boundary $\pm\Delta z = \pm c\tau$. This is the D'Alembert solution for coupled equations. It has long been known [39] that the 2-D time domain Green's function for Helmholtz equation, which contains a delta function singularity coinciding with a pole, is a non-integrable expression. The 2-D time domain Maxwell equation dyadic Green's functions, Eqns. (195)-(203), have terms with this same ill defined mathematical behavior, which obviates physical interpretation.

However, the elements of the 3-D Green's function in (208) contain several interesting features that are revealed by the two examples in the section above. In the first example, that of a radiating current source, virtually all of the components of $G_{11}^{(3)}$ and $G_{15}^{(3)}$ are needed in order to propagate the field. In this example the unit step $U(-r)$ and delta function $\delta(r)$ do not contribute to the answer, but a $-\pi/3$ term produced by $U\left(ct-r\right)$ is cancelled by a $\pi/3$ produced by the source region term $\delta'\left(r\right)$. This shows that the source region terms are a necessary part of the Green's function in the propagator equation, the second integral in (169). The same conclusion can be drawn by a similar investigation of the third integral in Eqn. (169), which is a mathematical description of Huygens' principle

In the second example above, that of a radiating dipole, all components of the resulting field are causal, thereby restricting energy traveling outward from the source to the velocity c as expected. However, after being turned on at $t=0$, the field due to the source region terms is confined to the position of the contributing source. In this case it can be said that these terms interact only with non-radiating currents, that is, currents whose effect is not felt in the radiated field. From this example it can be concluded that when finding the field radiated by current sources, which is accomplished with the first integral in (169), it is not necessary to include the source region terms.

CHAPTER V

SUMMARY AND RECOMMENDATIONS

5.1. Summary

An exact formulation for the time domain voltage and current on a lossy transmission line and multiconductor transmission line has been presented. It is shown that the set of analytical expressions in terms of voltage and current reduce to a set of numerical equations that are easily implemented and easily extended to the nonuniform transmission line case. In addition, the method is extended to solve for Maxwell's equations. 1-D, 2-D, and 3-D Green's functions are evaluated separately and verified with initial condition and radiation condition.

In chapter II, a numerical dispersion relation was derived showing that the EP method is not subject to numerical dispersion. A special feature of this method is that it is accurate to $\mathcal{O}(h^5)$, where h is the spatial numerical grid increment, whereas 2nd order FDTD is accurate to $\mathcal{O}(h^2)$. Both methods are explicit techniques requiring a knowledge of the voltage and current at only three previous time spatial points. The primary reason for this improvement is that the FDTD method is based upon a numerical discretization of the transmission line differential equations, while EP is a numerical evaluation of the exact propagator solution to the coupled set of transmission line equations.

Accuracy is also gained with the EP method because voltage and current are calculated at each point in the numerical grid, whereas with the FDTD method voltage

and current are calculated at alternate grid points as prescribed by the Yee interleaving scheme. This translates to an increased computational burden placed on the EP method because the number of calculations of voltage and current is doubled and in the initial time step some special functions must be evaluated. However, as demonstrated with the examples, the advantage of this method is that exceptionally accurate results can be obtained even with very few grid points in the lossy transmission line section both for low and high loss as well as for the short and long line cases. It should also be noted that because the EP method voltage and current are computed at each numerical grid point and because there is no numerical dispersion, characterization of the line capacitance, inductance, characteristic impedance, and device parameters is more accurate than with the FDTD interleaving method. It is concluded that the EP method presented here is an accurate and viable alternative to other time domain methods.

In chapter III, it was demonstrated that the proposed technique is general time domain analytical solution applicable to both the TEM line and quasi-TEM line. For the TEM lines, the propagator for *N*-conductor coupled lines is derived using the propagator method and relying on the property ($[L][C] = \bar{\mathbf{I}} / v_p^{\,2}$) of homogeneous structures. The present time voltages and currents are found through a spatial convolution of the propagator with the initial voltage and current. A simple closed-form time domain solution was obtained for coupled homogeneous TEM lines. This exercise demonstrates that the propagator method can be directly applied to Telegrapher's equations giving a closed form analytical solution for the coupled transmission lines.

Results were presented in terms of the time domain line voltage on a uniform

coupled stripline, confirming the validity of the proposed EP numerical model. The nonuniform coupled stripline example showed that the set of analytical expressions in terms of voltage and current for coupled transmission lines reduce to a set of numerical equations that are easily implemented and easily extended numerically to the nonuniform transmission line case. The asymmetric three coupled stripline example is evidence that the EP analytical/numerical method is valid for any type of lossless *N* conductor coupled TEM transmission lines.

First, the eigenvalues and eigenvectors of the N x N coupling capacitance matrix for an *N*-conductor coupled line is used to find the *N*-mode inductance and capacitance vectors for air and dielectric substrates. This step is an expansion of the procedure for obtaining the even and odd mode voltages and currents from the eigenvalues and eigenvectors of the 2 x 2 capacitance matrix for a 2-conductor line. Next, the corresponding characteristic impedance and phase velocity for each mode are calculated from the N-mode capacitances. Finally, a 2N x 2N propagator matrix is found and an explicit numerical algorithm is developed to evaluate the EP equations. A direct time domain numerical method such as the one presented here does not require multiple frequency domain calculations that must be Fourier Transformed to the time domain. This is the case for most of the popular commercial transmission line codes.

A simulation of two uniform coupled microstrip lines is presented, confirming the validity of the proposed model. From the three coupled microstrip line example, it is noted that the propagator technique presented here is valid for any type of symmetrical lossless quasi-TEM line. In addition, it is shown that the set of analytial expressions in

terms of voltage and current reduce to a set of numerical equations that are easily implemented and easily extended to the nonuniform transmission line case

In chapter IV, the propagator method has been used to obtain the time domain dyadic Green's functions for Maxwell's equations in 1-, 2-, and 3-dimensions in free space. The propagator method is shown to be a straightforward procedure, relying on familiar differential and integral calculus. It is expected that in order to solve boundary value problems in electromagnetics, it will be necessary to create a propagator method that incorporates features of the eigenfunction expansion method. However, by using the propagator method one can calculate the fields directly, thereby avoiding potentials, which are a primary component of the eigenfunction expansion method.

In the 3-D case the source region Green's function terms, $\delta'(r), \delta(r), U(-r)$, to our knowledge have not been previously reported in the Section 1.3. That these terms are a necessary part of the Maxwell equation Green's function was demonstrated by allowing the time increment to approach zero thereby producing the expected identity dyadic, which could not be obtained otherwise. It was also shown by example that a given initial field, in our case a plane wave, can be accurately propagated only if the source region terms are included in the Green's function expression.

Additionally, it was also discovered that when finding the field due a current source, that portion of the field produced by the source region terms is confined to the source location. Therefore, when calculating or computing the field radiated by a current source, the source region terms need not be included in analytical or numerical methods involving the 3-D Green's function because they only interact with the non-radiating

portion of the source current.

5.2. Recommendations for future research

Since resistance and conductance for real microwave circuit area are played an important role in a multiconductor transmission line, it must be included in the propagator and it is suggested as a next step. Although it is difficult to find general solution in multiconductor lossy transmission line due to its complexty in operation matrix, it is possible to solve this problem if single lossy transmission line technique is applied.

Analysis of asymmetric coupled transmission lines in an inhomogenous medium is second area needing research. It seems that there is no problem in TEM line. Because fundamental N-mode concept can't be applied to asymmetric case in quasi-TEM line, it is important to find new modified mode concept to calculate eigenvalue and eigenvector of operator matrix.

It is also suggested to apply absorbing boundary condition (ABC) in electromagnetic field. At the boundary, to match plane wave of arbitrary incidence, polarization, and frequency, perfect matched layer (PML) is essential to adapt for propagator method. Moreover, proposed technique for electromagnetic field is ideal case. Therefore, it must include conductivity and resistivity in Maxwell's equation and find new Green's functions.

REFERENCES

[1] T. Dhaene and D. D. Zutter, “Selection of Lumped Models for Coupled Lossy Transmission Lines,” *IEEE Trans. Computer-Aided Design*,” vol. 11, no.7, pp. 805-815, July 1992.

[2] T. Komuro, “Time-Domain Analysis of Lossy Transmission Line with Arbitrary Terminal Network,” *IEEE Trans. Circuits and Systems*, vol. 38, pp. 1160-1164, Oct. 1991.

[3] F. H. Branin, “Transient Analysis of Lossless Transmission Lines,” *Proc. IEEE*, vol.55, pp. 2012-2013, Nov. 1967.

[4] A. J. Gruodis and C. S. Chang, “Coupled Lossy Transmission Line Characterization and Simulation,” *IBM J. Res. Develop.*, vol.25, pp.25-41,1981.

[5] I. M. Elfadel, H. M. Huang, A. E. Rudehli, A. Dounavis, and M. S. Nakhla, “A Comparative Study of Two Transient Analysis Algorithms for Lossy Transmission Lines with Frequency-Dependent Data,” *IEEE Trans. Advanced Packag.*, vol. 25, no.2, pp. 143-153, May 2002.

[6] S. Grivet-Talocia, H. M. Huang, A. E. Rudehli, F. Canavero, and I. M. Elfadel, “Transient Analysis of Lossy Transmission Lines: An Efficient Approach Based on the Method of Characteristics,” *IEEE Trans. Advanced Packag.*, vol. 27, no.1, pp. 45-56, Feb. 2004.

[7] Q. Xu, Mazumder P., Z. F. Li, “Transmission Line Modeling by Method of Characteristics,” *IEEE 14th Int. Conf. VLSI Design*, pp.359-364, Jan. 2001.

[8] S.Y. Lee, A. Konard, and R. Saldanha, “Lossy Transmission Line Transient Analysis by the Finite Element Method,” *IEEE Trans. Magnetics*, vol. 29, pp. 1730-1732, Mar. 1993.

[9] R. Lucic, V. Jovic and M Kurtovic, “Simulation of Electomagnetic Transients on Single Transmission Lines via the Finite Element Method,” *Int. Conf. and*

Exhibition on Electromagnetic Compatibility, EMC York 99, pp. 41-46, July 1999.

[10] S. H. You and E. F. Kuester, "Guaranteed Passive Direct Lumped-Element Modeling of Transmission Lines," *IEEE Transa. Microwave Theory Tech.*, vol. 53, no.9, pp. 2826-2834, Sep. 2005.

[11] A. Taflove and S. C. Hagness, *Computational Electromagnetics: The Finite-Difference Time-Domain Method*, 2nd edition, Boston: Artech House, 2000.

[12] X. Zhong, Y. Liu and K. K. Mel, "A New Time-Domain Method Based on the General Transmission-Line Equations," *Microwave and Optical Tech. Letters*, vol. 32, no.1, Jan. 2002.

[13] T. Sekine, K. Kobayashi, and S. Yokokawa, "Transient Analysis of Lossy Nonuniform Transmission Line Using the Finite Difference Time Domain Method," *Electronics and Communications in Japan*, Part 3, vol.85, no. 8, pp. 1018-1026, Aug. 2002.

[14] W. J. R. Hofeer, "The Transmission Line Matrix Method - Theory and Applications," *IEEE Trans. Microwave Theory Tech.*, vol. 33, no.10, pp. 882-893, Oct. 1985.

[15] A. Centeno and J. Conlay, "A Comparison of Numerical Dispersion in FDTD and TLM Algorithms," *Asia-Pacific Conf. on Applied Electromagnetics*, pp. 128-131, Shan Alam, Malaysia, July 2003.

[16] K. Lu, "An Efficient Method for Analysis of Arbitrary Nonuniform Transmission Lines," *IEEE Trans. Microwave Theory Tech.*, vol. 45, no.1, pp. 9-14, Jan. 1997.

[17] Q. Xu and P. Mazumder, "Accurate Modeling of Lossy Nouniform Transmission Lines by Using Differential Quadrature Methods," *IEEE Trans. Microwave Theory and Tech.*, vol. 50, no.10, pp. 2233-2246, Oct. 2002.

[18] R. E. Collin, *Foundations for Microwave Engineering*, Singapore: McGRAW Hill Physical and Quantum Electronics Series, 1966.

[19] A. R. Chavez, P. Moreno, J. L. Naredo, and L. Guardado, “Fast Transient Analysis of Nonuniform Multiconductor Frequency-Dependent Treansmission Lines,” *IEEE Trans. Power Delivery*, vol. 21, no.2, pp. 809-815, Apr. 2006.

[20] A. Djordjevic, and T. Sarkar, “Analysis of Time Response of Lossy Interconnects Based on Recursive Convolution Formulation,” *IEEE Trans. Circuits Syst.I*, vol. 39, no.11, pp. 879-892, Nov. 1987.

[21] A. Dounavis, R. Achar, and M. S. Nakhla, “Efficient Sensitivity Analysis of Lossy Multiconductor Transmission Lines with Nonlinear Terminations,” *IEEE Trans. Microwave Theory Tech.*, vol. 49, no.12, pp. 2292-2299, Dec. 2001.

[22] F. H. Branin, “Transient Analysis of Lossless Transmission Lines,” *Proc. IEEE*, vol.55, pp. 2012-2013, Nov. 1967.

[23] Z. F. Li, Q. W. Xu, and J. Z. Zhu, “Fast Simulation of Lossy Transmission Lines by the Modified Method of Characteristics,” *Elect. Letter*, vol. 33, no.11, pp. 942-944, May 1997.

[24] F. Romeo, and M. Santomauro, “Time-Domain Simulation of n Coupled Transmission Lines,” *IEEE Trans. Microwave Theory Tech.*, vol. MTT-35, no. 2, pp. 131-137, Feb. 1987.

[25] D. S. Gao, A. T. Yang, and S. M. Kang, “Modeling and Simulation of Interconnection Delays and Crosstalks in High-speed Integrated Circuits,” *IEEE Trans. Circutis Syst.*, vol. 37, no. 1, pp. 1-9, Jan. 1990.

[26] Q. Xu, Mazumder P., Z. F. Li, “Transmission Line Modeling by Modified Method of Characteristics,” *IEEE 14th Int. Conf. VLSI Design*, pp.359-364, Jan. 2001.

[27] S. Grivet-Talocia, H. Huang, A. E. Ruehli, F. Canavero, and I. M. Elfadel, “Transient Analysis of Lossy Transmission Lines: An Efficient Approach Based on the Method of Characteristics,” *IEEE Trans. Advanced Packag.*, vol. 27, no.1, pp. 45-56, Feb. 2004.

[28] A. Ruehli, and T. A. Johnson, *Circuit analysis computing by waveform relaxation,* in *Wiley Encyclo. of Electri. and Electro. Eng.*, J. Webster, ED. New York: Wiley. 1999, vol.3.

[29] N. Nakhla, A. Ruehli, M. Nakhla, and R. Achar, "Simulation of Coupled Interconnects Using Waveform Relaxation and Transverse Partitioning," *IEEE 13th Elect. Perform. of Electr. Packa.*, pp.25-28, Oct. 2004.

[30] S. Barmada, and M. Raugi "Transient Numerical Solution of Nonuniform MTL Equations with Nonlinear Loads by Wavelet Expansion in Time or Space Domain," *IEEE Trans. Circutis Syst. I*, vol. 47, no.8, pp. 1178-1190, Aug. 2000.

[31] S. Grivet-Talocia, "Adaptive Transient Solution of Non- uniform Multiconductor Transmission Lines Using Wavelets," *IEEE Trans. Antennas Propagat.*, vol.48, no.10, pp.1563-1573, Oct. 2000.

[32] C. R. Paul, *Analysis of Multiconductor Transmission Lines,* New York: Wiley, 1994.

[33] T. Sekine, K. Kobayashi, and S. Yokokawa, "Transient Analysis of Lossy Nonuniform Transmission Line Using the Finite Difference Time Domain Method," *Electronics and Communications in Japan*, Part 3, vol.85, no. 8, pp. 1018-1026, Aug. 2002.

[34] T. L. Lu, L. Guo, X. Cui, and X. Gu. Hagness, "Research of Experiments and the FDTD Method of Multi-condcutor Transmission Lines for Transient Analsysis," *IEEE EMC Symp.*, no. 138, pp. 708-712, 2004.

[35] A. Cheldavi, S. Safavi-Naeini, and M. Kamarei, "Time-Domain Analysis of Nonuniform Coupled Planar Lines in VLSI Circuits," *IEE Pacific Rim Conf. on Comm. Comp. and Singal Proc.*, pp. 169-172, Aug. 1999.

[36] M. K. Amirhosseini and A. Cheldavi, "Time Domain Analysis of Circulant Symmetric Coupled Transmission Lines," *IEE Proc.-Microw. Antennas Propag.*, vol. 150, no.5, pp. 325-331, Oct. 2003.

[37] H. Levine and J. Schwinger, “On the Theory of Diffraction by an Aperture in an Infinite Plane Screen. II.” *Physical Review*, Vol. 75, no. 9, May 1949, pp. 1423-1432

[38] R. E. Collin, “Dyadic Green’s Function Expansions in Spherical Coordinates,” *Electromagnetics*, vol. 6, no. 3, pp. 183-207, 1986

[39] C.-T. Tai, *Dyadic Green Functions in Electromagnetic Theory*, New York: IEEE Press, 1971

[40] P.M. Morse and H. Feshbach, *Methods of Theoretical Physics*, Vols. 1 and 2, New York: McGraw Hill, 1953

[41] L. B. Felson and N. Marcuvitz, *Radiation and Scattering of Waves*, Englewood Cliffs, NJ: Prentice-Hall, 1973

[42] T. B. Hensen and A. D. Yaghjian, *Plane-Wave Theory of Time-Domain Fields*, New York: IEEE Press,1999

[43] G. Barton, *Elements of Green’s Functions and Propagation*, Oxford: Clarendon Press, 1989

[44] R. P. Feynman and A. R. Hibbs, *Quantum Mechanics and Path Integrals*, New York: McGraw Hill, 1965

[45] C. Grosche and F. Steiner, *Handbook of Feynman Path Integrals*, Berlin: Springer, 1998

[46] M. Kac, “Some stochastic problems in physics and mathematics,” *Colloquium lectures in the pure and applied sciences*, no. 2, Magnolia Petroleum Co. and Socony Mobile Oil Co. (1956). Rocky Mountain J. of Math, 4, 497-509, 1974.

[47] S. K. Foong, “Functional integration and wave propagation,” *in Functional Integration: Basics and Applications*, Cecile DeWitt-Morette, Ed. New York: Plenum Press, 1997, pp. 97-130.

[48] L. M. Rubin, “Application of Path Integrals in Modeling Transmission Line Loss,”

IEEE Trans. Comp., Packag., Manufact. Technol. B, vol. CPMTB-19, no.4, pp. 775-788, Nov. 1996.

[49] T. Hirono, W. Lui, S. Seki, and Y. Yoshikuni, "A Three-Dimensional Fourth-Order Finite-Difference Time-Domain Scheme Using a Symplectic Integrator Propagator," IEEE Trans. Microwave Theory Tech., vol. 49, no.4, pp. 1640-1648, Sep. 2001.

[50] Z. Shao, Z. Shen, Q. He, and G. Wei, "A Generalized Higer Order Finite-Difference Time-Domain Method and Its Application in Guided-Wave Problems," IEEE Trans. Microwave Theory Tech., vol. 51, no.3, pp. 856-861, Mar. 2003.

[51] R.D. Nevels, J. A. Miller, and R. E. Miller, "A Path Integral Time-Domain Method for Electromagnetic Scattering," *IEEE Trans. Antennas Propagat.*, vol. 48, no.4, pp. 565-573, April 2000.

[52] R. Nevels and J. Miller, "A Simple Equation for Analysis of Nonuniform Transmission Lines," *IEEE Trans. Microwave Theory Tech.*, vol. 49, no.4, pp. 721-724, April 2001.

[53] J. Jeong and R. Nevels, "Novel Time Domain Analysis Technique for Lossy Nonuniform Transmission Lines," in *Antennas Propagat. Int. Symp.*, vol. 3A, pp. 848-851, July 2005.

[54] D. Pavlidis and H. L. Hartnagel, "The Design and Performance of Three-Line Microstrip Couplers," *IEEE Trans. Microwave Theory Tech.*, vol. MTT-24, pp. 631-640, Oct. 1976.

[55] V. K. Tripathi, "On the Analysis of Symmetrical Three-Line Microstrip Circuits," *IEEE Trans. Microwave Theory Tech.*, vol. MTT-25, pp. 726-729, Sep. 1977.

[56] P. M. DeRusso, R. J. Roy and C. M. Close, *State Variables for Engineers*, New York: Wiley, 1965.

[57] T. H. Lee, *The Design of CMOS Radio Frequency Integrated Circuits*, Cambridge:

University Press, 1998.

[58] O. P. Rustogi, "Linearly Tapered Transmission Line and Its Application in Microwaves," *IEEE Trans. Microwave Theory Tech.*, vol. MTT-17, pp. 166-168, Mar. 1969.

[59] *Advanced Design System (ADS)*, Agilent Technologies, Palo Alto, CA.

[60] S. Yamamoto, T. Azakami, and K. Itakura, "Coupled Strip Transmission Line with Three Center Conductors," *IEEE Trans. Microwave Theory Tech.*, vol. MTT-14, pp. 446-461, Oct. 1966.

[61] D. M. Pozar, *Microwave Engineering*, 2nd Ed. New York: Wiley, 1998.

[62] N. Boulejfen, A. B. Kouki, and F. M. Ghannouchi, "Frequency- and Time-Domain Analysis of Nouniform Lossy Coupled Transmission Lines with Linear and Nonlinear Terminations," *IEEE Trans. Microwave Theory Tech.*, vol. MTT-48, pp. 367-379, Mar. 2000.

[63] A. R. Djordjevic, M. B. Bazdar, T. K. Sarkar, and R. F. Harrington, *LINPAR for Win32 Platforms*, Ver 2.0, Boston: Artech House, 1999.

[64] M. Kirschning, and R. H. Jansen, "Accurate Wide-Range Design Equations for the Frequency-Dependent Characteristic of Parallel Coupled Microstrip Lines," *IEEE Trans. Microwave Theory Tech.*, vol. MTT-32, pp. 83-90, Jan. 1984.

[65] K. C. Gupta, R. Garg, I. Bahl, and P. Bhartia, *Microstrip Lines and Slotlines*, 2nd Ed. Boston: Artech House, 1996.

[66] C. Chen, *Theory of Electromagnetic Waves*, New York: McGraw Hill, 1983

[67] Yu. A. Brychkov and A. P. Prudnikov, *Integral Transforms of Generalized Functions*, New York: Gordon and Breach, 1989

[68] G. A. Campbell and R. M. Foster, *Fourier Integrals for Practical Applications*, nos. 209D, 619, 871.2, 872, NJ: Van Nostrand Company, 1948.

APPENDIX A

Eqn. (18) is evaluated by using some lesser known forms of the Fourier Transform [67]

$$\Im\left[\frac{dF(k_z)}{dk_z}\right] = \frac{1}{2\pi}\int_{-\infty}^{\infty}\left[\frac{dF(k_z)}{dk_z}\right]e^{jk_z\overline{z}}dk_z = -i\overline{z}\,\Im\left[F\left(k_z\right)\right] \quad (223)$$

$$\frac{1}{2\pi}\int_{-\infty}^{\infty}\frac{\sin\left[tv_p\sqrt{k_z^2-k_l^{\,2}}\right]}{\sqrt{k_z^2-k_l^{\,2}}}e^{jk_z\overline{z}}dk_z = \frac{1}{2}J_0\left[k_l\sqrt{(\overline{z})^2-\left(tv_p\right)^2}\right] \quad (224)$$

$$\frac{1}{2\pi}\int_{-\infty}^{\infty}\left\{\cos\left[tv_p\sqrt{k_z^2-k_l^{\,2}}\right]\right\}e^{jk_z\overline{z}}dk_z =$$

$$\frac{1}{2}\left[\delta\left(\overline{z}+tv_p\right)+\delta\left(\overline{z}-tv_p\right)\right]+\frac{bt}{4}\frac{J_1\left[\frac{b}{v_p}\sqrt{(\overline{z})^2-\left(tv_p\right)^2}\right]}{\sqrt{(\overline{z})^2-\left(tv_p\right)^2}} \quad (225)$$

and the properties of Bessel function $J_0(-x)=J_0(x),\quad J_1(-x)=-J_1(x)$. Combinations of (224) and (225) produce K_{11} and K_{22} . K_{12} is found by first expressing A_{12} in the differential form

$$A_{12} = jZ_0e^{-at}\frac{1}{tv_p}\frac{d}{dk_z}\left\{\cos\left[tv_p\sqrt{k_z^2-k_l^{\,2}}\right]\right\} \quad (226)$$

and then applying (223) and (225) in succession. K_{21} can be found in the same way.

APPENDIX B

In order to obtain (24) and (25), the integrations in (22) and (23) are performed by Simpson's numerical integration rule

$$\int_{x-h}^{x+h} f\left(x'\right)dx' \cong \left[f\left(x+h\right)+ f\left(x-h\right)+4 f\left(x\right)\right]\frac{h}{3}-\frac{h^5}{90} f^{(4)}\left(\xi\right) \qquad (227)$$

Note that this Simpson's rule requires only a 3 point interval, shown in Fig. 17, and has an error bound $-\frac{h^5}{90} f^{(4)}\left(\xi\right)$, where h is the distance between grid points, $f^{(4)}$ is the 4th derivative of the function of integration and ξ is any value in $\left(x-h, x+h\right)$.

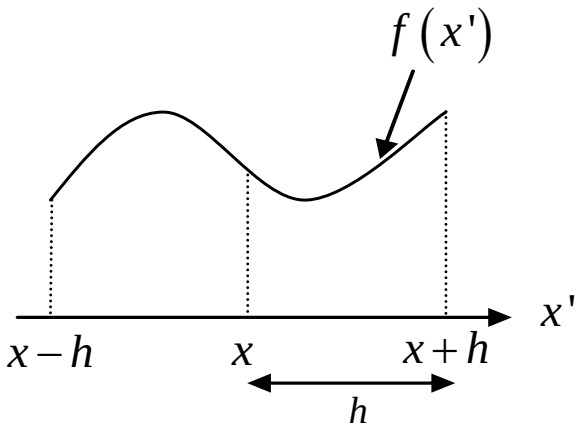

Fig. 17 Illustration of Simpson's integration rule.

Because $h \ll 1$, higher order terms are neglected in the numerical expression.

Also, the following Bessel properties are used to obtain the terms in Eqns. (22) and (23)

$$\lim_{x\to 0}\left[J_v(x)\right]=\left(\frac{1}{2}x\right)^v\Big/\Gamma(v+1) \tag{228}$$

$$J_0(jx)=I_0(x) \tag{229}$$

$$J_1(jx)=jI_1(x) \tag{230}$$

where Γ is Gamma function and I_0, I_1 are zero and first order modified Bessel functions repectively. Eqn. (228) is valid only when v is fixed integer.

As an example of the construction of the numerical equations, after Simpson's rule is applied the fifth term of (22) becomes,

$$Fifth\ term \simeq \frac{bt^2 v_p}{3}\left[\begin{array}{c} f(z+tv_p)V(z+tv_p)+f(z-tv_p)V(z-tv_p) \\ +4\dfrac{J_1\left[\dfrac{b}{v_p}\sqrt{-(tv_p)^2}\right]}{\sqrt{-(tv_p)^2}}V(z) \end{array}\right] \tag{231}$$

where $f(z\pm tv_p)=\lim_{\overline{z}\to z\pm tv_p}\dfrac{J_1\left[\dfrac{b}{v_p}\sqrt{(\overline{z})^2-(tv_p)^2}\right]}{\sqrt{(\overline{z})^2-(tv_p)^2}}$

From the equation (228),

$$f(z\pm tv_p)=\lim_{\overline{z}\to z\pm tv_p}\frac{\frac{1}{2}\frac{b}{v_p}\sqrt{(\overline{z})^2-(tv_p)^2}}{\sqrt{(\overline{z})^2-(tv_p)^2}}=\frac{1}{2}\frac{b}{v_p} \tag{232}$$

Also, in (231)

$$4\frac{J_1\left[\frac{b}{v_p}\sqrt{-\left(tv_p\right)^2}\right]}{\sqrt{-\left(tv_p\right)^2}}V(z)=4\frac{J_1\left(jbt\right)}{jtv_p}V(z)=4\frac{I_1\left(bt\right)}{tv_p}V(z) \qquad (233)$$

Inserting (232) and (233) into (231) gives

$$Fifth\ term\simeq\frac{\left(bt\right)^2}{6}\left[V(z+tv_p)+V(z-tv_p)\right]+\frac{4\left(bt\right)}{3}I_1(bt)V(z) \qquad (234)$$

The other terms in (24) and (25) can be constructed in the same way.

APPENDIX C

The most common technique for finding the dyadic Green's function for Eqn. (166) is the eigenfunction expansion method [38]. This requires an inhomogeneous differential equation with the left hand side given in (172), but with a Dirac delta forcing function. That the causal part of the propagator is a solution to such an inhomogeneous equation can be shown as follows: A unit step multiplier, $U(t-t')$, is inserted in (172) yielding,

$$\frac{\partial U\left(t-t'\right)\bar{\mathbf{K}}}{\partial t}-\bar{\mathbf{S}}\cdot U\left(t-t'\right)\bar{\mathbf{K}}=0 \tag{235}$$

When the time derivative is carried out and (173) and (176) are incorporated into the result, the traditional Green's function inhomogeneous differential equation

$$\frac{\partial\bar{\mathbf{G}}}{\partial t}-\bar{\mathbf{S}}\cdot\bar{\mathbf{G}}=\bar{\mathbf{I}}\delta(\mathbf{r}-\mathbf{r}')\delta(t-t') \tag{236}$$

readily follows. In essence the unit step ensures causality of the Green's function.

APPENDIX D

```
      module lossy_TL

! All variables used in this program are defined in this module.
! All subroutine including main part must have 'use lossy_TL'.
! nx = cell size
! nt = time step
! Vs = a source

      implicit none

      integer :: i,n,k,nx_end
      integer,parameter :: nx=300,ns=1601
      integer,parameter :: nx_start=30,nx_end1=200
      integer,parameter :: nx_source=15,nx_collect=nx_start-1
      integer,parameter :: nt=1000                !time step
      integer,parameter :: dbl=selected_real_kind(p=14,r=200)
      integer,parameter :: db=selected_int_kind(8)
      real(kind=dbl):: di,nn,h,skin_dept,t
      real(kind=dbl),dimension(nx)::ds,sum
      real(kind=dbl),dimension(nx):: AA,vi,vi1,w,alpac,alpad,alpa,A,B
      real(kind=dbl),dimension(nx)::Zc,Ra,La,Ca,Ga
      real(kind=dbl)::mu,ro,er1,er2,sigma,rho
      real(kind=dbl)::ep1,ep2,Rm,loss_tang
      real(kind=dbl),dimension(nx)::f,C0,ee,ee_f,fb,fa,mo,mc,m
      real(kind=dbl),dimension(nx):: LR,R11,R22
      real(kind=dbl):: pi,beta,dtd,dx,dy,temp,df,omega,dt
      real(kind=dbl) :: I0,I1,Zs,Zl,ds_air,eta,w0,w1
      real(kind=dbl),dimension(nx) :: V_in,V_tot,Vs,I_in,I_tot,Is
      real(kind=dbl),dimension(nx) ::V_in_u,V_tot_u,Vs_u,I_in_u,I_tot_u
      real(kind=dbl),dimension(ns) ::dR,dR1,drr,freqs,R1
      integer :: ip,nsnap,iplot(50)
      integer, parameter :: nsnap=50             !number of snapshot
      real(kind=dbl),dimension(2) ::dyy,dls,dlf
      real(kind=dbl),dimension(nx) ::dxx, dV_in,dV_tot
      complex :: j ,dum,B1,A1,gam,ep,Zin
      complex,dimension(ns) ::ef_in,ef_ref,R2

      end module lossy_TL
!*********************************************************************
      use lossy_TL

!     call data needed to calculate
      call data

!     call initialization subroutine
      call initialize                  !initialize the arrays

!     snapshots plots of the V and I field at these time steps
```

```
      do n=1,nt
         nn=n
        call V_lossless
        call V_total
        call dft

        open(unit=50,file='V_in.txt')
            write(50,*) (nn-nx_start+nx_source)/100,Vs(nx_source)

        open(unit=60,file='V_ne.txt')
            write(60,*) (nn-nx_start+nx_source)/100,V_tot(nx_start)

        open(unit=70,file='V_fe.txt')
            write(70,*) (nn-nx_start+nx_source)/100,V_tot(nx_end-1)
        do ip=1, nsnap
           iplot(ip)=(ip)*10
!          if (n.eq.iplot(ip)) call plot3d
        end do
      end do

! call analytical solution in freq. domain
      call analytic

! plot reflection plot
      call plot_reflection

      end
!***********************************************************************
      subroutine data

      use lossy_TL

      j = CMPLX(0.,1.)
      pi=4.*ATAN(1.)
      mu=4.*pi*1.e-7
      eo=1.e-9/(36*pi)
      eta=sqrt(mu/eo)
      er1=9.7
      loss_tang=2e-4
      er2=0
      sigma=5.8e7
      ep=eo*(er1-j*er2)
      ep1=eo*er1
      ep2=eo*er2
      ds_air=0.003
      di=0.1                  !Lossy TL length
      Zs=10.
      Zl=100.
      h=5.e-4
      t=2.e-5
      nx_end=118
```

```
 w0=5e-4
 w1=15e-4
 sum(nx_start)=0.0
 w(nx_start)=w0
 w(nx_end)=w1

 do i=nx_start,nx_end1
   freqs(1) = 0.0
   do k = 2, ns
       freqs(k) =0!4.e9!freqs(k-1) + 10.E06
       omega=2*pi*freqs(k)
       Rm=sqrt(omega*mu/2/sigma)
       if (w(i)/h<=1) then
             f(i)=0.02*(er1-1)*(1-w(i)/h)**2
             C0(i)=2*pi*eo/log(8.*h/w(i)+w(i)/4/h)
       else
             f(i)=0.
             C0(i)=eo*(w(i)/h+1.393+0.667*log(w(i)/h+1.444))
       end if
             ee(i)=(er1+1)/2+(er1-1)/2/sqrt(1+12*h/w(i))
+                  +f(i)-0.217*(er1-1)*t/sqrt(w(i)*h)
             fb(i)=47.746/h/sqrt(er1-ee(i))*atan(er1*sqrt((ee(i)
+                   -1)/(er1
+                -ee(i))))
             fa(i)=fb(i)/(0.75+(0.75-0.332*er1**(-1.73))*w(i)/h)
             mo(i)=1+1/(1+sqrt(w(i)/h))+0.32*(1+sqrt(w(i)/h))**
+                  (-3)
       if (w(i)/h<=0.7) then
             mc(i)=1+1.4/(1+w(i)/h)*(0.15-0.235*exp(0.45*freqs(k)
+                  /1.e9/fa(i)))
       else
             mc(i)=1.
       end if
             m(i)=mo(i)*mc(i)
       ee_f(i)=er1-(er1-ee(i))/(1+(freqs(k)/1.e9/fa(i))**m(i))
       ds(i)=ds_air/sqrt(ee_f(i))
       w(i+1)=w(i)+(w1-w0)/di*ds(i)
       sum(i+1)=sum(i)+ds(i)
       skin_depth=(1/Rm/sigma)*100/2.54*1000
       if (w(i)/h<=0.5) then
                LR(i)=1
       else
                LR(i)=0.94+0.132*w(i)/h-0.0062*(w(i)/h)**2
       end if
       R11(i)=Rm/w(i)*LR(i)*(1/pi+1/pi**2*log(4*pi*w(i)/t))
       R22(i)=Rm/w(i)*w(i)/h/(w(i)/h+5.8+0.03*h/w(i))
       Zc(i)=1/C0(i)*sqrt(mu*eo/ee_f(i))
       Ca(i)=C0(i)*ee_f(i)
       La(i)=mu*eo/C0(i)
       Ga(i)=er1/ee_f(i)*(ee_f(i)-1)/(er1-1)*omega*er2/er1*Ca(i)
       Ra(i)=R11(i)+R22(i)
       alpad(i)=Ga(i)*Zc(i)/2
       alpac(i)=Ra(i)/2/Zc(i)
```

```
            alpa(i)=(alpad(i)+alpac(i))*8.686
            vi(i)=1/SQRT(La(i)*Ca(i))
            vi1(i)=1/SQRT(eo*mu*ee_f(i))
            dt=ds(i)/vi(i)
            A(i)=(Ga(i)/Ca(i)-Ra(i)/La(i))*ds(i)/(2*vi(i))
            B(i)=EXP(-(Ga(i)/Ca(i)+Ra(i)/La(i))*ds(i)/(2*vi(i)))
            AA(i)=A(i)
          end do
        end do

        end
!***********************************************************************
        subroutine dft

        use lossy_TL

! To find reflection coefficient, store data

        j=(0,1)
        temp=V_tot(nx_collect)-V_in(nx_collect)

        do k=1,ns
          dum=-1.*j*2.*pi*(n-1)*freqs(k)*dt
          ef_in(k)=ef_in(k)+dt*V_in(nx_collect)*CEXP(dum)
          ef_ref(k)=ef_ref(k)+dt*temp*CEXP(dum)
          R2(k)=ABS(ef_ref(k)/ef_in(k))
        end do

        end
!***********************************************************************
        subroutine analytic

        use lossy_TL

          j = CMPLX(0.,1.)
!         call data
! generate the analytical data

        do k=1, ns
          omega=2*pi*freqs(k)
          gam=sqrt((Ra(i)+j*omega*La(i))*(Ga(i)+j*omega*Ca(i)))
          A1=(exp(gam*di)-exp(-1.*gam*di))/(exp(gam*di)+exp(-1.*gam*di))
          Zin=Zc(i)*(Zl+Zc(i)*A1)/(Zc(i)+Zl*A1)
          B1=(Zin-Zs)/(Zin+Zs)
          R1(k)=abs(B1)
        end do

        end
!***********************************************************************
        subroutine initialize

! Initialize all the arrays
```

```
      use lossy_TL

           V_in=0.0
           I_in=0.0
           V_tot=0.0
           I_tot=0.0
           Vs=0.0
           V_in_u=0.0
           I_in_u=0.0
           V_tot_u=0.0
           I_tot_u=0.0
           ef_in=(0.0,0.0)
           ef_ref=(0.0,0.0)
           R2=(0.0,0.0)
           R1=(0.0,0.0)

      end
!**********************************************************************
! Voltage without lossy center section

      subroutine V_lossless

      use lossy_TL

      call source

      V_in_u(1)=0.0
      I_in_u(1)=0.0

      do i=2,nx-1
        V_in_u(i)=0.5*((V_in(i+1)+V_in(i-1))
     +             -(I_in(i+1)-I_in(i-1))*Zs)+Vs(i)

        I_in_u(i)=0.5*((I_in(i+1)+I_in(i-1))
     +              -(V_in(i+1)-V_in(i-1))/Zs)

      end do

      V_in_u(nx)=0.0
      I_in_u(nx)=0.0

      do i=1,nx
        V_in(i)=V_in_u(i)
        I_in(i)=I_in_u(i)
      end do

      end
!**********************************************************************
! Voltage with lossy center section

      subroutine V_total

      use lossy_TL
```

```
      call source

      V_tot_u(1)=0.0
      I_tot_u(1)=0.0

      do i=2,nx-1
          V_tot_u(i)=0.5*((V_tot(i+1)+V_tot(i-1))
     +                -(I_tot(i+1)-I_tot(i-1))*Zs) +Vs(i)

          I_tot_u(i)=0.5*((I_tot(i+1)+I_tot(i-1))
     +              -(V_tot(i+1)-V_tot(i-1))/Zs)

      if(i.gt.nx_start.and.i.lt.nx_end) then

          V_tot_u(i) = B(i)*0.5 * (
     +             (1+((A(i)**2)/6)-(A(i)/3))*(V_tot(i+1)
     +             + V_tot(i-1))
     +             -Zc(i)*(1+((A(i)**2)/6))*(I_tot(i+1)-I_tot(i-1))
     +             +(4*A(i)/3)*(bessi1(AA(i))-bessi0(AA(i)))*V_tot(i) )

          I_tot_u(i) = B(i)*0.5 * (
     +             (1+((A(i)**2)/6)+(A(i)/3))*(I_tot(i+1)
     +             + I_tot(i-1))
     +             -(1+(A(i)**2)/6)*(V_tot(i+1) - V_tot(i-1))/Zc(i)
     +             +(4*A(i)/3)*(bessi1(AA(i))+bessi0(AA(i)))*I_tot(i) )

        else if (i.gt.nx_end-1.and.i.lt.nx) then

          V_tot_u(i)=0.5*((V_tot(i+1)+V_tot(i-1))
     +                -(I_tot(i+1)-I_tot(i-1))*Zl)

          I_tot_u(i)=0.5*((I_tot(i+1)+I_tot(i-1))
     +              -(V_tot(i+1)-V_tot(i-1))/Zl)
      end if

      end do

      V_tot_u(nx)=0.0
      I_tot_u(nx)=0.0

      do i=1,nx
        V_tot(i)=V_tot_u(i)
        I_tot(i)=I_tot_u(i)
      end do

      end
!**********************************************************************
! Bessel function

      FUNCTION bessi0(x)
      REAL bessi0,x
      REAL ax
```

```
      DOUBLE PRECISION
      p1,p2,p3,p4,p5,p6,p7,q1,q2,q3,q4,q5,q6,q7,q8,q9,y
      SAVE p1,p2,p3,p4,p5,p6,p7,q1,q2,q3,q4,q5,q6,q7,q8,q9
      DATA
      p1,p2,p3,p4,p5,p6,p7/1.0d0,3.5156229d0,3.0899424d0,1.2067492d0,
     +                     0.2659732d0,0.360768d-1,0.45813d-2/
      DATA q1,q2,q3,q4,q5,q6,q7,q8,q9/0.39894228d0,0.1328592d-1,
     +        0.225319d-2,-0.157565d-2,0.916281d-2,-0.2057706d-1
     +        ,0.2635537d-1,-0.1647633d-1,0.392377d-2/
      if (abs(x).lt.3.75) then
      y=(x/3.75)**2
      bessi0=p1+y*(p2+y*(p3+y*(p4+y*(p5+y*(p6+y*p7)))))
      else
      ax=abs(x)
      y=3.75/ax
      bessi0=(exp(ax)/sqrt(ax))*(q1+y*(q2+y*(q3+y*(q4
     +                +y*(q5+y*(q6+y*(q7+y*(q8+y*q9))))))))
      endif
      return
      END

      FUNCTION bessi1(x)
      REAL bessi1,x
      REAL ax
      DOUBLE PRECISION
      p1,p2,p3,p4,p5,p6,p7,q1,q2,q3,q4,q5,q6,q7,q8,q9,y
      SAVE p1,p2,p3,p4,p5,p6,p7,q1,q2,q3,q4,q5,q6,q7,q8,q9
      DATA p1,p2,p3,p4,p5,p6,p7/0.5d0,0.87890594d0,0.51498869d0,
     +                0.15084934d0,0.2658733d-1,0.301532d-2,0.32411d-3/
      DATA q1,q2,q3,q4,q5,q6,q7,q8,q9/0.39894228d0,-0.3988024d-1,
     +        -0.362018d-2,0.163801d-2,-0.1031555d-1,0.2282967d-1
     +       ,-0.2895312d-1,0.1787654d-1,-0.420059d-2/
      if (abs(x).lt.3.75) then
      y=(x/3.75)**2
      bessi1=x*(p1+y*(p2+y*(p3+y*(p4+y*(p5+y*(p6+y*p7))))))
      else
      ax=abs(x)
      y=3.75/ax
      bessi1=(exp(ax)/sqrt(ax))*(q1+y*(q2+y*(q3+y*(q4+
     +         y*(q5+y*(q6+y*(q7+y*(q8+y*q9))))))))
      if(x.lt.0.)bessi1=-bessi1
      endif
      return
      END
!*********************************************************************
! The excitation of the gaussian pulse
! It should be added at each time step.

      subroutine source

      use lossy_TL

      beta=40.
```

```
      Vs(nx_source)=exp(-((n-5*beta)/beta)**2)

      end
!**********************************************************************
! Plot the reflection coeffcient

      subroutine plot_reflection

      use lossy_TL

!  Matlab required variables
      integer :: m_eng, engopen
      integer :: engevalstring, engputfull, stat, engclose
      integer :: mxcalloc,drr_pointer, dR_pointer,dR1_pointer

      do k=1,ns
       drr(k)=freqs(k)/1.e9
       dR(k)=R2(k)
       dR1(k)=R1(k)
      end do

      open(unit=10,file='eqn_data.txt')
      do k=1,ns
         write(10,*) drr(k),dR(k)
      end do

      open(unit=20,file='anal_data.txt')
      do k=1,ns
         write(20,*) drr(k),dR1(k)
      end do

      m_eng = engopen('matlab ')
      dR_pointer = mxcalloc(ns,8)
      dR1_pointer = mxcalloc(ns,8)
      drr_pointer=mxcalloc(ns,8)

      call mxcopyreal8toptr(dR,dR_pointer,ns)
      call mxcopyreal8toptr(dR1,dR1_pointer,ns)
      call mxcopyreal8toptr(drr,drr_pointer,ns)

      stat=engputfull(m_eng, "dR" , ns, 1, dR_pointer ,0)
      stat=engputfull(m_eng, "dR1" , ns, 1, dR1_pointer ,0)
      stat=engputfull(m_eng, "drr", ns, 1,drr_pointer, 0)

      stat=engevalstring(m_eng, "plot(drr, dR, 'r' ,drr,dR1,'b--')")
      stat=engevalstring(m_eng, "xlabel('FREQUENCY(GHz)')")
      stat=engevalstring(m_eng, "ylabel('REFLECTION COEFFICIENT')")
      stat=engevalstring(m_eng, "legend('Eqn','Analytic')")
      stat=engevalstring(m_eng, "axis([0 6 0 1])")
      PAUSE

      stat = engclose(m_eng)
```

```
      end
!**********************************************************************
! plot the V_in and V_tot

      subroutine plot3d

      use lossy_TL

!  Matlab required variables
      integer :: m_eng, engopen
      integer :: engevalstring, engputfull, stat, engclose
      integer :: mxcalloc, Vt_pointer,Vi_pointer,dxx_pointer,y_pointer
      integer :: dyy_pointer,dls_pointer,dlf_pointer

      dyy(1)=1.0
      dyy(2)=-1.0
      dls(1)=nx_start
      dls(2)=nx_start
      dlf(1)=nx_end
      dlf(2)=nx_end

      do i = 1,nx
        dxx(i)=I
        dV_in(i)=V_in(i)
        dV_tot(i)=V_tot(i)
      end do

!  Start matlab engine and allocate space for matrix to be passed to
!  matlab
      if( n==10) m_eng = engopen('matlab ')
      Vt_pointer = mxcalloc(nx, 8)
      Vi_pointer = mxcalloc(nx, 8)
      dxx_pointer = mxcalloc(nx, 8)
      dyy_pointer = mxcalloc(2, 8)
      dls_pointer = mxcalloc(2, 8)
      dlf_pointer = mxcalloc(2, 8)
!  First we convert the data to a format that matlab understands
      call mxcopyreal8toptr(dV_in,Vi_pointer,nx)
      call mxcopyreal8toptr(dV_tot,Vt_pointer,nx)
      call mxcopyreal8toptr(dxx,dxx_pointer,nx)
      call mxcopyreal8toptr(dyy,dyy_pointer,2)
      call mxcopyreal8toptr(dls,dls_pointer,2)
      call mxcopyreal8toptr(dlf,dlf_pointer,2)
! Now move the data into matlab
      stat=engputfull(m_eng, "dxx", nx, 1, dxx_pointer, 0)
      stat=engputfull(m_eng, "dyy", 2,  1, dyy_pointer, 0)
      stat=engputfull(m_eng, "dls", 2,  1, dls_pointer, 0)
      stat=engputfull(m_eng, "dlf", 2,  1, dlf_pointer, 0)
      stat=engputfull(m_eng,"dV_in",nx,1,Vi_pointer,0)
      stat=engputfull(m_eng,"dV_tot",nx,1,Vt_pointer,0)
! now generate all six plots on page  and wait 5 seconds
      stat=engevalstring(m_eng,"subplot(2,1,1)")
      stat=engevalstring(m_eng,"plot(dxx,dV_in,dls,dyy,':',dlf,dyy,':')
```

```
     +        ")
      stat=engevalstring(m_eng,"subplot(2,1,2)")
      stat=engevalstring(m_eng,"plot(dxx,dV_tot,dls,dyy,':',dlf,dyy,':'
     +       )")

!  Now close matlab
      if(n.eq.nt) stat = engclose(m_eng)

      end
!***********************************************************************
```

VITA

Jaehoon Jeong was born in Gyeongsangnam-Do, Republic of Korea. He received the Bachelor of Science degree in electrical and electronics engineering from Hong-Ik University, Seoul, Korea, in 2002 and the Doctor of Philosophy degree in Electrical Engineering, Texas A&M University, in 2006.

From Feb. of 1997 to Apr. of 1999, he was in the military service as a radar and wireless communication engineer. In 2002, he was a Technology Engineer with the Hyosung Corporation Ltd., Seoul, Korea. He was a Research Assistant with the Electromagnetics and Microwave Laboratory, Texas A&M University, College Station under the advisement of Dr. Robert D. Nevels. His research interests are mathematical and numerical techniques in transmission line analysis, electromagnetic field analysis and scattering. He can be reached through Professor Robert D. Nevels, Department of Electrical and Computer Engineering, Texas A&M University, College Station, TX 77843-3128. His permanent address is Haengsin 2-dong, Goyang Si Deokyang-gu, Gyeonggi-Do, Republic of Korea, 412-724.